NUREG/CR-1538
EGG-2047
Distribution Category: R3

PBF/LOFT LEAD ROD TEST SERIES TEST RESULTS REPORT

Dominic J. Varacalle, Jr.
Richard W. Garner
Shu Shiozawa[a]
Walter E. Driskell
Dennis R. Evans
W. Robert Cox
Jose A. Fernandez
Thomas E. Brake

Published July 1980

EG&G Idaho, Inc.
Idaho Falls, ID 83415

Prepared for the
U.S. Nuclear Regulatory Commission
Washington, D.C. 20555
Under DOE Contract No. DE-AC07-76IDO1570
FIN No. A6041

a. Visiting engineer from the Japanese Atomic Energy Research Institute

ABSTRACT

Results of the Power Burst Facility/Loss-of-Fluid Test (PBF/LOFT) Lead Rod sequential blowdown test series conducted in the PBF are presented. The tests were performed to evaluate the extent of mechanical deformation that would be expected to occur to low pressure (0.1 MPa) light water reactor design fuel rods when subjected to a series of large, double-ended cold leg break loss-of-coolant accident (LOCA) tests, and to determine whether subjecting these deformed fuel rods to subsequent testing would result in rod failure. The extent of mechanical deformation (buckling, collapse, or waisting of the cladding) was evaluated by comparison of cladding temperature and pressure measurements with out-of-pile experiment data, by comparison of steady state fuel centerline temperature response, and by posttest visual examinations and cladding diametral measurements.

SUMMARY

The PBF/LOFT Lead Rod (LLR) Test Program provided evidence that unpressurized pressurized water reactor (PWR) type fuel rods deformed by prior loss-of-coolant experiments (LOCEs) will not fail when subjected to successive preconditioning cycles, large break LOCA transients, and reflood and quench cycles.

The PBF/LLR Test Program was conducted by the Thermal Fuels Behavior Program of EG&G Idaho, Inc., to provide experiment information on the behavior of nuclear fuel under normal and loss-of-coolant accident conditions. The tests in this program were conducted in the Power Burst Facility reactor at the Idaho National Engineering Laboratory. The program was conducted for the U. S. Nuclear Regulatory Commission under funding provided by the Japanese Atomic Energy Research Institute.

The results of the PBF/LLR tests have direct application to evaluating the extent of fuel rod deformation that would be expected to occur during the LOFT[a] Power Ascension Test Series and the consequences of continued operation of the LOFT core with deformed fuel rods. The PBF/LLR Test Program focused on fuel rod behavior rather than on the total system behavior as in the case of LOFT.

In the PBF reactor, the test fuel rods are contained within an in-pile tube (IPT) located at the center of the PBF core. The experiment hardware is composed of the IPT and its contents, the primary coolant system (PCS), the blowdown system, and the reflood and quench system.

The sequence of events during the LLR tests was as follows. Initially, the PCS was providing coolant to the IPT at typical commercial PWR flow, temperature, and pressure conditions. The blowdown portion of the experiment began with isolation of the PCS from the IPT. Next, blowdown was initiated by opening the high speed blowdown valves to the blowdown tank in the cold leg, followed by reactor scram. The system depressurized in approximately 30 s. Reflood and quench followed the system depressurization for cooling of the fuel rods.

The PBF/LLR Test Series originally consisted of three tests, designated LLR-3, LLR-5, and LLR-4, that were designed and performed to simulate the behavior of LOFT design fuel rods during the LOFT Power Ascension Test Series[b] Tests L2-3, L2-5, and L2-4, respectively. Each test was performed with four, unpressurized, separately shrouded LOFT design fuel rods. A total of seven fuel rods were tested in the program. The fuel rods consisted of a 0.914-m-long stack of fresh, 93% theoretical density, UO_2 fuel pellets clad with zircaloy-4. The fuel was enriched with 9.5 wt% ^{235}U and the rods were prepressurized to 0.103 MPa. Test conditions at initiation of the LLR-3, LLR-5, and LLR-4 system depressurizations were approximately 595 K inlet coolant temperature, 15.5 MPa system pressure, and 41, 46, and 57 kW/m peak linear power, respectively, in the test rods. Each test involved a power cycling phase and steady state operation phase to precondition the fuel and build up a fission product inventory. The rods were then exposed to a blowdown similar to that expected in LOFT during a simulated PWR double-ended cold leg break LOCA. Thermal-hydraulic parameters and fuel rod pressures, temperatures, and coolant flow conditions were monitored throughout the tests.

Prior to the performance of the PBF/LLR tests, expectations were that Test LLR-5 would result in waisting of the cladding and that Test LLR-4 would be performed to provide the desired information on the effects of pellet-cladding interaction during subsequent testing with deformed fuel rods. However, the measured fuel rod cladding temperatures during Tests LLR-3 and LLR-5 were lower than anticipated, and the maximum desired fuel rod cladding deformation may not have

a. The Loss-of-Fluid Test facility is the major testing facility for evaluating the systems response of a PWR over a wide range of loss-of-coolant experiment conditions. As such, the LOFT core is intended to be used for sequential LOCEs, provided no significant fuel rod failures occur. During the LOFT large break LOCE transients, a system depressurization (30 s duration) typical of that expected during a double-ended cold leg break in a PWR is maintained. Since the fuel rods are fabricated unpressurized, the cladding is subjected to a compressive stress during most of the blowdown, which causes cladding collapse onto the fuel column as cladding temperatures approach 1050 K at a system pressure of 7 MPa.

b. The LOFT test series includes five successive 200% cold leg break LOCEs, with initial core powers ranging from 34.2 to 52.5 kW/m.

occurred until the highest power test (Test LLR-4) was performed. Since a major objective of the LLR tests was to investigate the effect of waisting on rod behavior during subsequent power ramps and blowdown transients, Test LLR-4A was added to the test program. This experiment was performed at the same test conditions as Test LLR-4.

Maximum measured cladding temperatures during Test LLR-3 ranged from 880 to 990 K. Rod 312-3 failed during the test due to a waterlogged condition that occurred sometime prior to the blowdown. On the basis of the cladding temperatures attained during this test, no mechanical deformation is expected to have occurred to the remaining rods. Maximum measured cladding temperatures ranged from 985 to 1015 K during Test LLR-5, which probably resulted in two-point buckling of the cladding at the thermocouple locations. However, the cladding elongation measurements obtained during this test and the subsequent tests of the LLR series indicated that departure from nucleate boiling (DNB) occurred earlier than indicated by the thermocouples, and probably at lower elevations. Higher cladding temperatures and cladding collapse may have occurred at rod elevations lower than the thermocouples during Test LLR-5.[a] Maximum measured cladding temperatures during Test LLR-4 ranged from 1065 to 1165 K. When Rod 312-1 was removed after the test for postirradiation examination, the rod exhibited collapse and waisting 35 to 55 cm above the bottom of the fuel stack. Comparable deformation of the other three rods probably occurred during this test, on the basis of out-of-pile deformation criteria. Maximum measured cladding temperatures during Test LLR-4A ranged from 1070 to 1260 K. Subsequent examination of the four rods from this test revealed that all four had achieved either the collapse or the waisting regime of mechanical deformation, but none of the rods failed.

During the postirradiation examination, all the rods were found to be uniformly covered with a black layer of zirconium dioxide. The cladding on all the rods (excluding Rods 312-3 and 312-4 from Test LLR-3) collapsed onto the fuel pellets, with waisting evidenced at a nominal distance of 30 to 60 cm from the bottom of the heated length.

The coolant data obtained in the measurement spools, the fuel rod flow shrouds, and the IPT during Test LLR-5 (representative of all the tests) were evaluated and compared with calculations from the RELAP4 computer code. Good agreement between test data and calculated coolant pressure, temperature, and mass flow rate in the hot and cold leg blowdown measurement spools was achieved. However, the RELAP4 pretest and posttest calculations of cladding temperature were significantly higher than the measured cladding temperatures throughout the blowdown portion of the transients.

Fuel centerline temperature measurements made during the tests were also compared with FRAP computer code calculations. The code overpredicted the steady state centerline temperature of a fresh rod and underpredicted the temperature of a collapsed fuel rod. Transient centerline temperatures were underpredicted in all cases.

The reflood dynamics witnessed during Test LLR-5 were compared with FLOOD4 computer code calculations. The code overpredicted the fuel rod quench times recorded during the test.

---

a. Preliminary results of the Thermocouple Effects Test Program, recently performed at the PBF for the specific purpose of evaluating the effect of cladding external surface thermocouples on fuel rod response during blowdown transients, indicate that the cladding thermocouples may indeed delay the onset of DNB, resulting in lower measured cladding surface temperatures.

CONTENTS

NOTE: All of the appendices to this report are presented on microfiche attached to the inside of the back cover.

FIGURES

TABLES

NOMENCLATURE

A	flow area
a	air
E_r	radial strain
f	liquid phase
fg	difference in saturated liquid and vapor
g	vapor phase
G	mass velocity
j	superficial velocity
m	mass flow
Q	volumetric flow rate
v	specific volume
w	water
X	quality
α	void fraction
ρ	density
σ	surface tension
μ	viscosity

PBF/LOFT LEAD ROD TEST SERIES TEST RESULTS REPORT

1. INTRODUCTION

The behavior of light water reactors (LWRs) following a postulated loss-of-coolant accident (LOCA) must conform to operating criteria specified in the Code of Federal Regulations. To ensure that the behavior of both the cooling system and the nuclear core is understood and properly modeled, in-pile experiments are being conducted in the Loss-of-Fluid Test (LOFT)[1] Facility and Power Burst Facility (PBF) at the Idaho National Engineering Laboratory by EG&G Idaho, Inc., for the U.S. Nuclear Regulatory Commission (NRC).

The LOFT facility is the major testing facility for evaluating the systems response of an LWR over a wide range of loss-of-coolant experiment (LOCE) conditions. The LOFT core is intended to be used for sequential LOCEs. The LOFT Power Ascension Test Series is a series of 200% cold leg break LOCEs with an initial core power of 50, 75, and 100% of full power (52.5 kW/m) as shown in Table 1. A system depressurization typical of that expected during a double-ended cold leg break in a pressurized water reactor (PWR) is simulated. The as-built internal fuel rod pressure will be 0.103 MPa for all the experiments except LOCE L2-6, in which the central bundle will be prepressurized. Cladding peak temperatures are calculated to rise to approximately 1300 K during the 100% power LOCA test. During most of the blowdown, the cladding will be subjected to a compressive stress that causes uniform cladding collapse onto the fuel column as cladding temperatures approach 1050 K at a system pressure of 7 MPa. At slightly higher temperatures (1100 K), cladding waisting (cladding collapse into gaps formed at pellet interfaces) may also occur. In preparation for a subsequent experiment in the L2 series, the LOFT core will be subjected to a series of preconditioning power ramps and steady state operation for 20 to 40 h. Pellet-cladding interaction (PCI) during the power ramps could potentially cause cladding failures at waisted locations throughout the high power region of the 1300-rod LOFT core.

The extent of the mechanical deformation and the propensity for failure of the LOFT fuel during this series of nuclear blowdown tests has been of concern because of the necessity to develop criteria for fuel replacement. Therefore, a series of special tests, designated the PBF/LOFT Lead Rod (PBF/LLR) tests, were conducted by the Thermal Fuels Behavior Program in the Power Burst Facility to provide in-pile information on the thermal and mechanical deformation behavior of low internal pressure, LWR-type fuel rods subjected

TABLE 1. LOFT L2 POWER ASCENSION TEST SERIES PROGRAM PLAN

Test	Power Level (kW/m)	Break Size (%)	Break Type	Fuel Condition
L2-2	26.3	200	Cold leg	Unpressurized
L2-3	39.4	200	Cold leg	Unpressurized
L2-5	39.4	200	Cold leg	Unpressurized
L2-4	52.5	200	Cold leg	Unpressurized
L2-6	39.4	200	Cold leg	Pressurized center module

to a series of multiple LOCA blowdowns and subsequent power ramps from a wide range of initial power levels. The LLR Test Program examined the consequences of continued operation of a nuclear core with deformed fuel rods.

The PBF/LLR tests were specifically designed to simulate the test conditions during the LOFT Power Ascension Tests L2-3 through L2-5. The tests provided an evaluation of the LOFT fuel over a wide range of initial fuel rod powers. Thus, an assessment of the state of the LOFT core before any one L2 test and the anticipated effect of the next test can be obtained by utilizing a combination of LLR test data and analytical predictions.

The primary objectives for the PBF/LLR tests were to (a) experimentally evaluate the extent of cladding collapse that would be expected to occur during the LOFT LOCA transients; (b) evaluate the effects of collapsed cladding and pellet-cladding interaction on the mechanical response of deformed fuel rods subjected to subsequent power increases, long-term preconditioning, and loss-of-coolant conditions; (c) provide experimental data to evaluate the Fuel Rod Analysis Program (FRAP) computer code for use in requalification of the LOFT core; and (d) evaluate the accuracy of the LOFT fuel rod thermocouples. The PBF/LLR Test Program consisted of four tests: LLR-3, LLR-5, and LLR-4, corresponding to the planned LOFT L2-3, L2-5, and L2-4 experiments, respectively, and Test LLR-4A, a follow-on test to the original program. Each of the LLR tests was performed with four, separately shrouded, LOFT design fuel rods with active fuel lengths of 0.914 m.

Each of the four LLR tests involved a power cycling preconditioning phase and a steady state operation phase to precondition the fuel and build up the fission product inventory. The power calibration phase consisted of several power cycles to provide fuel preconditioning and calibration of the test rods with the PBF core power. The rods were then further preconditioned at a test rod peak power density of 41 kW/m during Test LLR-3, 47 kW/m during Test LLR-5, 57 kW/m during Test LLR-4, and 56 kW/m during Test LLR-4A. For each test the system conditions prior to blowdown were approximately 595 K initial coolant temperature, 0.584 L/s coolant flow rate through each flow shroud (3412 kg/m^2-s) for Tests LLR-3 and LLR-5 and 0.78 L/s (4557 kg/m^2-s) for Tests LLR-4 and LLR-4A, and 15.5 MPa system pressure. Upon completion of the preconditioning phase for each test, blowdown was initiated by opening the high speed valves in the cold leg, simulating a 200% double-ended cold leg break. Cladding temperatures during the tests ranged from 880 to 1260 K.

Table 2 lists the maximum measured cladding temperatures of the fuel rods used for the LLR tests. In general, the measured cladding peak temperatures increased when the initial rod power was increased and were higher at lower axial elevations. In Test LLR-3, two of the rods (Rods 312-3 and 312-4) were at a lower power density than the other two rods. The high power rods were encased in zircaloy-4 flow shrouds and the low power rods were encased in stainless steel flow shrouds to model the LOFT center and peripheral fuel rods, respectively. For the subsequent tests, all the rods were encased in zircaloy-4 shrouds.

A brief discussion of the test hardware and the test conduct is presented in Section 2. A detailed description of the fuel rods, test assembly, and blowdown system is presented in Appendix A (presented on microfiche attached to the inside of the back cover). The thermal-hydraulic response of the coolant during the blowdown transients is described in Section 3. The data from Test LLR-5 (typical of the LLR tests) are described and compared with pretest analyses conducted with the RELAP4[2] code. Included are discussions of the system depressurization, coolant temperature, break flow, and coolant volumetric flow through the fuel assembly. The behavior of the fuel rods is described in Section 4 and compared with posttest analyses conducted with the FRAP-T5[3] code, and pre- and posttest analyses with the RELAP4 code. Included are discussions of steady state behavior as a function of rod power, transient cladding surface and fuel centerline temperatures, cladding axial elongation, and cladding circumferential strain. Section 5 presents a scenario of the reflood phenomena that occurred in the LLR tests. The conclusions pertinent to the tests results are discussed in Section 6. A detailed experiment description is contained in Appendix A and a discussion concerning the pretest steady state fuel rod power is given in Appendix B. The RELAP4 computer code models are described in Appendix C, the FRAP-T models in Appendix D, and the FLOOD4 models in Appendix E. All of the appendices to this report are presented on microfiche attached to the inside of the back cover. Companion reports[4,5] present the data taken during the tests and the detailed postirradiation analyses of the test rods.

TABLE 2. MAXIMUM MEASURED CLADDING TEMPERATURES OF LLR FUEL RODS

Rod	Temperature (K)			
	Test LLR-3	Test LLR-5	Test LLR-4	Test LLR-4A
312-1[a]	950	1000	1125	--
312-2[b]	920	1015	1165	1150
312-3[a]	990	--	--	--
312-4[a]	880	--	--	--
345-1[a]	--	1000	1060	1070
345-2[c]	--	c	c	c
399-2[d]	--	--	--	1260

a. Measured at 0.533 m from bottom of heated length.

b. Measured at 0.457 m from bottom of heated length.

c. Not instrumented with cladding thermocouples.

d. Measured at 0.314 m from bottom of heated length.

2. EXPERIMENT DESIGN AND CONDUCT

The PBF/LLR LOCA experiments were designed to study the LOFT fuel rod behavior expected to occur during the LOFT L2 Power Ascension Tests. The performance of LOCA experiments in the PBF differs from similar blowdown experiments performed in the Semiscale[6] and LOFT Programs in that only the core portion of the experiment is depressurized in the PBF, whereas the entire systems are depressurized in the Semiscale and LOFT facilities as would occur during a LOCA in a commerical PWR. In the PBF, the core portion of the experiment (that is, the four test fuel rods) is contained within the in-pile tube located at the center of the core, which provides a test environment with typical PWR coolant pressures, temperatures, and flow rates.

2.1 Experiment Design

The PBF/LLR LOCA experimental hardware is composed of the loop coolant system, the IPT (which contains the test train), the blowdown system, the reflood system, and the quench system.

The PBF primary loop coolant system, which provides a steady state flow path for the system coolant, contains high speed isolation valves in both legs, a high speed loop flow bypass valve, a pump, a pressurizer, a heater, and heat exchangers.

The four test fuel rods used for the LLR tests, the separate flow shrouds for each test fuel rod, and the associated instrumentation formed the fuel train. The fuel train was contained within the test train, which was in turn contained within the IPT. The test train was designed to support the fuel train, such that the four test fuel rods were positioned symmetrically about the central axis of the IPT. The test train also supported the instrumentation for measurement of coolant conditions within the IPT.

The blowdown system contains the effluent from the IPT during the blowdown transient. The system is composed of an initial coolant conditions instrument spool, a blowdown coolant conditions instrument spool in each leg, two blowdown valves in each leg, two Henry nozzles in each leg, the header, the blowdown tank, and the associated piping.

The reflood system is composed of piping from the quench system; a high speed, high flow valve; a high speed, low flow valve; and the test train center hanger rod. During reflood, coolant from the quench tank is injected directly down the center hanger rod into the plenum volume beneath the lower particle screen.

The quench system is composed of a high speed cold leg blowdown isolation valve, a high speed quench activation valve, pump, quench tank, water storage tank, and water makeup tank. The quench system provides long-term cooling of the experiment and IPT.

2.1.1 Fuel Train. The fuel train consisted of the four test fuel rods, flow shrouds, and associated instrumentation. Figure 1 presents an illustration

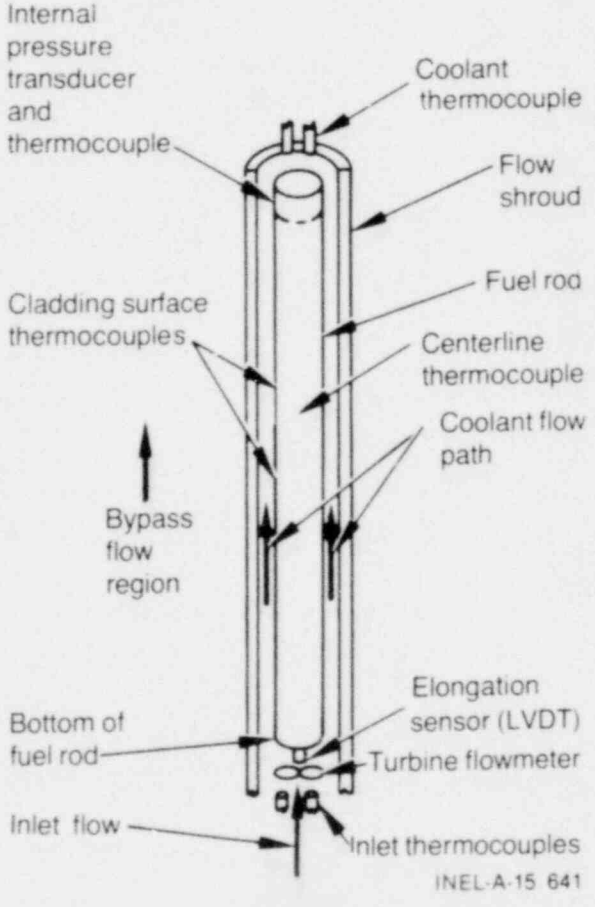

Figure 1. PBF/LLR test configuration schematic.

of a test fuel rod within a circular shroud, and the associated instrumentation. The dimensional characteristics of the four LLR fuel rods were typical of LOFT and 15 x 15 PWR fuel rods, except for the active length (0.91 m) and plenum volume. LOFT cladding was used to fabricate the fuel rods. The plenum volume was scaled proportionally to the active fuel length of a PWR. All seven of the test rods used in this series were backfilled with helium to atmospheric pressure, which corresponds to the backfill pressure used for the LOFT L2 Test Series fuel rods. The fuel rod pellets were fabricated by Exxon Nuclear Company using the typical LOFT technique. Except for pellet enrichment and centerline holes, the fuel pellets were identical to LOFT pellets. Centerline holes permitted the insertion of the fuel centerline thermocouples. The ^{235}U enrichment (9.5%) for the four PBF rods was higher than that for the LOFT rods (4%) to obtain the desired peak linear heating rate in the PBF. The fuel rod designations for each test, and fuel and cladding thermocouple locations for each rod are listed in Table 3. The nominal dimensional characteristics for the fuel rods are summarized in Table 4.

Circular flow shrouds were used in the LLR tests to encase each fuel rod. Thus, a typical LOFT bundle configuration was not modeled; however, the flow area of the flow shroud was relatively close to the LOFT stipulated flow area. The orientation of the fuel rods within the IPT is shown in Figure 2 (the rod numbers shown are for Test LLR-3 only). In Test LLR-3 two of the rods (Rods 312-3 and 312-4) were encased in stainless steel shrouds, whereas the other two rods (Rods 312-1 and 312-2) were encased in zircaloy-4 flow shrouds to obtain a power tilt of 0.87 to 1.0, which represents the ratio of power between the LOFT peripheral and central rods. Zircaloy shrouds were used for all four fuel rods for the subsequent tests.

TABLE 3. FUEL ROD DESIGNATIONS AND CLADDING SURFACE THERMOCOUPLE LOCATIONS FOR PBF/LLR TESTS

Rod	LLR Tests	Shroud	Thermocouple Location[a] (m) 180° Cladding Thermocouple	0° Cladding Thermocouple	Centerline Thermocouple	b
312-1	3,4,5	Zircaloy	0.533	0.533	0.533	yes
312-2	3,4,5,4A	Zircaloy	0.533	0.457	0.457	no
312-3	3	Stainless steel	0.533	0.533	0.533	yes
312-4	3	Stainless steel	0.533	0.533	0.533	no
345-1	4,5,4A	Zircaloy	0.533	0.533	0.533	yes
345-2	4,5,4A	Zircaloy	--	--	0.457	no
399-2	4A	Zircaloy	0.457	0.314	0.457	yes

a. From bottom of active fuel. All rods were unpressurized (0.1034 MPa).

b. Instrumented with three bulk coolant thermocouples and three flow shroud thermocouples at fuel midplane and 120 mm above and below the midplane.

TABLE 4. PBF/LLR TEST FUEL ROD DESIGN CHARACTERISTICS

Characteristics	Nominal Value
Fuel	
Material	UO_2
Pellet outside diameter	0.9294 ± 0.00127 cm
Pellet length	1.524 ± 0.0635 cm
Pellet enrichment	9.5 ± 0.5 wt%
Density	93.0 ± 1.5% theoretical density (nondensifying)
Fuel stack length	0.9144 m
End configuration	Dished
Burnup	0 MWd/t
Centerhole diameter	0.185 cm
Insulator Pellet	
Material	Al_2O_3 (99% pure, ASTM D2442)
Length	0.508 ± 0.0254 cm
Diameter	0.889 ± 0.005 cm
Cladding	
Material	Zircaloy-4
Tube outside diameter	1.07 ± 0.0038 cm
Tube inside diameter	0.948 ± 0.0038 cm
Thickness	0.061 cm (nominal)
Overall length	99.06 cm
Fuel Rod	
Plenum void volume	2.95 cm^3
Fill gas	He
Fill gas purity	94.9% He, 5% Ar, 0.1% impurities
Initial gas pressure	0.1034 MPa
Diametral gap	0.0191 cm
Overall length	99.8601 cm

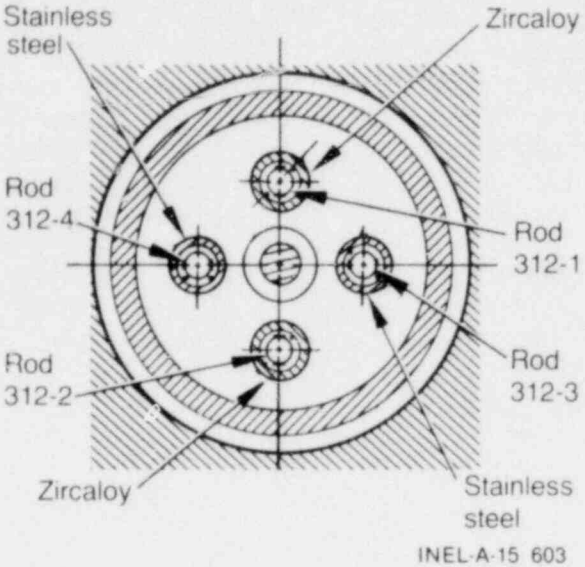

Figure 2. Test train orientation for LLR tests.

The instrumentation associated with each fuel rod consisted of one strain gage type pressure transducer to measure fuel rod plenum pressure; two LOFT-type cladding surface thermocouples laser welded (LOFT technique) to the cladding (except Rod 345-2, which was not instrumented with cladding thermocouples to provide a comparison to study the effects of external thermocouples); one centerline thermocouple; one plenum temperature thermocouple, which was unshielded from thermal radiation; and one linear variable differential transformer (LVDT) to measure the fuel rod axial elongation.

The instrumentation associated with each fuel rod flow shroud consisted of two turbine flowmeters located at the shroud inlet and exit to measure the coolant volumetric flow, thermocouples mounted in the coolant flow stream to measure coolant bulk temperature at the flow shroud inlet and exit, coolant thermocouples in selected shrouds at three locations along the fuel rod to measure the axial coolant temperature distribution, differential thermocouples to measure the coolant temperature increase from inlet to exit, three thermocouples mounted on the shroud outside surface to measure the axial temperature distribution for selected shrouds, and aluminum-cobalt alloy flux wires located on the outside of each shroud to give the time integrated axial power distribution in the rod.

Top hat orifices were mounted on the fuel rod side of each of the turbine meters at the inlet and exit of each shroud. These orifices were designed to increase the steady state pressure drop across the flow shrouds during blowdown.

2.1.2 Test Train. An illustration of the LLR test train is shown in Figure 3. The test train was

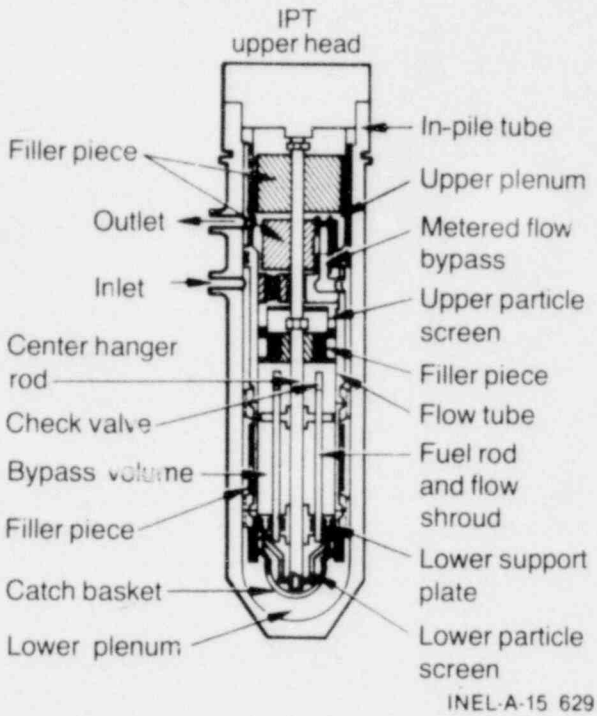

Figure 3. Test train assembly for LLR tests.

designed to support the four fuel rods symmetrically about the central axis of the IPT. The center hanger rod provided the principal structural support and the flow path for the reflood water. The fuel trains were primarily supported by the lower support plate and were positioned at the top by a spider. A particle screen was mounted in the lower and upper plenums of the test train to contain fuel particles in the event of a fuel rod failure. Filler pieces were inserted in the IPT exit volume, the upper plenum, and the downcomer region to reduce the large volumes of water in the test train. Check valves were located at the exit of each fuel rod flow shroud to prevent atypical coolant fallback from the upper plenum during the blowdown. A metered flow bypass path between the IPT inlet and the upper plenum was provided across the IPT flow tube to control the system thermal hydraulics during blowdown. The LLR test train included a direct injection, constant flow rate reflood capability to simulate the reflood portion of the LOFT transients.

During preblowdown steady state reactor operating conditions, the coolant enters the PBF IPT, where approximately 75% of the coolant flows upward through the metered bypass flow path from the IPT to the upper plenum. The remaining 25% of the coolant passes downward outside the IPT flow shroud to the vicinity of the catch basket. The coolant then enters each of the four test rod flow shrouds, passes each fuel rod, and exits through a tube to the common upper plenum region. The total IPT flow then passes through the upper particle screen where it mixes with the metered bypass flow and then exits through the outlet nozzle. The test train was designed to minimize coolant leakage between the IPT inlet and the upper plenum.

During transient blowdown conditions, the check valves located on top of each flow shroud close instantaneously with the differential pressure reversal from the lower to upper plenum. The pressure differential forces the fuel rod coolant to reverse direction and pass downward to the lower plenum and up the downcomer. All of the coolant above the lower support plate passes through the metered bypass flow path to the downcomer, where it mixes with coolant from the lower plenum and flow shrouds. The coolant then flows out the inlet nozzle, in transit to the blowdown tank.

Instrumentation for measurement of coolant parameters in the IPT included three thermocouples located in the IPT upper plenum region to measure bulk coolant temperature, one thermocouple located in the coolant volumetric bypass volume at the midplane of the active fuel length, two coolant thermocouples located in the lower plenum to measure bulk coolant temperature, one pressure transducer to measure IPT overpressure in the catch basket, two pressure transducers to measure system pressure in the upper plenum, one pressure transducer to measure the system pressure in the lower plenum, seven neutron detectors spaced along the length of the active core region to measure neutron flux and determine the axial flux profile, three gamma detectors to measure the gamma flux located at core centerline, six liquid level detectors (two below the lower support plate, and one in each flow shroud below the rod) to measure water level, and a turbine flowmeter located in the metered bypass piping to measure volumetric flow.

2.1.3 PBF-LOCA Test System. The PBF-LOCA test system, illustrated in Figure 4, includes the PBF IPT (discussed in the previous two subsections), the loop coolant system, the blowdown system, the reflood system, and the quench system. The loop coolant system provided steady state cooling of the test fuel rods during preblowdown operation. The two high speed isolation valves provided the means of isolating the loop coolant system from the rest of the PBF-LOCA test system. Isolation was necessary for protection of the loop coolant system, which was not designed to withstand blowdown conditions. After isolation, the loop continued to operate through the high speed bypass valve.

The blowdown system includes the high speed blowdown valves, nozzles, header, blowdown tank, and related piping. Coolant conditions prior to blowdown were measured in the initial conditions instrument spool, and during and following blowdown in the hot and cold leg instrument spools. A small line connected the hot and cold blowdown piping legs with a controllable valve (warmup line and valve). This line provided a small flow rate to keep the two legs at a constant temperature prior to blowdown. The blowdown header and tank collected and contained the coolant ejected from the IPT and piping during blowdown, reflood, and quench.

The quench system provided the coolant for posttest cooling of the test fuel rods. Quenching was accomplished by opening the quench valve and closing the cold leg blowdown isolation valve to permit coolant from the quench tank (pressurized by a nitrogen gas system) to enter the IPT. After the quench tank was emptied (in about 60 s), coolant was pumped from the storage tank for up to four hours to provide long-term cooling.

Instrumentation for the measurement spools included a resistance temperature detector (RTD) to measure the preblowdown temperature of the coolant; an exposed ribbon thermocouple to measure the coolant temperature during the transient; a flush-mounted pressure transducer to measure the preblowdown and subcooled decompression; a water cooled, stand-off mounted pressure transducer to measure the preblowdown and saturated decompression; a full flow turbine flowmeter to measure preblowdown coolant velocity to the IPT in the inlet condition spool and in the blowdown leg spools during the transient; a

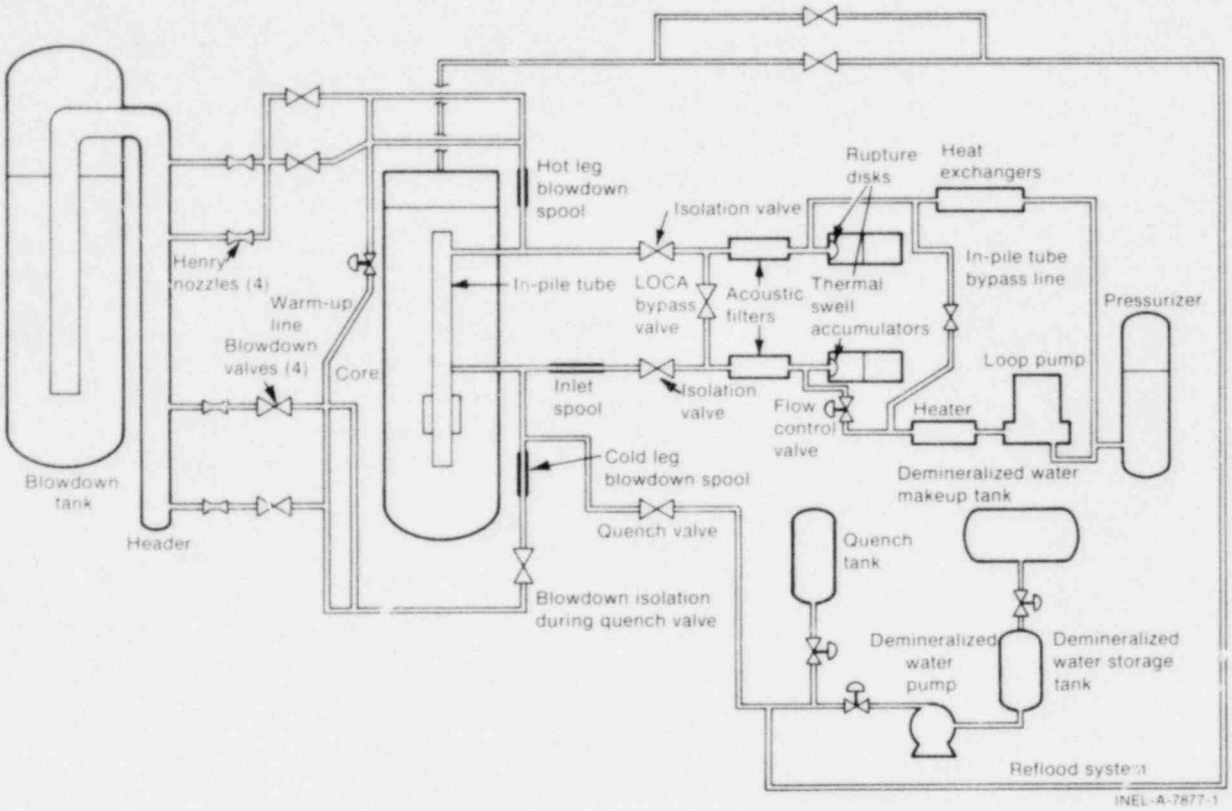

Figure 4. PBF-LOCA blowdown loop.

drag disk in the blowdown leg spools to measure the coolant momentum flux during the transient; a three-beam gamma densitometer on the blowdown leg spools to measure coolant density; and a pressure difference transducer to measure the preblowdown pressure difference across the test train and the blowdown leg spool-to-spool pressure difference during the transient. Each of the multibeam densitometers located in the cold and hot legs was used to measure coolant density along three chords through the piping and to determine the flow regime within the piping.

The instrumentation designation, location, range, response time, and signal conditioning are detailed in Reference 4.

2.2 Experiment Conduct

The LLR Test Program consisted of four separate blowdowns from nuclear power operation. The order of the tests (Tests LLR-3, -5, -4, and -4A) was chosen to match the LOFT schedule for the L2 Power Ascension Test Series. The sequence of events during the LLR tests is as follows. Initially, the loop coolant system provided coolant to the IPT at typical LOFT flow, temperature, and pressure conditions. The transient portion of the experiment began with the opening of the loop bypass valve, and then isolation of the loop coolant system from the IPT. Next, blowdown was initiated by opening the two high speed blowdown valves in the cold leg. Converging-diverging nozzles with cylindrical throat diameters equal to their length formed the break plane during blowdown. The IPT depressurized in approximately 35 s. The following subsections describe the preblowdown operation, pretest conditions, and the blowdown operation.

2.2.1 Preblowdown System Operation. The preblowdown operation consisted of a nonnuclear heatup phase to bring the system pressure and temperature to near test conditions. The reactor was then brought to criticality and stabilized at low power to achieve the desired temperature and pressure. During this period, the measurement transducers were evaluated and problems corrected to qualify them prior to blowdown.

Tests were also conducted to quantify flow leakage between the IPT and upper plenum. The

blowdown system warmup line valve was closed to stop coolant bypass flow external to the IPT primary coolant loop. The total measured coolant flow rate entering the IPT was then compared with the sum of the coolant flow rate passing through the four fuel rod shrouds. The approximate leakage during the LLR tests was less than 7% of the total shroud flow. Potential primary leakage locations included the test assembly lower support plate, a labyrinth seal at the top of the IPT between the IPT and flow shroud, and two zircaloy-to-stainless-steel joints in the flow shroud.

Steady state test conduct was initiated with the preconditioning phase for each test, which consisted of (a) several power ramps from low powers to successively higher powers to provide data for calibration of the test rods with the PBF core power by means of an energy balance on the coolant flowing through the fuel rod flow shrouds, and (b) steady state operation (for 2 h) at a peak linear power consistent with the LOFT counterpart test to provide approximately 80% of the maximum decay heat buildup for an infinite reactor time. This decay heat buildup initiated fuel pellet cracking and restructuring and allowed the pellet-cladding mechanical interaction to stabilize. After power calibration and decay heat buildup, fuel rod power and coolant conditions were adjusted to the desired initial values for the tests. The measured initial conditions for the LLR tests prior to blowdown are shown in Table 5.

Details of the power calibration procedure and results, and the power histories for the four tests are presented in Appendix B.

2.2.2 Transient System Operation. Transient test operation was initiated with isolation of the IPT and experimental hardware from the PBF primary coolant system, and a simultaneous system blowdown. Blowdown commenced with the opening of the two high speed (~100 ms) cold leg blowdown valves, shown in Figure 1, to simulate a 200% double-ended cold leg break LOCA. Approximately 3.75 s after initiation of blowdown, the large cold leg blowdown valve was closed until 22 s, at which time it was reopened. This valve sequencing was necessary to match the LOFT L2 Test Series predicted depressurization rates. Valve operation was controlled by a time sequential programmer. The break planes were formed by converging-diverging nozzles, with a cylindrial throat section having equal length and diameter. The throats were sized to control the blowdown flow and depressurization rates. The coolant ejected from the IPT was collected in the system blowdown tank. Reflood was performed by injecting coolant from a quench tank directly into the IPT. After reflood, additional posttest quench cooling was provided to completely flood the fuel rods and terminate the test.

Fuel rod maximum cladding temperatures were increased by continued reactor operation after initiation of blowdown. Approximately 1-s of fission heat is estimated to provide up to 10% of the initial steady state stored energy in the fuel rods. Table 5 presents the time after blowdown at which the PBF reactor was scrammed for each test. The PBF reactor power was essentially maintained at the steady state power level for these time periods after initiation of blowdown.

TABLE 5. MEASURED INITIAL CONDITIONS FOR THE LLR TESTS PRIOR TO BLOWDOWN

Test	Maximum Rod Power (kW/m)	System Pressure (MPa)	Inlet Temperature (K)	Average Shroud Differential Temperature (K)	Shroud Flow (L/s)	Fission Heat Period[a] (s)
LLR-3	41	15.6	595	11.1	0.58	0
LLR-5	47	15.5	598	10.5	0.60	2.0
LLR-4	57	15.6	600	10.1	0.80	2.6
LLR-4A	56	15.5	600	11.5	0.78	2.85

a. Fission heat period refers to the time following initiation of blowdown that the PBF core power was maintained in an effort to provide higher cladding temperatures during blowdown.

3. SYSTEM THERMAL-HYDRAULIC RESPONSE DURING BLOWDOWN

The LLR system thermal-hydraulics were influenced by thecore heat transfer, neutronics, and system component interactions. Since thermal-hydraulic measurements within the flow shrouds were not sufficiently detailed to permit direct determination of the fuel rod boundary conditions, the RELAP4/MOD6 code was used to confirm the expected system thermal-hydraulic behavior and calculate the coolant behavior in each fuel rod flow shroud. The variables that affect system response and, thus, fuel rod behavior, include coolant pressure, density, temperature, and flow. The system pressure, in conjunction with the fuel rod internal pressure and cladding temperature, govern fuel rod cladding deformation. The pressure distribution within the system provides the driving potential for coolant flow through the fuel rod flow shrouds. The coolant temperature and density define the fluid state of the mass flow leaving the system. The system break flow rate, and hence the fuel rod shroud mass flow rate, directly influence the cladding surface heat flux, the cladding temperature, the system depressurization, and the coolant mass ejection.

In the following sections the coolant break flow rate, system depressurization, fuel rod shroud volumetric flow rate, coolant temperature, and coolant density are evaluated and discussed. The data are also compared with pretest and posttest calculations performed with RELAP4.

RELAP4 is a code that can predict the transient behavior of water cooled nuclear reactors (or simulators) subjected to postulated accident conditions, such as those resulting from a LOCA. It is a program that predicts the interrelated effects of coolant thermal-hydraulics, system heat transfer, and core neutronics. The code solves the governing conservation equations for mass, momentum, and energy using homogeneous flow theory and thermal-equilibrium conditions. Detailed descriptions of the RELAP4 nodalization and models are discussed in Appendix C. This calculational model of the PBF blowdown loop configuration was achieved using a special version of RELAP4/MOD6/UPDATE4.[a] A description of this special version is also provided in Appendix C.

a. RELAP4/MOD6, Update 4, Version III. Idaho National Engineering Laboratory Configuration Control Number H00441IB.

The coolant thermal-hydraulic behavior during the blowdown of each of the PBF/LLR tests was similar. For this reason, only the results from Test LLR-5 are described in this report as being typical of the thermal-hydraulics observed during all the tests. Measurement accuracy and resolution of the data are not sufficient to distinguish minor differences from test to test.

3.1 System Depressurization

During a large cold leg break LOCE at LOFT, the loss of coolant rapidly depressurizes the system, the core coolant reverses flow direction, and the core eventually experiences a critical heat flux (CHF), resulting in a rapid increase in fuel rod cladding temperatures.

Several modifications to the PBF-LOCA system and the typical PBF-LOCA test train were required for the LLR experiments. These modifications included (a) installation of different sized converging/diverging blowdown nozzles and selective blowdown valve sequencing in the system to define the system depressurization, (b) check valves located at the outlet of the fuel rod flow shrouds to prevent coolant flow from the upper plenum during blowdown, and (c) an inlet metered flow bypass from the downcomer to the upper plenum to control the system hydraulic response.

Depressurization of the IPT during the LLR tests was influenced primarily by the system coolant temperature distribution and the metered bypass flow rate. The pressure distribution within the IPT from the upper to lower plenum during the LLR tests varied from that witnessed in earlier Loss-of-Coolant Test LOC-11 blowdowns.[7] The following discussion encompasses an evaluation of the system depressurization in the hot and cold leg measurement spools, the upper and lower plenums, and the volumetric bypass.

Figure 5 illustrates the measured and calculated system depressurization obtained with the flush-mounted pressure transducer in the cold leg spool piece during Test LLR-5. The RELAP4 prediction also represents the LOFT required depressurization for this test. As shown in the figure, good agreement was obtained between the LLR data and the LOFT required depressurization.

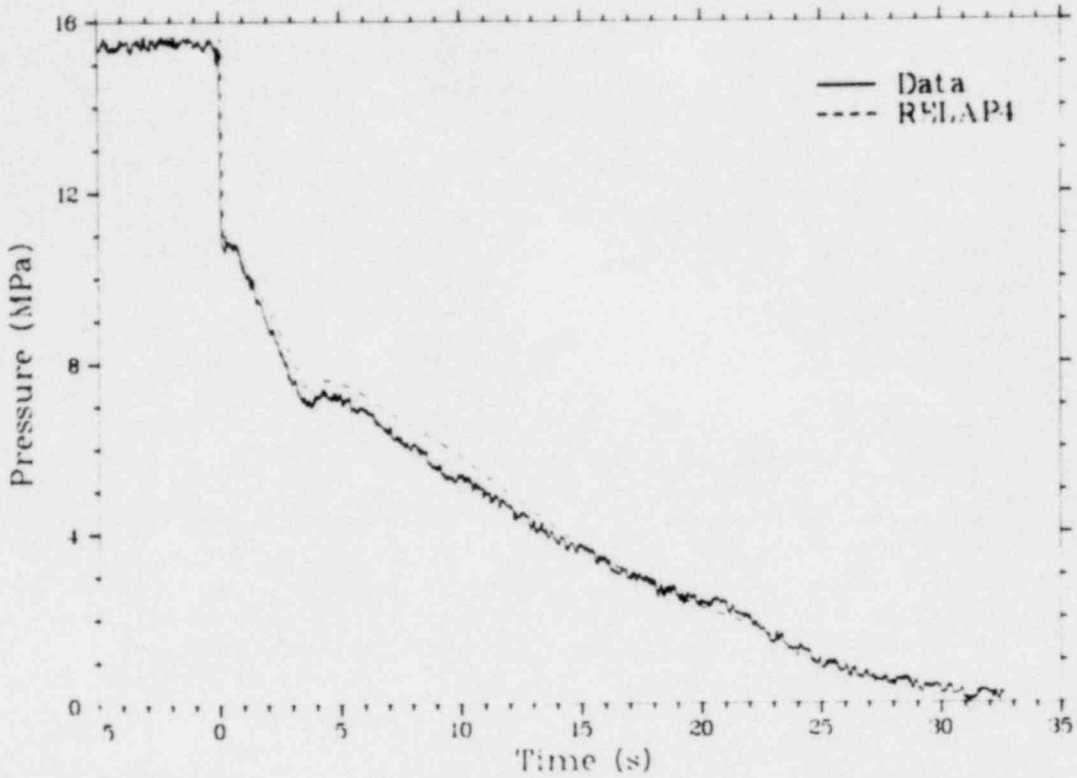

Figure 5. Comparison of calculated and measured system depressurization in the cold leg blowdown spool during Test LLR-5.

A steady state pressure of approximately 15.5 MPa was achieved prior to the LLR-5 blowdown. With the initiation of the transient, pressure waves propagated through the system at sonic velocities, and the system depressurized until the saturation pressure of the coolant was reached. The coolant pressure decreased rapidly during this subcooled depressurization from the initial value to a saturation pressure of 10.7 MPa, which corresponded to a system saturation temperature of 589 K. (The LOFT required inlet coolant temperature for Test LLR-5 was 595 K.) The lower system saturation temperature (589 K) resulted because of difficulties in keeping the isolated piping to the hot and cold leg blowdown valves at system temperature. Prior to blowdown, a warmup line was opened to elevate the water temperature in these lines from approximately 530 to 595 K, but once the warmup line was closed to conduct the transient, the temperatures in the dead legs decreased approximately 2 K per minute due to radiation and free convection heat losses to the ambient atmosphere. The IPT inlet temperature was maintained at 600 K prior to the test in an attempt to offset this occurrence. In spite of this facility problem, the subcooled and saturated portions of the blowdown matched the LOFT desired trends extremely well.

With the onset of the blowdown, the coolant at the highest system temperature (in the shrouds and at the shroud outlet) flashed. Since the volume of water involved was minimal, the volume of steam produced was not sufficient to bring the total system to saturation conditions and, thus, the subcooled depressurization was momentarily retarded and this continued until the lower plenum flashed and again was momentarily retarded. This cascade effect continued for 50 ms, until the system coolant generated enough vapor to attain saturation conditions and the system pressure had dropped to the level of the coolant vapor pressure. The sonic velocity was drastically reduced at this point, the pressure waves propagating through the system were damped out, and choking at the break point occurred. After this initial decrease to saturation conditions, the data show the depressurization to be slightly lower than the LOFT required depressurization (as calculated by RELAP4 pretest calculations) for the majority of the saturated blowdown. The slight increase in measured system pressure at 3.75 s is attributed to the closing of the large cold leg blowdown valve. The code calculations follow this trend closely. From this point, the data indicate a less rapid depressurization than the code calculations until 22 s, at which time the measured and calculated

results coincide. This difference is attributed to the difference in the calculation of the break flow rate. The effect of reopening the large cold leg blowdown valve is evidenced at 22 s as the slope of the depressurization data increases for the remainder of the transient. The changes in system pressure during the opening and closing of the large cold leg blowdown valve correspond closely to the observed spikes in break mass flow rate data discussed in Section 3.4.

Figure 6 presents a comparison of the predicted (pretest) and measured pressure differential between the cold and hot leg blowdown spools (which is representative of the differential between the IPT lower and upper plenums). At steady state, the cold leg spool pressure was approximately 0.18 MPa higher than the hot leg spool pressure. When blowdown was initiated, the pressure differential was reversed, resulting in a 0.55-MPa differential from the upper plenum to the lower plenum. This pressure differential caused the check valves on the top of each flow shroud to rapidly close, resulting in coolant voiding and a saturated steam environment around each fuel rod. At 3.75 s into the transient, the large cold leg blowdown valve was closed, resulting in a decrease in the pressure differential to 0.05 MPa, at which value it remained until 22 s. At this time, the large cold leg blowdown valve was reopened, causing the pronounced increase in the pressure differential. The comparison between the RELAP4 pretest calculations and the experimental data shows good agreement.

Figure 7 illustrates the measured pressures at four different locations in the PBF IPT and blowdown loop. The pressure response in the cold leg spool piece, the lower plenum, the upper plenum, and the hot leg spool piece differ significantly during the first 10 s of the transient due to the constricted flow paths in the IPT. Since the only flow path for the rod coolant during the transient is out the cold leg, the fuel rods are subjected to the pressure environment in the lower plenum throughout the blowdown. The metered bypass region is the only major flow path in the IPT for the coolant around and above the flow shrouds and in the hot leg piping to leave the IPT. The depressurization in these regions would therefore be expected to be retarded due to the high resistance flow path through the bypass.

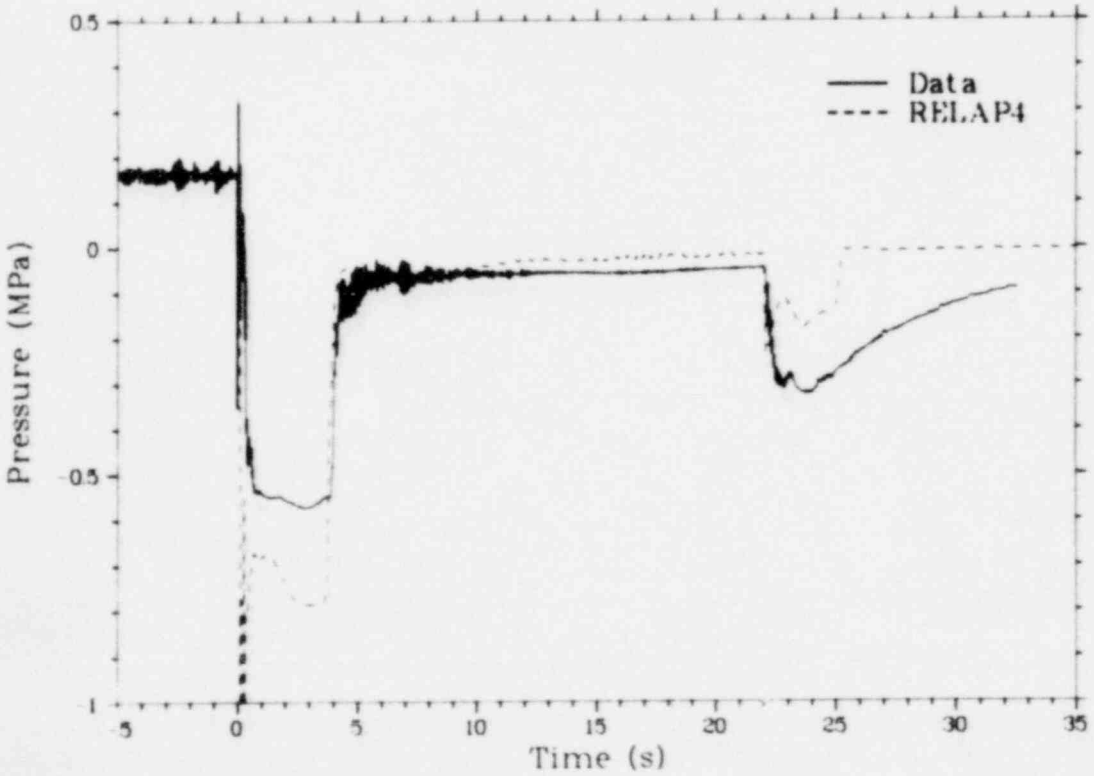

Figure 6. Comparison of calculated and measured pressure differential between cold and hot legs during Test LLR-5.

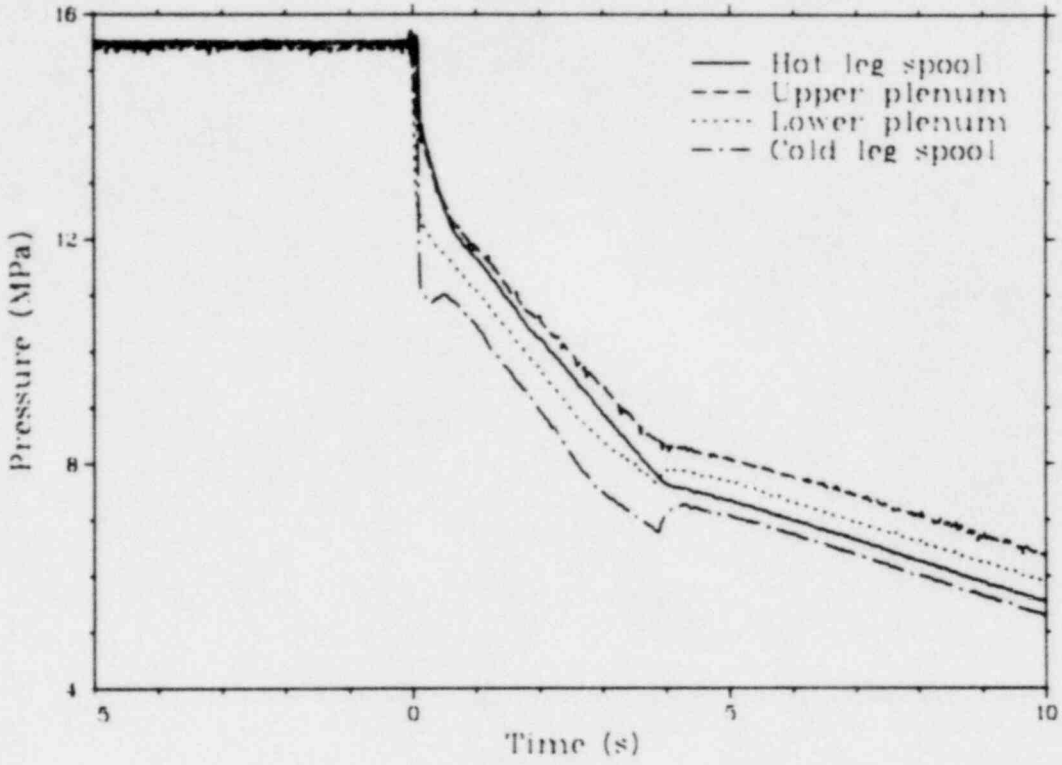

Figure 7. Coolant pressures within the IPT during Test LLR-5.

3.2 System Coolant Temperatures

With the initiation of the blowdown transient, the system subcooled depressurization reduced the coolant temperature at the various locations in the IPT and piping legs to saturation conditions. The local qualities continued to rise throughout the two-phase portion of the blowdown until superheated conditions (quality = 1) existed at some of the locations in the system. The degree of superheat at these locations was determined by the energy transfer from the relatively massive IPT structure and piping due to thermal radiation and convective heat transfer. Measurement of the actual coolant temperature in this superheated single-phase gas situation is complicated by the effects of thermal radiation from surrounding surfaces on the thermocouple. The subsequent paragraphs discuss the coolant temperature response within the system spool pieces and IPT at several locations.

Figure 8 shows a comparison between the pretest RELAP4 calculation and the coolant temperature measurement in the cold leg spool piece during Test LLR-5. The fluid temperature gradually decreases as the system pressure presented in Figure 5 decreases, following saturation until 22 s. The RELAP4 predictions are in reasonable agreement with the measurement during this period of time, slightly overpredicting the data for the first 17 s. At 23.5 s, the data indicate a superheated environment in the spool piece. Calculations of the fluid state (Section 3.3) based on the density (Figure 12) in the spool piece and coolant temperature indicate that qualities during the time period from 20 to 30 s range from approximately 0.3 to 0.8. Therefore, this superheat spike is attributed to the influence of radiation on the thermocouple, and a two-phase mixture is postulated to have existed for up to 30 s in the transient. The RELAP4 predictions for this time also indicated a two-phase mixture would exist.

Figure 9 illustrates the coolant temperatures in the hot leg, cold leg, and initial conditions spool pieces. As shown, the three measurements follow the same trends for the first 23 s of the transient. The fact that the hot leg and initial conditions thermocouples do not indicate any superheat for

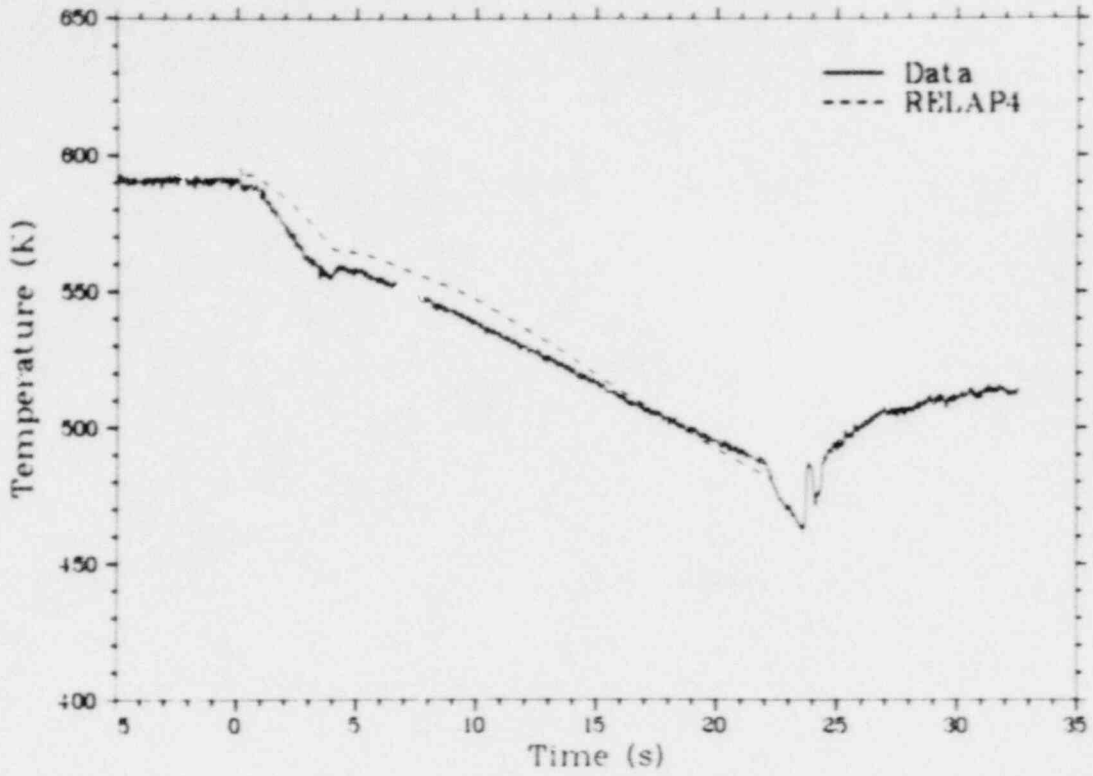

Figure 8. Comparison of calculated and measured coolant temperature in the cold leg blowdown spool during Test LLR-5.

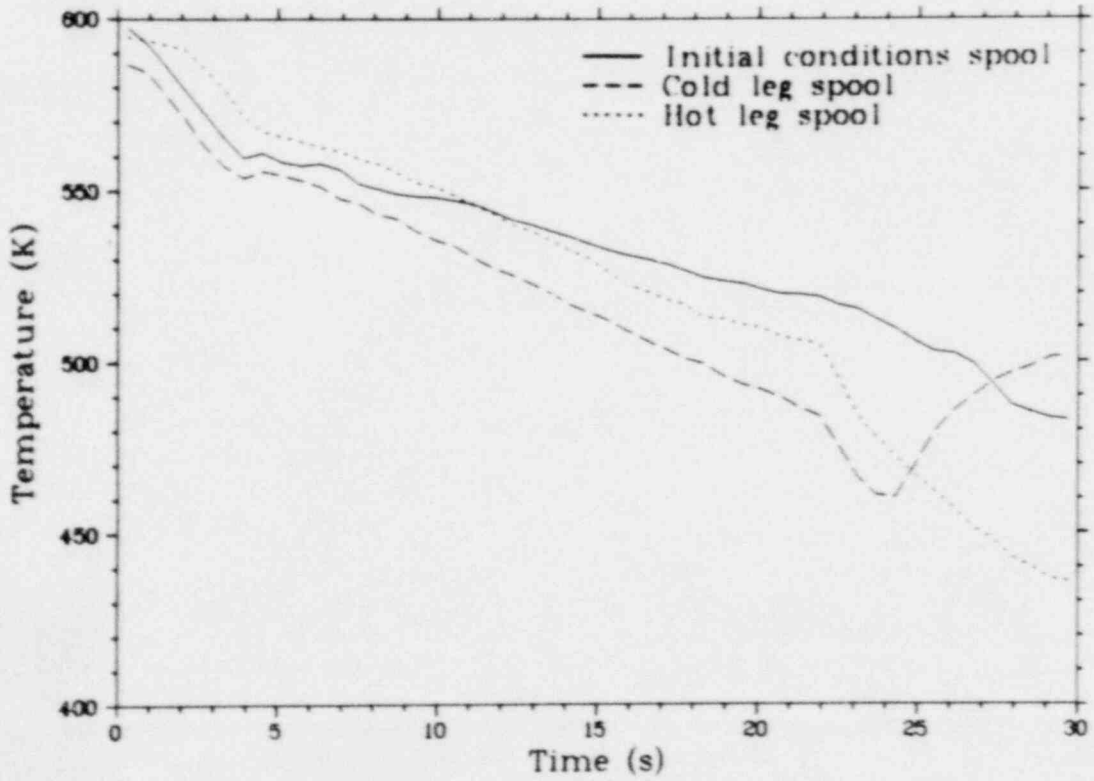

Figure 9. Coolant temperature measurements in the spool pieces during Test LLR-5.

the first 30 s of the transient, further indicates that the superheat spike recorded in the cold leg spool at 23 s is an instrument anomaly.

Figure 10 presents the coolant temperature at five different locations in the PBF system. The measurements in the lower plenum (catch basket), in the volumetric bypass at the fuel rod midplane, above the shroud outlet, at the IPT outlet nozzle, and at the metered bypass inlet are compared with pretest RELAP4 calculations in the lower and upper plenum. The thermocouples all follow the same saturation line decrease from the initial steady state values, following the local pressures for most of the blowdown transient. The changes in slope at 3.75 and 22 s in all the curves is attributed to the sequencing of the large cold leg blowdown valve. The coolant temperature in the lower portion of the lower plenum follows a saturation line decrease for the entire blowdown. During this interval, the calculations slightly overpredict the data. None of the thermocouples in the upper plenum indicated superheat until 18 s, at which time the thermocouple located at the IPT exit indicated some separation. This condition persisted for 5 s, and the measurement then followed a saturation line decrease for the remainder of the blowdown.

The calculations for coolant temperatures illustrated in Figure 11 in the upper plenum did not predict any superheating until 25.5 s. The measured coolant temperature at the IPT exit in the upper plenum indicated a significantly higher temperature than the RELAP4 calculations past 15 s of the transient.

3.3 System Coolant Density

The coolant density in the hot and cold leg spool pieces was measured with three-beam gamma densitometers during the PBF/LLR experiments. The cross-sectional average density is derived by assuming a flow regime somewhere between stratified and dispersed flow, and a linear density profile in the pipe through the upper and lower chordal densities. The gradient is then integrated over the cross-sectional area, and then combined with the result from the middle beam density. The density obtained from integrating the gradient was weighted by 2/3 and the center beam density was weighted by 1/3.

Figure 12 provides a comparison of the densities from the cold leg densitometer for the upper, lower, and center beams. The density does not

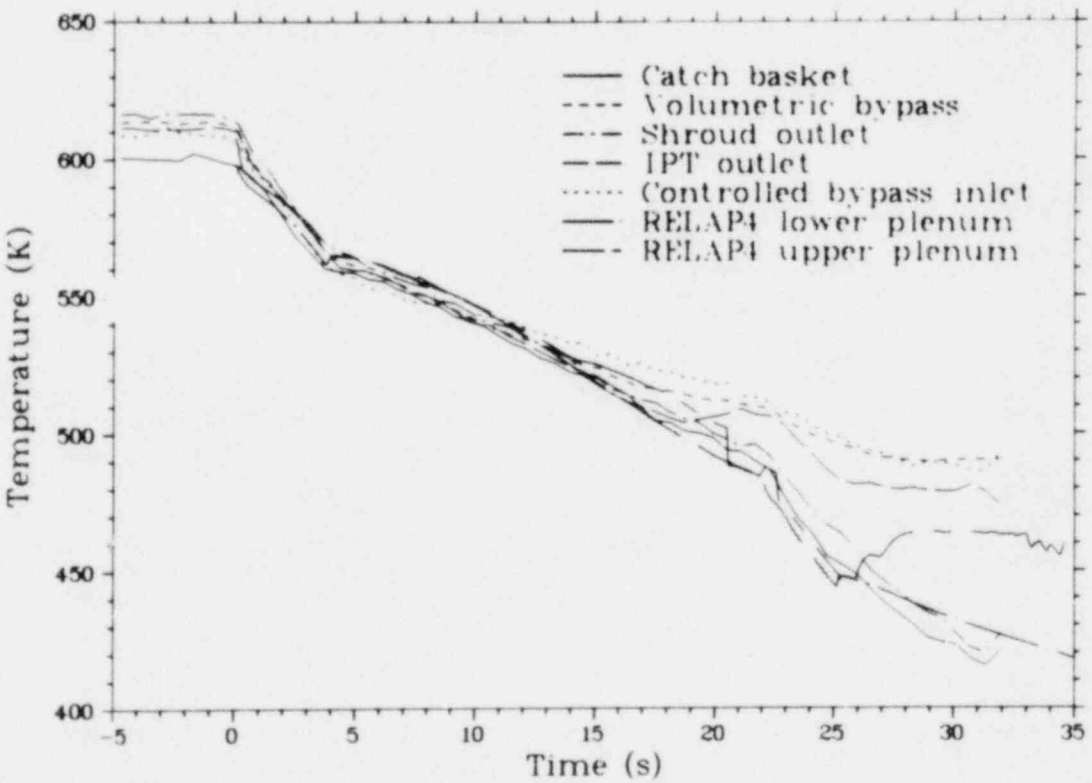

Figure 10. Coolant temperatures within the IPT during Test LLR-5.

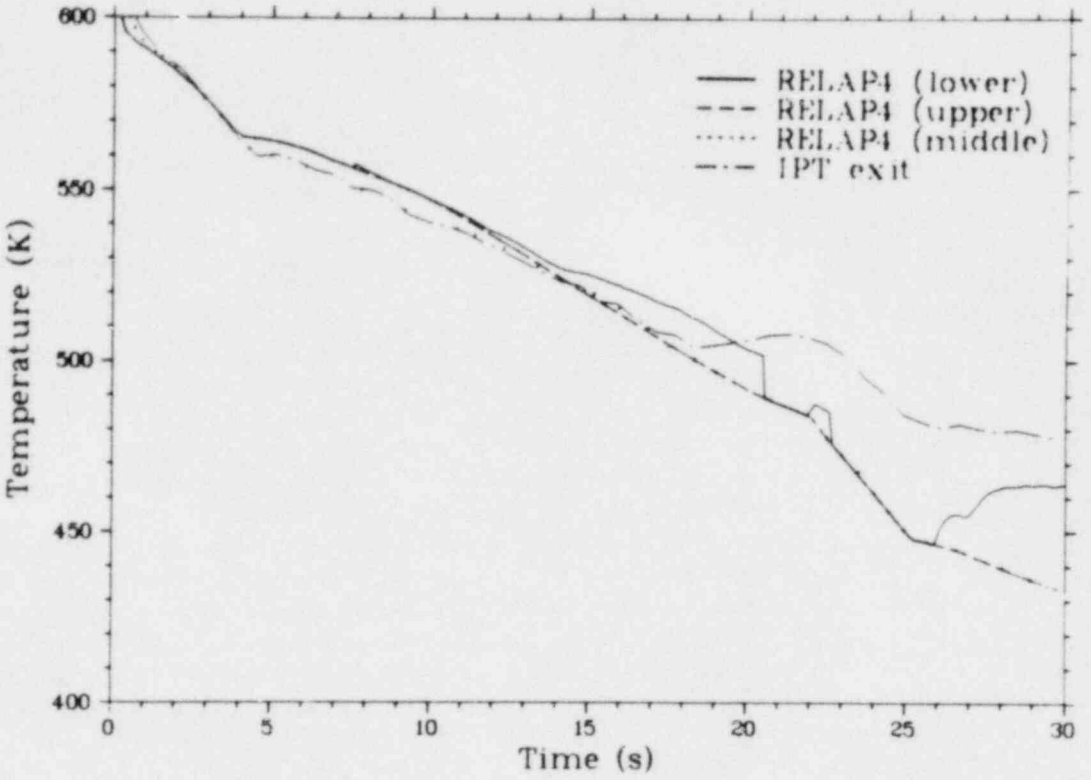

Figure 11. Comparison of calculated and measured coolant temperature in the upper plenum during Test LLR-5.

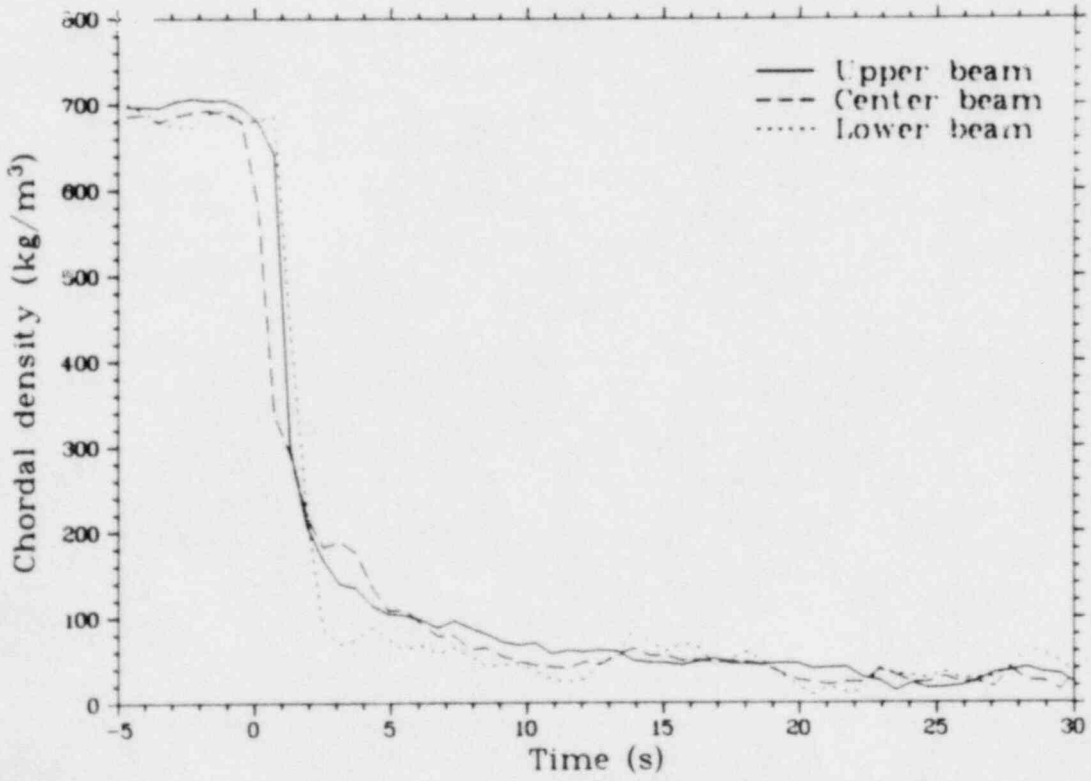

Figure 12. Comparison of measured density from three beams of the cold leg densitometer during Test LLR-5.

appear to be uniform across the pipe for the entire transient. The lower beam indicates a higher density than the other two beams during the first 1.25 s of the transient. After 6 s, the upper and lower beams evenly bracket the center beam density, which suggests a linear density gradient. However, the gradient is opposite that seen in Test LOC-11C,[7] in which the lower beam indicated the highest transient density of all three beams. Figure 13 presents the predicted (pretest) and average measured coolant density in the cold leg spool piece as a function of time. The experimental data compare well with the RELAP4 prediction. However, the average measured density is higher than the calculated density during the first second of the transient, and lower than the calculated density from about 2 to 4 s. The fact that the cold leg density remained constant for approximately the first second of the transient is attributed to measurement error, since the pressure and temperature measurements indicated saturation was achieved within 50 ms. Since the RELAP4 model of the IPT blowdown and primary coolant system piping is coarse and does not allow the temperature and pressure distribution to be modeled, the density from 2 to 4 s is significantly overpredicted, and past 12.5 s it is underpredicted.

There are several bends and one 90-degree elbow just upstream of the cold leg spool piece in the PBF cold leg piping. Centrifugal forces would, therefore, tend to separate the liquid and vapor phases during the LLR blowdowns, complicating the flow patterns. These flow patterns in the cold leg spool piece are important for two reasons. First, because of their influence on the spool instrumentation, and second, due to the concern regarding whether the RELAP4 code is predicting the correct flow conditions and, consequently, break flow rate for the system. The flow patterns observed in cocurrent two-phase flow in horizontal and inclined tubular channels are discussed in detail by Alves.[8] In general, the patterns are complicated by asymmetry of the phases resulting from the influence of gravity. However, Alves lists six generally accepted flow patterns: bubbly, plug, stratified, wavy, slug, and annular flow. Bubbly flow is characterized by the gas or vapor phase being distributed as discrete bubbles in the upper half of the pipe in a continuous liquid phase. In plug flow the vapor bubbles are approximately the diameter of the pipe, while the liquid flow is contained in liquid slugs. Stratified flow occurs only at very low liquid and vapor velocities. In this pattern the two phases flow separately, with a relatively smooth interface. Once the vapor

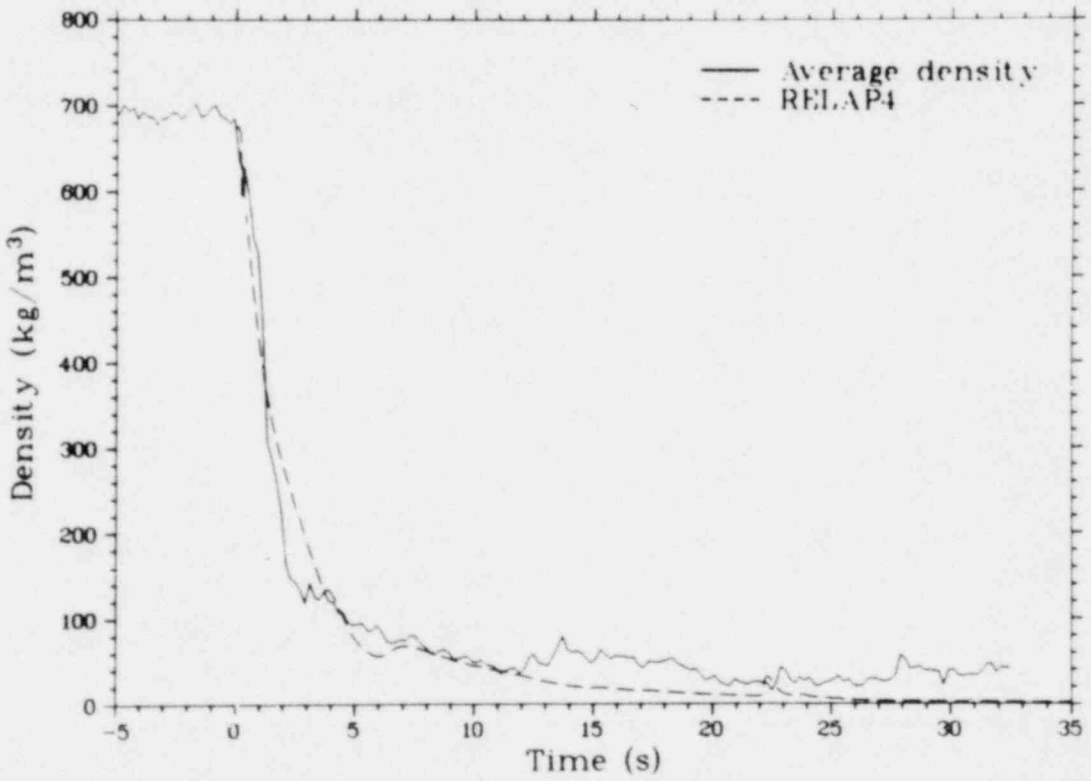

Figure 13. Comparison of average measured density versus calculated density in the cold leg spool piece during Test LLR-5.

velocity increases, the interface becomes disturbed by waves traveling in the direction of flow; hence, wavy flow. A further increase in vapor velocity causes the waves at the interface to be picked up to form a frothy slug pattern. Finally, a still higher vapor velocity results in annular flow and the formation of a gas core with a liquid film around the periphery of the pipe. Since the metal temperature of the PBF spool piece is initially in the vicinity of 600 K during blowdown, the presence of a heat flux from the wall alters the flow pattern from that which would have occurred in a long, unheated channel at the same local flow conditions due to departure from thermodynamic and hydrodynamic equilibrium. If this consideration is assumed negligible, Collier[9] suggests a method of representing the various transitions from flow pattern to flow pattern in the form of a flow pattern map. The respective patterns are represented as areas on a graph, the coordinates of which are the actual superficial phase velocities (j_f or j_g) or generalized parameters containing these velocities.

One flow pattern map, that of Baker[10], has become generally accepted and widely used for horizontal channels. Baker plotted the observations of various workers for a steam-water system in terms of the coordinates (G_g/λ) and (G_f/ψ), where G_g and G_f are the superficial mass velocities of the vapor and liquid phases given by

$$G_g = j_g \rho_g = GX \tag{1}$$

$$G_f = j_f \rho_f = G(1-X). \tag{2}$$

The factors λ and ψ are defined by

$$\lambda = \left[\left(\frac{\rho_g}{\rho_a}\right)\left(\frac{\rho_f}{\rho_w}\right)\right]^{1/2} \tag{3}$$

and

$$\psi = \frac{\sigma_w}{\sigma_f}\left[\left(\frac{\mu_f}{\mu_w}\right)\left(\frac{\rho_w}{\rho_f}\right)^2\right]^{1/3}. \tag{4}$$

Figure 14 shows the Baker flow pattern map for horizontal flow for steam-water. If the observed cold leg pressure, volumetric mass flow, and average density in the cold leg are evaluated with respect to this map at various time points during the blowdown transient, a flow pattern history can be constructed. Both vapor and liquid specific volume are derived by using state relationships. Quality is derived from Equation (5), and void fraction from Equation (6).

$$X = v - (v_f/v_{fg}) \tag{5}$$

$$\alpha = Xv_g/(v_f + Xv_{fg}) \tag{6}$$

Table 6 presents the derived quality and void fraction for the upper, lower, and middle beams of the gamma densitometer in the cold leg spool piece. These data indicate that the flow pattern in the cold leg is annular flow with a liquid film on the periphery of the pipe and a higher velocity gas core. Figure 15 presents the average derived quality from these calculations and compares it with pre- and posttest RELAP4 analyses. The RELAP4 calculations reasonably predict the data for the first 10 s, then predict significantly higher qualities for the remainder of the transient.

By using the average derived density, void fraction, and volumetric flow, the Baker flow pattern map can be constructed for the cold leg. As shown in Figure 14, the flow at 1 s is in the froth region (wispy-annular). Sometime between 1 and 2 s the flow pattern changes to a dispersed flow (misty type flow in which droplets are entrained in a steam environment). This flow pattern remains until approximately 16 s into the transient, at which time it changes to an annular type flow for the majority of the remainder of the blowdown transient, with one short transition to slug flow.

3.4 System Flow Rate

The flow leaving the PBF-LOCA blowdown system in transit to the blowdown tank during a LOCE is a difficult variable to calculate. The use of specially designed converging-diverging nozzles, with cylindrical throat sections of length equal to the diameters, optimized the capability to calculate break flow. In the RELAP4 model a combination of the Henry-Fauske (subcooled flow) and homogeneous equilibrium model (saturated flow) correlations for critical flow was used to describe the flow at the throats of the

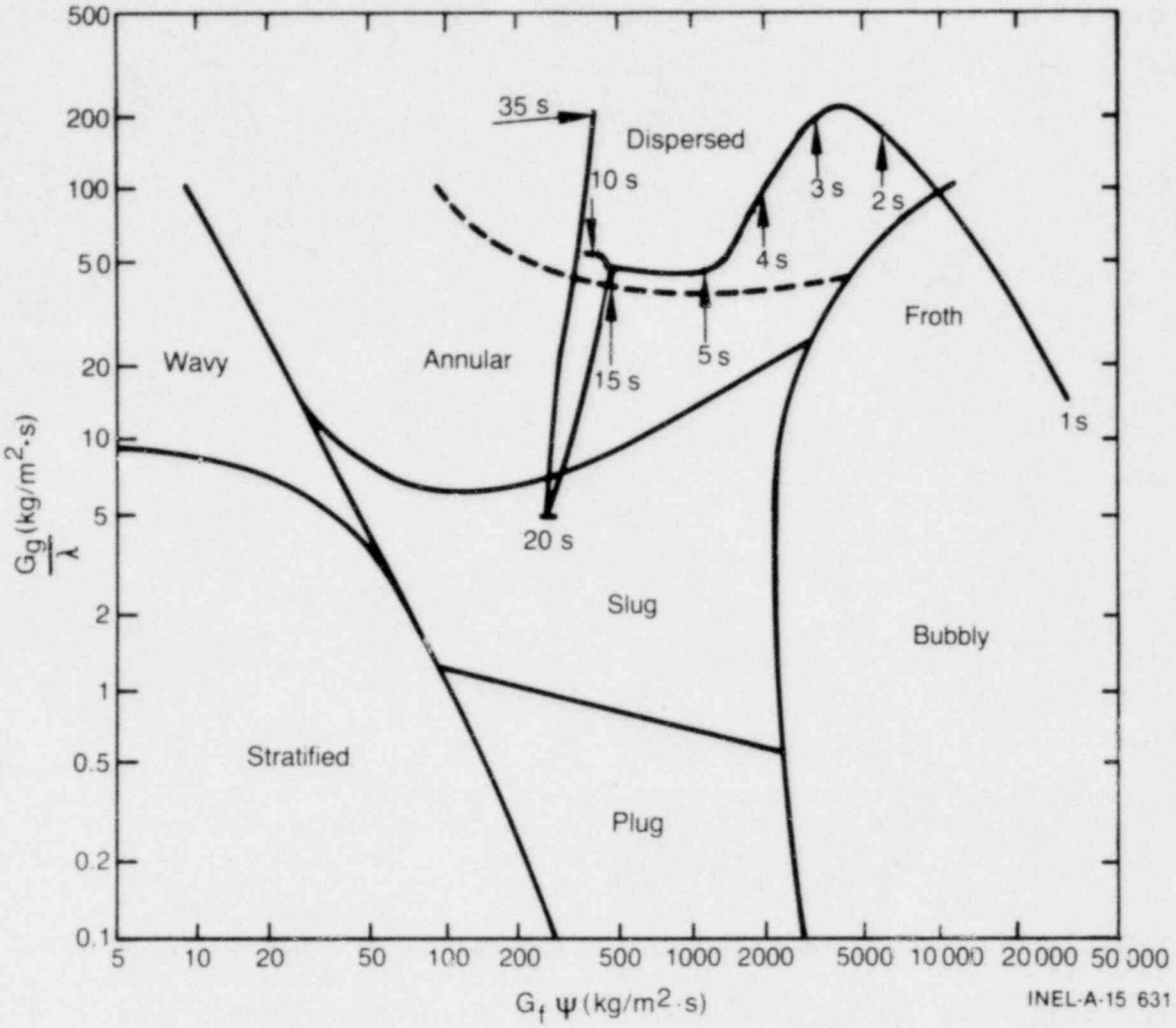

Figure 14. Baker flow pattern map for horizontal flow in the cold leg spool piece during Test LLR-5.

blowdown nozzles. Results of previous PBF-LOCA tests showed that a break flow multiplier[a] of 1.0 (RELAP4 default values) would provide the best agreement between the code calculations and the LLR data.

The mass flow rate in the cold and hot leg measurement spools was determined from the average coolant density and coolant volumetric flow rate obtained by combining information from the gamma densitometer and a turbine flowmeter. Because of the IPT differential pressure reversal, shown in Figure 6, the check valves on top of the flow shrouds shut instantaneously upon initiation of the blowdown and forced the two-phase coolant in the volumetric bypass region (above the lower support plate) into the upper plenum and out the metered bypass flow path in transit to the blowdown tank. Figure 16 presents the measured and predicted metered bypass volumetric flow rate. Approximately 33% of the total initial system fluid volume passes through the metered bypass during blowdown. As is evident, RELAP4 significantly underpredicted the volumetric flow rate through this flow path. This flow constitutes several flow sources, including the hot leg piping to the isolation valve, the hot leg blowdown piping, the upper plenum, and the volumetric bypass volume. An underprediction of the volumetric flow rate by such a margin may be due to an error in the fluid state calculated by RELAP4. To more closely model the relative water volumes in a PWR relative to the core region for the LLR test train, filler pieces

a. The multiplier is a constant selected to optimize comparison between the code calculation and the experimental data.

TABLE 6. COMPARISON OF DERIVED QUALITY AND VOID FRACTION FROM DENSITY IN COLD LEG SPOOL PIECE

Time (s)	X_{low}	α_{low}	X_{center}	α_{center}	X_{upper}	α_{upper}
1	0.01	0.13	0.16	0.69	0.06	0.41
2	0.27	0.84	0.18	0.77	0.20	0.79
3	0.40	0.93	0.19	0.82	0.19	0.82
4	0.36	0.93	0.19	0.84	0.21	0.86
5	0.49	0.95	0.26	0.88	0.27	0.88
6	0.48	0.95	0.31	0.91	0.29	0.90
7	0.50	0.96	0.36	0.93	0.31	0.91
8	0.50	0.96	0.40	0.95	0.31	0.92
9	0.54	0.97	0.50	0.96	0.31	0.92
10	0.54	0.97	0.56	0.98	0.29	0.93
15	0.23	0.94	0.33	0.96	0.29	0.95
20	0.39	0.98	0.48	0.93	0.23	0.94
30	0.40	0.97	0.82	1.00	0.32	0.96

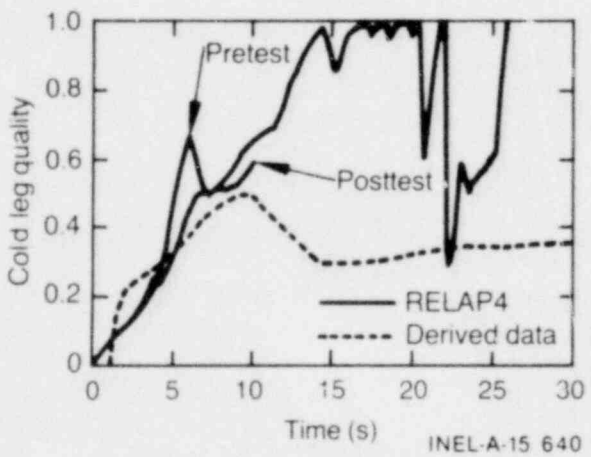

Figure 15. Comparison of analytical and derived quality during Test LLR-5.

were inserted in the IPT exit volume, the upper plenum, and the downcomer region. By adding this much mass to the upper plenum, the heat transfer in this region was further complicated, thus disallowing the code to predict the correct phase separation in the volumetric bypass and upper plenum volumes. A much higher quality water (lower density) existed in these two regions than was predicted in order for the code to underpredict the flow.

Figure 17 presents a comparison of the RELAP4 calculated hot leg volumetric flow rate with the data. The agreement between the prediction and data is reasonable, except for the initial measured flow spike.

The volumetric flow rate at the cold leg blowdown spool and the pretest RELAP4 calculation are shown in Figure 18. The initial flow spike to 60 L/s occurred when the cold leg blowdown valves, located between the measurement spool and the blowdown nozzles, were first opened. The turbine flowmeter in the cold leg spool was sized for only 50-L/s flow, and, with only a 120% overrange capability, readings above 60 L/s are questionable. A slug of fluid immediately filled the piping between the nozzle and the valve, and resulted in choked flow at the break plane, as the reduced pressure at the nozzle throat resulted in rapid steam formation. The piping downstream of the nozzles was initially pressurized to the blowdown tank pressure (0.14 MPa) and filled with air at ambient temperature (300 K). As the system pressure decreased to 4.8 MPa in 50 ms at the cold leg spool, the driving potential for flow out the break was reduced, resulting in a reduction in volumetric flow rate from 60 to 40 L/s within 0.5 s. The volumetric flow rate then increased to 60 L/s during the interval from 1.0 to 3.75 s. This is attributed to an increase in coolant quality from 0 to 0.28 during this time period, with a resultant decrease in density and increase in void fraction to approximately 0.85. The severe drop-off in flow

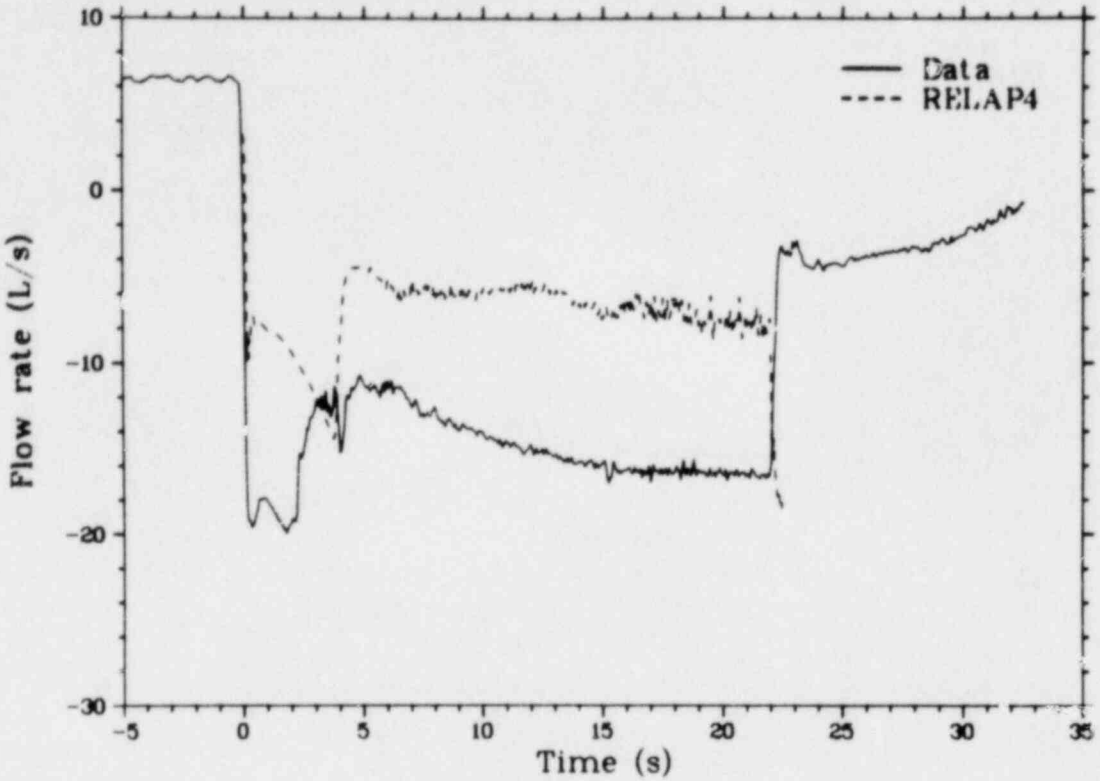

Figure 16. Comparison of calculated and measured volumetric flow in the metered bypass during Test LLR-5.

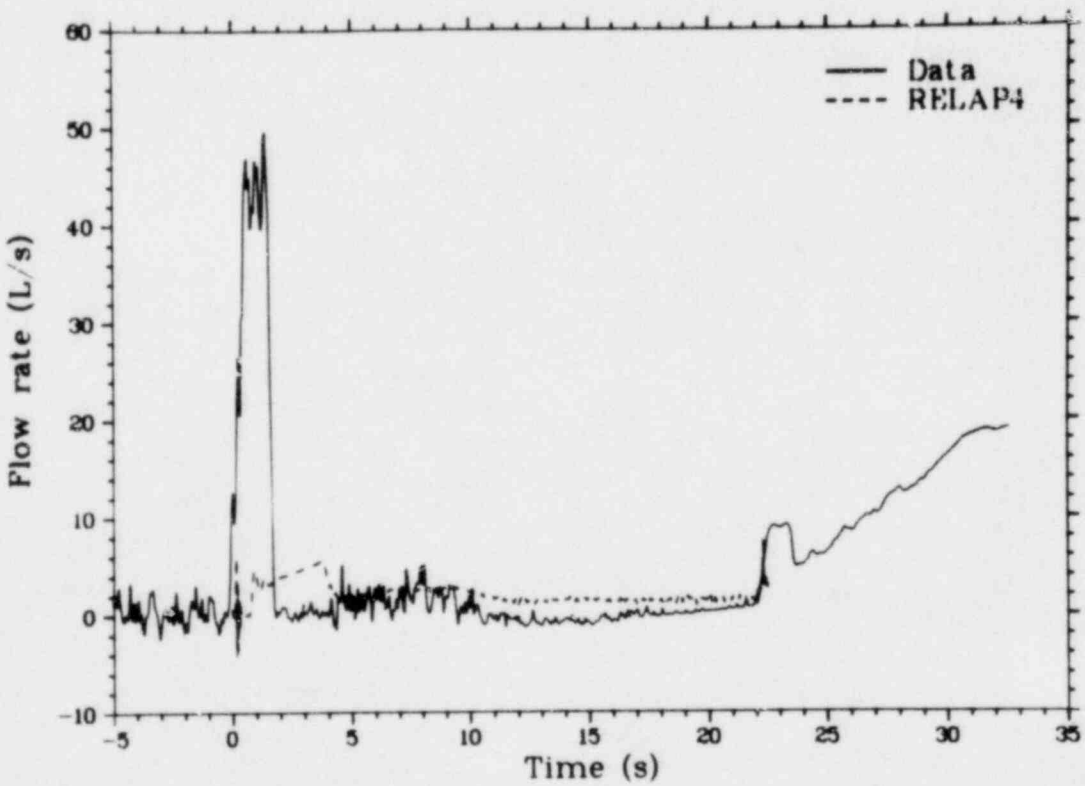

Figure 17. Comparison of calculated and measured volumetric flow in the hot leg blowdown spool during Test LLR-5.

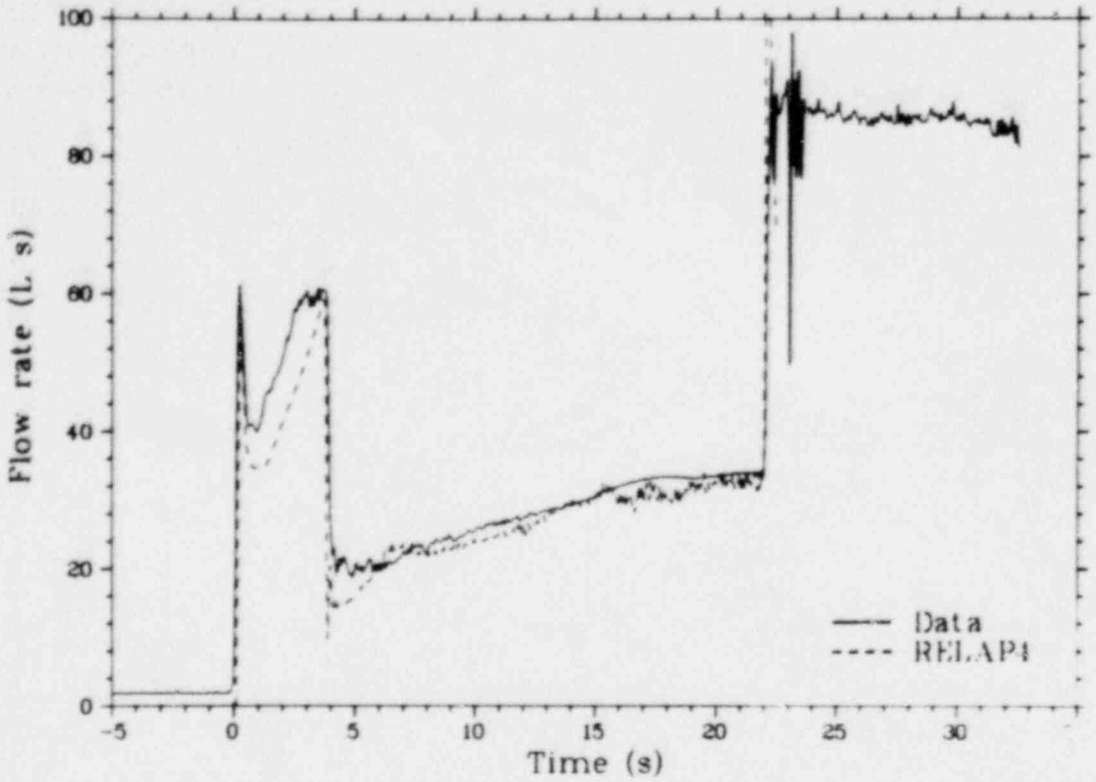

Figure 18. Comparison of calculated and measured volumetric flow in the cold leg blowdown spool during Test LLR-5.

rate at 3.75 s is attributed to the closing of the large cold leg blowdown valve. The flow then gradually increased due to the constantly increasing quality until 22 s, when the valve was reopened, resulting in high volumetric flow rates for the remainder of the blowdown transient. The RELAP4 code predicted the volumetric flow rate during both the subcooled and saturated portions of the blowdown extremely well, indicating that the code predicted the correct volume of two-phase mixture leaving the system, which also accounts for the good calculation of the system depressurization.

The cold leg spool average mass flow rate for Test LLR-5 is shown in Figure 19 along with the corresponding RELAP4 calculations. The mass flow rate was determined from the average coolant density and coolant volumetric flow rate. The overall agreement between the predicted and measured mass flow rates is good. Closer examination of the mass flow data in Figure 20 for the first 4 s of the transient indicates that the calculated coolant mass flow spike was slightly lower than that measured during the first 1.8 s of the transient. From 2 to 3.65 s the calculated density was higher than the measured density, resulting in a higher predicted mass flow. The mass flow rate then steadily decreased after this point, as the coolant density and pressure in the system decreased during blowdown.

An approximate inventory of the IPT, blowdown piping, and PCS piping to the isolation valves is compiled in Table 7, as derived from the RELAP4 model. The total mass ejected from the system, obtained by integrating the cold leg mass flow measurement, was approximately 112 kg for the first 35 s of blowdown. The initial inventory, as estimated in Table 7, was 124 kg. The correspondence between the integrated mass flow and mass inventory indicates the measurements are valid.

3.5 Fuel Rod Shroud Flow Rate

The steady state inlet volumetric flow rate to the IPT during Test LLR-5 was approximately 9.35 L/s, as measured at the inlet spool piece. Approximately 6.7 L/s passed through the metered bypass, with the remaining flow passing through the four flow shrouds (~2.4 L/s). A small amount of flow (~0.25 L/s) is attributed to

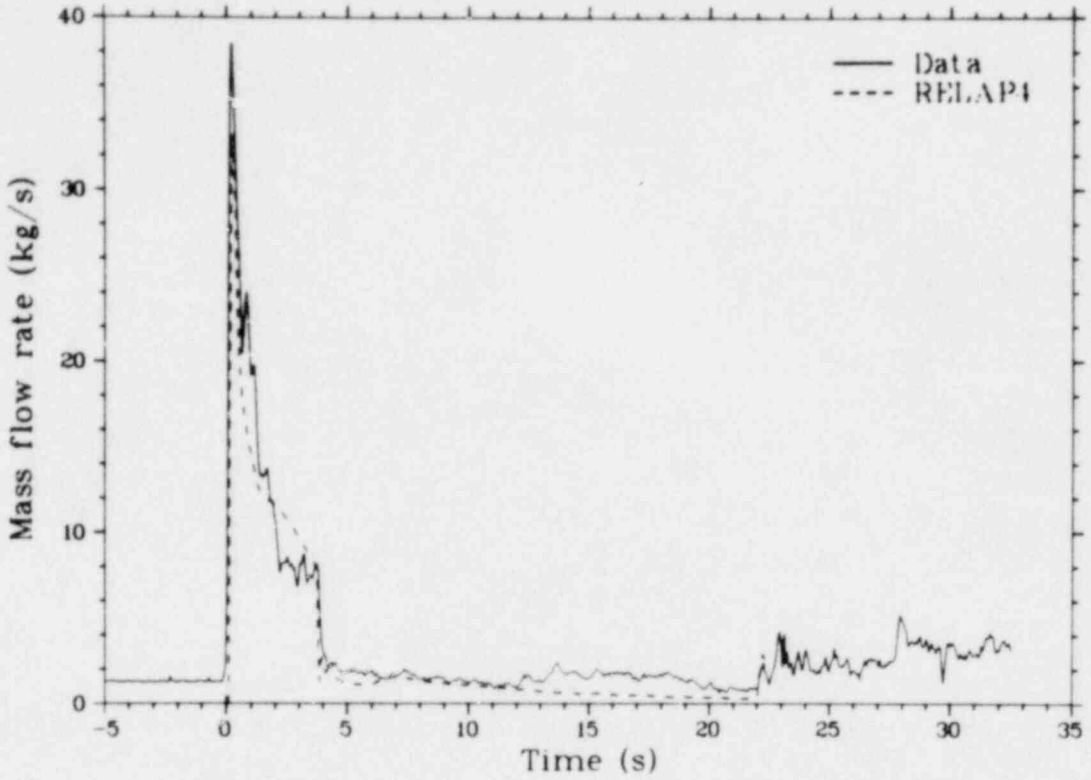

Figure 19. Comparison of analytical and derived mass flow in the cold leg blowdown spool (0 to 35 s) during Test LLR-5.

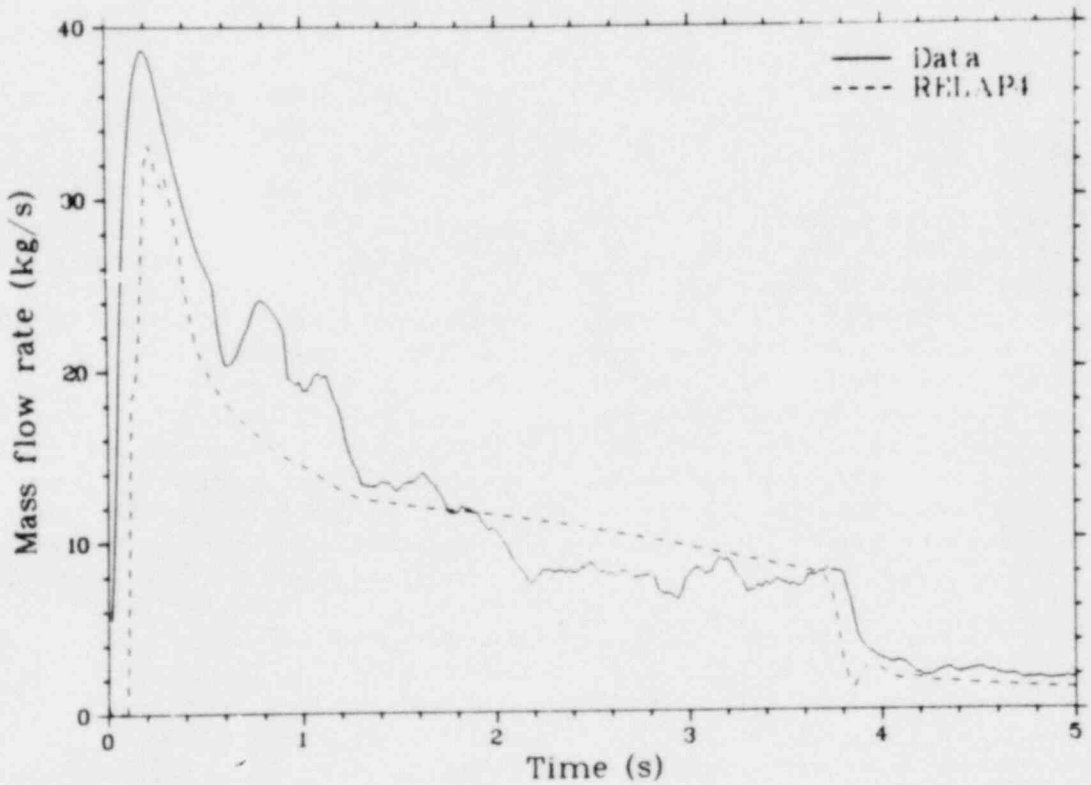

Figure 20. Comparison of analytical and derived mass flow in the cold leg blowdown spool (0 to 5 s) during Test LLR-5.

TABLE 7. PBF IN-PILE TUBE COOLANT VOLUMES AND MASS INVENTORY

	Volume (L)
Hot leg[a]	31.89
Cold leg[a]	44.38
Downcomer	15.11
Volumetric bypass	16.43
Lower plenum	3.64
Upper plenum	11.10
Reflood line[b]	48.08
Hanger rod	0.79
Shrouds (4)	7.47
	178.89

Total system mass (initial conditions 15.5 MPa, 600 K) = (0.179 m^3 x 691.3 kg/m^3) = 123.7 kg

a. Includes piping from IPT nozzle to isolation valve.

b. From top of IPT to flow control valves.

various leakages through the test train. The warm-up line from the cold leg to the hot leg was closed until just prior to blowdown.

The flow rate in the fuel rod shrouds during the blowdown was primarily controlled by depressurization of the lower plenum. Because of the unique configuration of the PBF/LLR test train, the upper and lower plenums depressurized independently. Upon initiation of blowdown, the coolant in the flow shrouds reversed direction, check valves located on the top of each flow shroud closed, and the shroud flow was isolated from the upper plenum throughout the blowdown transient, resulting in negative flow throughout the transient.

The shroud inlet and outlet volumetric flow rates for Rod 312-1 during Test LLR-5 are shown in Figures 21 and 22, respectively, along with the corresponding RELAP4 predictions. Both the data and predictions for the other test rods for all the LLR tests generally follow the trends illustrated for Rod 312-1.

On initiation of blowdown, flashing first occurred in the fuel rod flow shrouds where the highest enthalpy fluid was located. The volumetric flow rate indicated by the upper turbine flowmeter decreased sharply from the initial steady state upflow of 0.58 L/s, and reversed to a value of -0.25 L/s. This small, initial, negative flow spike lasted only momentarily, as the flow immediately stagnated in the upper portion of the flow shrouds.

Flashing of the high enthalpy fluid in the lower portion of the flow shrouds resulted in a large negative flow spike at blowdown initiation. With this initial negative flow spike, the lower turbine flowmeter was saturated at -1.5 L/s. As choking occurred at the blowdown nozzles, the flow decreased to -0.8 L/s. Beyond this point the data indicate a significant amount of volumetric flow until the large cold leg blowdown valve was closed at 3.75 s. The flow then decreased sharply and gradually stagnated until 22 s, when the reopening of the blowdown valve generated flow rates comparable to those obtained during the first 5 s.

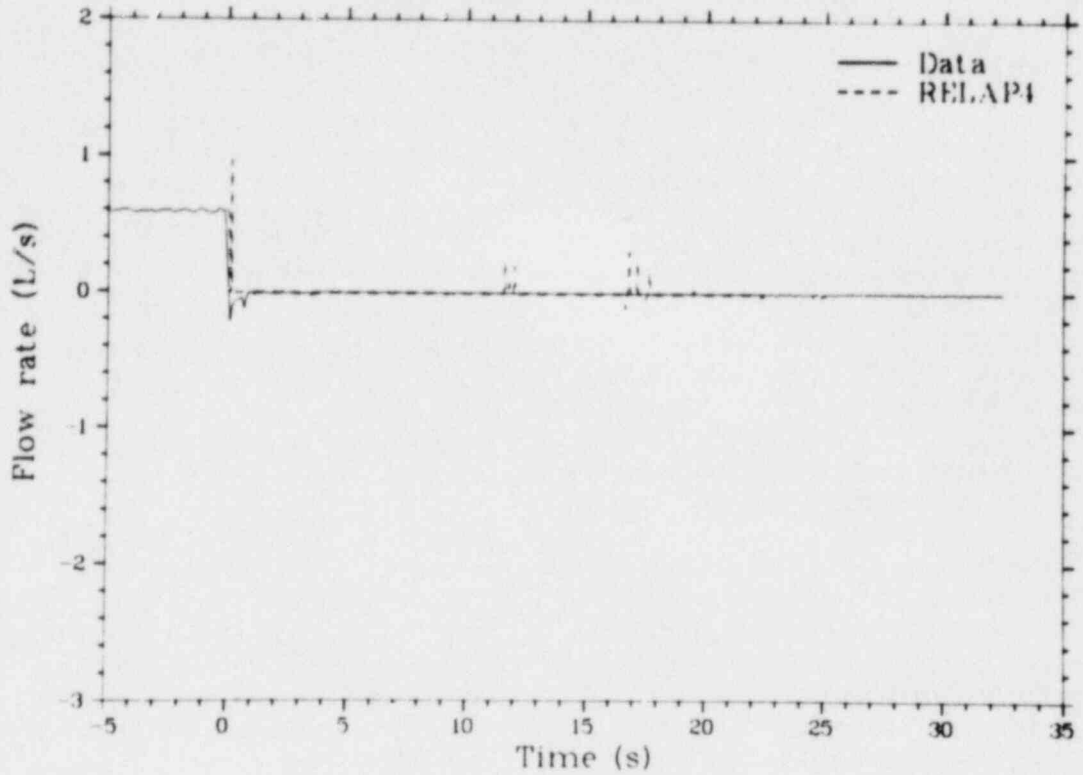

Figure 21. Comparison of calculated and measured upper turbine volumetric flow for Rod 312-1 during Test LLR-5.

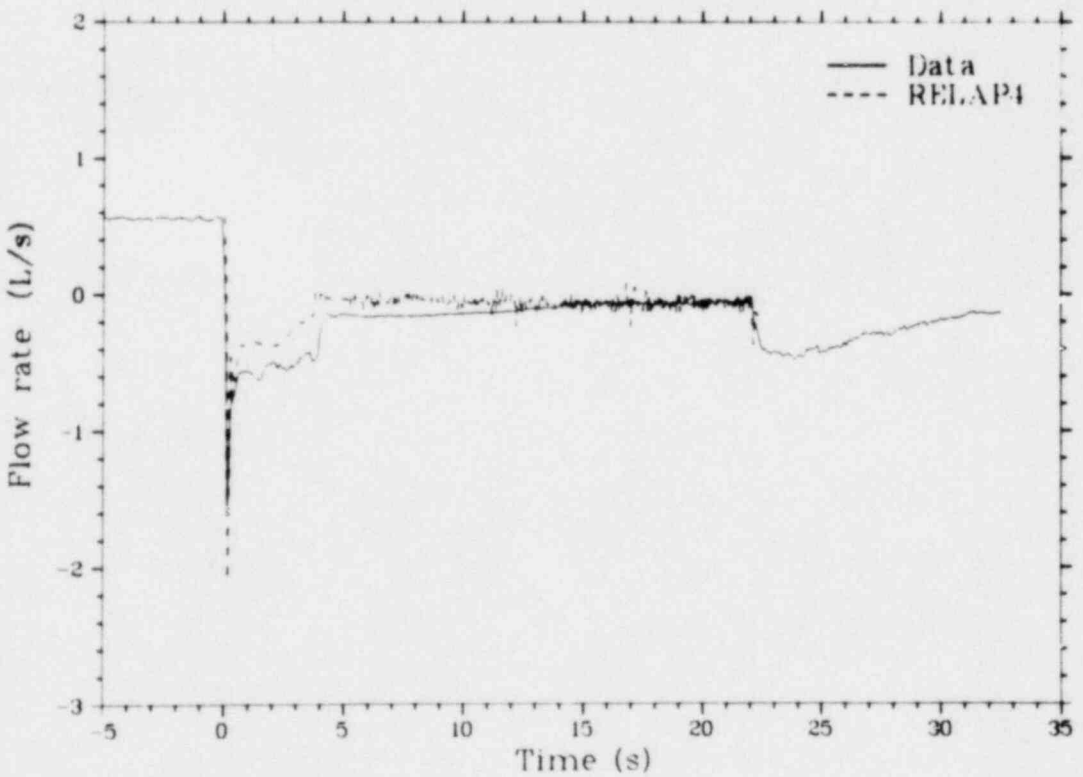

Figure 22. Comparison of calculated and measured lower turbine volumetric flow for Rod 312-1 during Test LLR-5.

The measured flow responses of all four of the fuel rod flow shrouds were essentially identical. This validates the modeling assumption of combining the four flow shroud paths into one for the RELAP4 nodalization. As shown in Figure 21, the RELAP4 calculations do not predict the small, initial, negative flow spike at the upper turbine flowmeter, but follow the measured data rather closely after this time period. The magnitude and duration of the initial negative flow spike was calculated well at the lower turbine flowmeter, however. After the initial flow spike, the lower volumetric flow rate for the first 4 s was as much as 0.2 L/s greater than the calculations, as shown in Figure 22. After 4 s the calculations follow the measured trends extremely closely.

Accurate calculation of the magnitude of the volumetric flow in the flow shrouds was complicated because of code modeling assumptions. The RELAP4 code is based on the assumption of homogeneous flow with thermodynamic equilibrium. In actuality, the conditions within the shrouds are nonhomogeneous and are not in thermodynamic equilibrium. Also, small differences between the actual and calculated coolant pressure and density can result in large differences in the volumetric flow rate. An indication of potential differences in density was suggested by the differences between the calculated and measured onset of superheated vapor in the shrouds, as discussed in Section 3.7.

3.6 Fuel Rod Shroud Coolant Density

The inability of the RELAP4 code to predict the time to CHF (discussed in Section 4.3) for the LLR tests can be directly related to the prediction of density and the corresponding flow patterns in the shrouds.

Since density measurements are not available in-core, the local thermal-hydraulic conditions throughout the core can only be approximated with the pre- and posttest RELAP4 calculations. Figure 23 presents the code calculations for density at the 0.457-m elevation. The posttest calculations indicate the density decreases to 160 kg/m^3 within 0.5 s. This decrease is due to the voiding (X = 0.3) in the flow shrouds and the high heat transfer rates from the fuel rods to the saturated steam environment. The density then decreases to

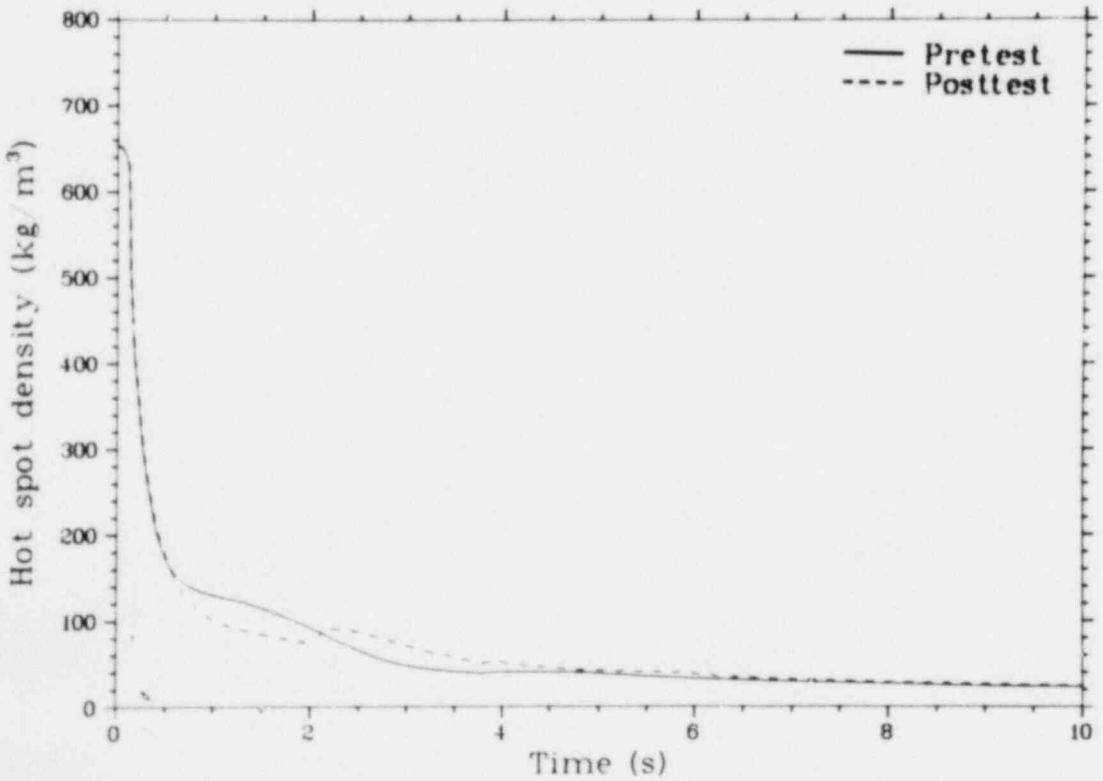

Figure 23. RELAP4 predictions for hot spot density.

70 kg/m^3 at 3 s as the calculated void fraction increases to 0.9. From this point, the hot spot density linearly decreases to a value approaching zero at 25 s. The code predicted a superheated steam environment at 5 s into the transient.

The flow patterns observed in vertical, cocurrent flow are similar to those seen for horizontal flow. Thus, bubbly, slug (similar to plug from horizontal flow), and annular flow are observable, as well as churn and wispy-annular flow. Churn flow is formed by the breakdown of the large vapor bubbles in slug flow. The gas or vapor flows in a more or less chaotic manner through the liquid, which is mainly displaced to the channel wall. Wispy-annular flow takes the form of a relatively thick liquid film on the walls of the pipe, together with a considerable amount of liquid entrained in a central gas or vapor core. Since the LLR shroud flow patterns are altered by the annular flow area resulting from the shroud/fuel rod geometry and the presence of the fuel rod and channel wall heat fluxes, the problem of estimating the flow patterns is complicated. Hewitt[11] and coworkers have constructed the flow pattern map shown in Figure 24 from their observations of high-pressure steam-water flow in small-diameter (1 to 3 cm) heated vertical tubes. The axes of the figure represent the superficial momentum fluxes of the liquid ($\rho_f j_f^2$) and vapor phases, respectively. These momentum fluxes can also be expressed in terms of the mass velocity (G) and the quality (X) by

$$\rho_g j_g^2 = \frac{(GX)^2}{\rho_g} \tag{7}$$

and

$$\rho_f j_f^2 = \frac{[G(1-X)]^2}{\rho_f} \quad . \tag{8}$$

If the density in the shrouds is assumed to be as given by the posttest calculation shown in Figure 23, the flow pattern map for the LLR flow shrouds (shown in Figure 24) is obtained. Since the highest enthalpy fluid is in the flow shrouds, this coolant flashes instantaneously at blowdown initiation. The flow map indicates an annular flow regime might have been maintained for the first 6.5 s of the transient when superheated steam conditions were attained. This flow regime suggests the formation of a high velocity vapor core with a liquid film around the periphery of the shroud and fuel rod. Prior to CHF, vapor that is formed at preferred positions on the surface of the rods intermittently detaches with the high velocity steam flow. With the production of more vapor, the bubble population increases with length, and coalescence takes place as CHF is attained and propagated up the rod. The flow shroud probably maintained a liquid film until 6.5 s to generate the high volumetric flow rate for the lower turbine flowmeter shown in Figure 22.

3.7 Fuel Rod Shroud Coolant Temperature

As blowdown was initiated, the coolant temperatures within the flow shrouds reached saturation within 50 ms. Local qualities continued to rise during the first several seconds of the transient until they reached unity between 6.5 and 7 s. The coolant temperatures then increased significantly above the saturation temperature throughout the remainder of the transient. This superheating was attributed to energy transfer by convection and radiation from the fuel rods and flow shrouds.

The coolant temperatures within the shroud of Rod 345-1 at several axial elevations are shown in Figure 25. With the initiation of blowdown, the coolant temperatures reached saturation conditions and decreased as the system pressure decreased until 6.5 to 7 s. At this point, the three coolant thermocouples at the fuel rod midplane and the thermocouple at the shroud inlet indicated a superheated steam environment, which was maintained throughout the remainder of the transient.

The coolant thermocouple at the shroud outlet indicated a saturation temperature decrease with pressure throughout the entire transient, decreasing to a value of 525 K at 30 s. Since this thermocouple was isolated from the high radiation environment in the active fuel length and recorded no superheat, the validity of the readings from the midplane thermocouples during superheated conditions is questionable. These thermocouples were not designed to accurately measure the coolant superheat, since measurement of a single-phase gas temperature requires shielding from the thermal radiation from surrounding surfaces. Thus, the indication of superheating by the thermocouples may have preceded the time at

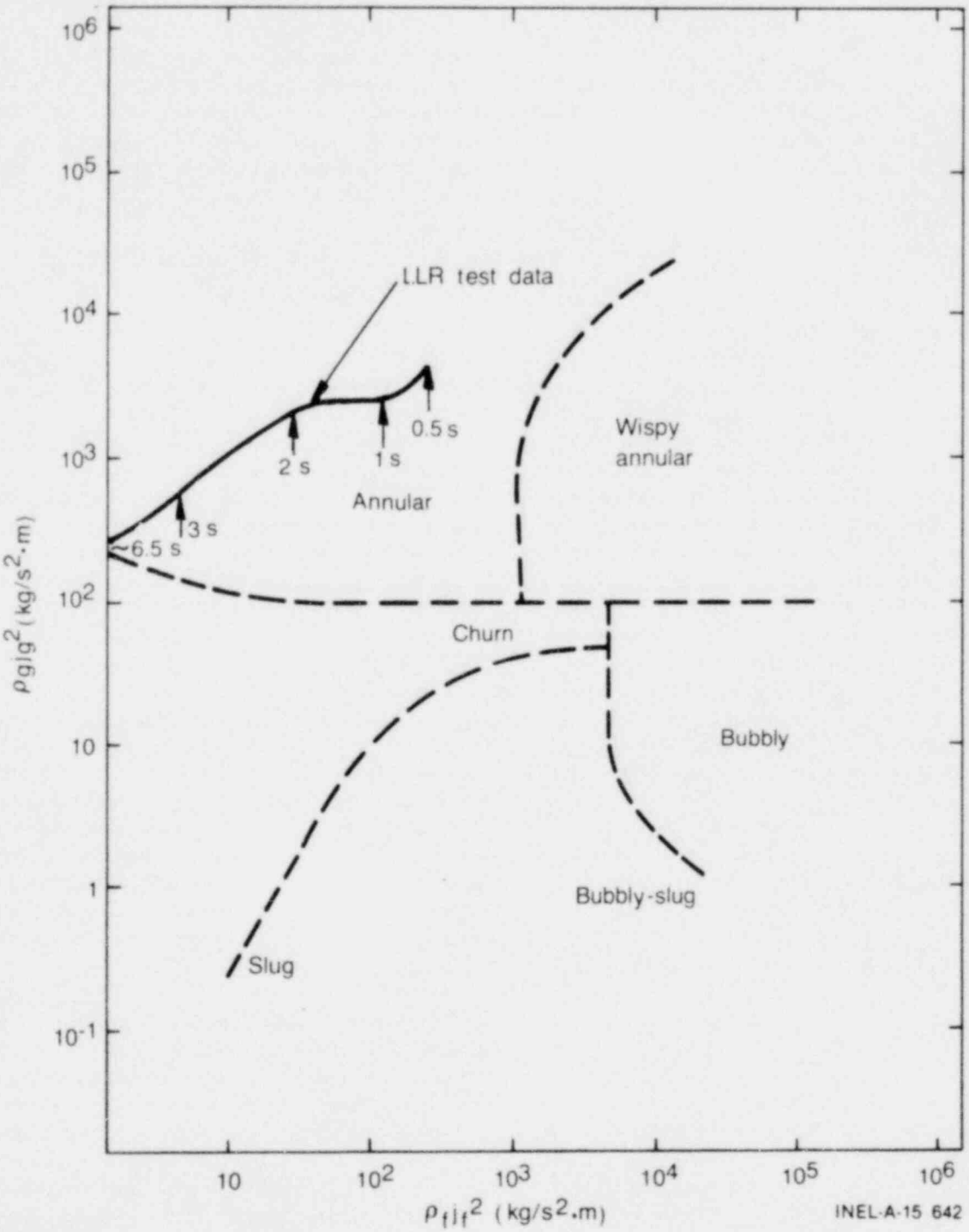

Figure 24. Hewitt flow pattern map for vertical flow in the flow shrouds during Test LLR-5.

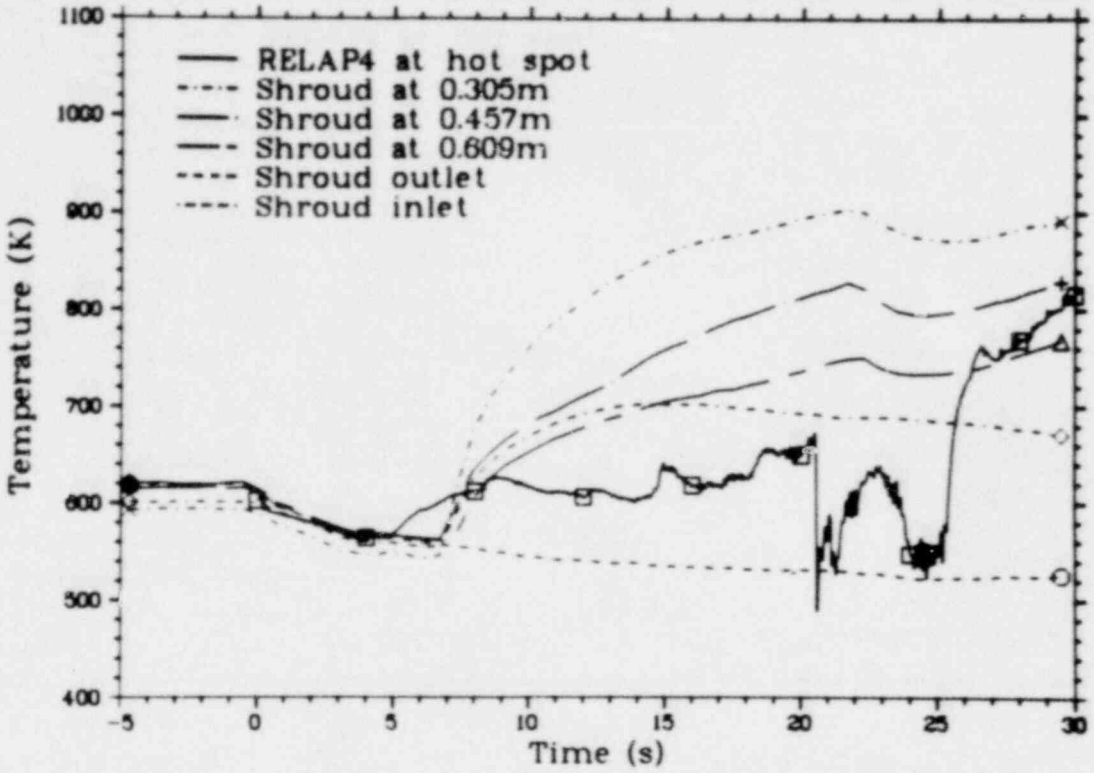

Figure 25. Coolant temperatures in Rod 345-1 shroud for Test LLR-5.

which the coolant actually exceeded the vapor saturation temperature at the midplane. Selected flow shrouds were instrumented with thermocouples to measure the metal temperature. As illustrated in Figure 26 for the Rod 345-1 shroud, the shroud metal temperature followed a saturation temperature decrease until 18 s, and then gradually achieved superheated temperatures approximately 50 K higher than the saturated coolant at the end of blowdown. Thus, the shroud thermocouple probably indicated the correct coolant superheat. As shown in Figure 25, the inlet thermocouple indicated superheated steam temperatures only as high as 700 K at 15 s, decreasing linearly to 665 K at 33 s. This measurement also indicates the midplane thermocouples were probably biased by radiation effects. The RELAP4 prediction for the 0.457-m location coolant temperature shown in Figure 25 indicated a quality of 1.0 would be reached at 5 s into the transient. The analytical predictions indicated slightly increasing superheated steam temperatures past this point for the remainder of the transient.

Figure 26 presents an indication of the radial temperature distribution from the cladding to the volumetric bypass during Test LLR-5 for the Rod 345-1 flow shroud. Radiation heat transfer from the hot fuel rod to the flow shroud became dominant once superheated conditions were attained in this shroud at 6.5 s. The RELAP4 prediction for the 0.533-m location coolant temperature shown in Figure 26 indicated a quality of 1.0 would be reached at 5 s into the transient. On the basis of RELAP4 calculations, when radiation becomes dominant, the magnitude of the radiation heat transfer coefficient is equal to that from convection. As shown, the temperature difference between the rod and the shrouds amounts to as much as 450 K. The volumetric bypass surrounding the flow shrouds is not influenced by the heat transfer from the active core region. Calculated heat transfer coefficients from this region to the shrouds amount to free convection values. High water levels were probably maintained due to the high resistance flow path to the cold leg, thus resulting in a moderately decreasing density for the majority of the transient.

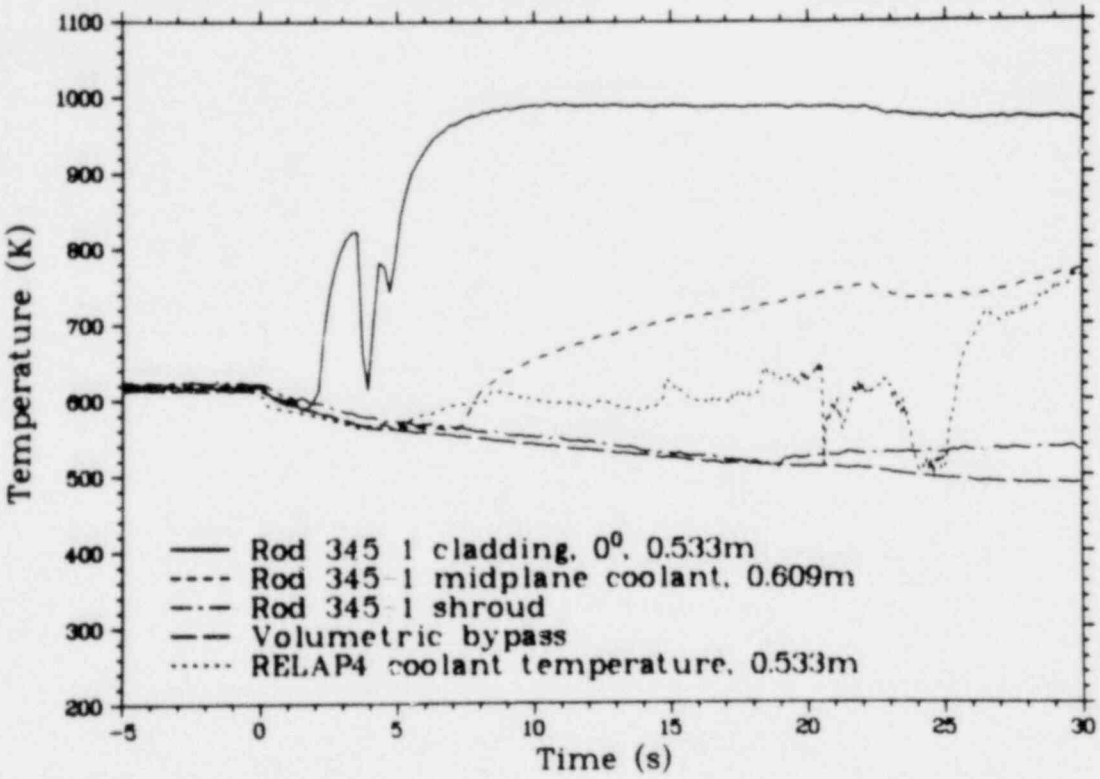

Figure 26. Radial temperature gradient for Rod 345-1 shroud.

4. FUEL ROD BEHAVIOR

At normal PWR operating conditions, hundreds of hours of operation are required for cladding collapse to occur. However, under severe conditions, such as during a hypothetical LOCA, the high cladding temperatures and fuel rod differential pressures could cause the cladding to collapse onto the fuel pellets in a matter of seconds.

The cladding deformation witnessed during the LLR transients was of particular interest to the LOFT Program. The LLR fuel rods were simultaneously subjected to high cladding temperatures and compressive stresses during the LOCA transients. These conditions caused uniform cladding collapse and waisting onto the fuel, with a decrease in the cladding diameter. The differential axial and radial thermal expansion between the fuel and cladding possibly exaggerated the pellet-cladding interaction (PCI) during the subsequent preconditioning operational period. Since collapse near the pellet interfaces (waisting) was severe, the cladding may have become permanently mechanically interlocked with the fuel. In the case of LOFT testing, if reactor cooldown or subsequent startup occurs too rapidly at this condition, the stress at the waisted pellet interface could cause a PCI-type of cladding failure. However, such failure was not witnessed in the LLR tests.

The mechanical deformation that was witnessed in the LLR tests can be directly compared with the fuel rod cladding temperature and pressure deformation criteria developed by Olsen[12] from investigations of zircaloy tubing deformation under isothermal, isobaric conditions. These tests by Olsen were conducted on LOFT-type cladding to determine the pressure-temperature loci for the deformation boundaries between two-point buckling (cladding contact at two points on the fuel pellet circumference, which results in an ovality of the cladding), uniform circumferential cladding collapse onto the fuel pellets (uniform loss-of-diameter of the cladding), and waisting (plastic flow of zircaloy cladding into small axial pellet gaps).

The results of the postirradiation examination (visual appearance, extent of cladding collapse, and cladding microstructural changes) also provided information to evaluate the LLR test rod damage. In addition, the fuel centerline temperature measurements during the steady state portion of the tests were indicative of changes from test to test in the performance of the rods during subsequent power excursions.

A detailed analysis of cladding deformation was performed for model and code development and evaluation. The FRAP-T5[a] computer code was used to confirm the actual fuel rod dynamics that occurred during the LLR tests. The code was developed to predict the coupled thermal-mechanical behavior of a nuclear fuel rod under normal and accident situations. It is the latest developmental model in the FRAP-T series. The code couples the major thermal and mechanical models that influence both fuel pellet and cladding responses. Subcodes are linked to FRAP-T to provide material properties for the fuel, cladding, and gap, and the 1967 ASME Steam Tables.

Specific capabilities modeled in FRAP-T5 include (a) radially varying energy generation within the fuel pellet, (b) radial and azimuthal heat conduction, (c) fuel-cladding mechanical interaction, (d) elastic-plastic cladding deformation, (e) transient fuel rod internal pressure, (f) dynamic gap conductance calculation, (g) using cladding surface heat transfer boundary conditions as predicted from thermal-hydraulic codes, and (h) cladding metal-water reaction. Of particular importance in LOCEs, the code has state-of-the-art fuel rod thermal models to predict stored energy. In addition, FRAP-T5 has models to account for radiation heat transfer to the surrounding test rod shrouds, which was important in the LLR tests. A detailed description of the FRAP code and the LLR model are included in Appendix D.

4.1 LLR Test Discussion

During the LLR tests, the fuel rods experienced critical heat flux (CHF) early in the blowdown and maximum measured cladding temperatures ranged from 880 to 1260 K. Table 2 presents the maximum measured cladding temperature for each fuel rod during the LLR tests. The maximum temperature of 1260 K was attained at the 0.314-m

a. FRAP-T5, Idaho National Engineering Laboratory Configuration Control Number H000583B.

location on Rod 399-2 during Test LLR-4A. The RELAP4 predictions indicated that the hot spot should have been at the 0.457-m elevation. However, these calculations did not consider the effect of the centerline thermocouple depressing the heat flux.

Test LLR-3, a 41-kW/m experiment, was conducted February 28, 1979 with four fresh fuel rods. The measured cladding temperatures for this test ranged from 880 to 990 K. Although the measured fuel rod cladding surface temperatures were lower than expected (990 K as compared with 1080 K), the cladding temperatures achieved on the zircaloy shrouded rods were close to those expected on the peripheral LOFT rods, indicating that the data are appropriate for evaluating the expected response of the LOFT rods. On the basis of the maximum measured cladding temperature, no mechanical deformation is assumed to have occurred to the fuel rods during Test LLR-3.

In keeping with the planned test sequence for LOFT, Test LLR-5, a 47-kW/m experiment was conducted March 24,1979. Two fresh rods (one without thermocouples) were installed for this test. The measured cladding temperatures ranged from 985 to 1015 K. On the basis of measured cladding temperature and rod pressure comparisons with Olsen's data, buckling is believed to have occurred at the thermocouple locations on the instrumented Test LLR-5 rods. Recent cladding surface thermocouple evaluation tests conducted at the PBF (Thermocouple Effects Tests) have shown that surface thermocouples act as cooling fins, delaying CHF and reducing the cladding temperatures at instrumented locations during a LOCA. Thus, on the basis of the responses of the elongation sensors and cladding thermocouples during Test LLR-5, the fuel rods could have first reached CHF at an elevation below the thermocouples at 0.5 s and then reached CHF at the thermocouple junctions at 1.9 s, despite the fact that the thermocouples were located at high power elevations. This delay in time to CHF at the thermocouple junctions could have resulted in less stored energy at the time of CHF and measured temperatures possibly 60 K lower than at lower elevations. Therefore, the Test LLR-5 rods may have experienced buckling and incipient collapse at axial elevations lower than the thermocouples.

Test LLR-4, a 57-kW/m experiment, was performed March 30, 1979 with the same fuel rods used in Test LLR-5. Measured cladding temperatures of 1060 to 1165 K resulted in mechanical deformation to the fuel rods. At approximately 15.4 s into the transient, the cladding surface thermocouples indicated quenching from inadvertant loop isolation valve cycling. This, however, did not affect the overall test rod thermal and mechanical response, as the maximum cladding temperature had been attained prior to the valve cycling. On the basis of comparisons with Olsen's data, the mechanical deformation of the fuel rods would be expected to include waisting. Subsequent postirradiation examination (PIE) of Rod 312-1, which was removed after this test, confirmed this deformation.

Since a major objective of performing the PBF/LLR Test Series was to evaluate the effect of cladding collapse and waisting on rod behavior during subsequent power ramps and depressurization transients, an additional LLR test. Test LLR-4A, was performed May 18, 1979 at the same test conditions as Test LLR-4. Rod 312-1 was removed prior to Test LLR-4A and replaced with a fresh rod (designated 399-2). This allowed determination of the mechanical deformation of a rod subjected to a single blowdown transient initiated from a power level of approximately 56 kW/m. During the power calibration and preconditioning power ramps, there were no observable indications that the deformed condition of the cladding on the other three test rods affected their behavior. Cladding temperatures for Test LLR-4A ranged from 1075 to 1260 K. These temperatures resulted in mechanical deformation to the fuel rods, including collapse and waisting. A program objective of subjecting deformed fuel rods to subsequent preconditioning and LOCA cycles was achieved, and no fuel rod failures were observed. Subsequent posttest examination revealed that all four Test LLR-4A rods had achieved the waisting regime of mechanical deformation.

In subsequent sections details of the steady state and transient performance of the LLR fuel rods are discussed. This discussion is presented in terms of fuel rod steady state centerline temperature response, the CHF phenomenon witnessed during the transients, and fuel rod thermal-mechanical responses during each test. Comparisons with RELAP4 pretest and posttest calculations and FRAP posttest calculations are also included.

4.2 Fuel Rod Steady State Thermal Response

A major objective of the LLR tests was to investigate fuel rod behavior during power ramps following conditions in which the cladding had been deformed. The measured and predicted fuel rod thermal behavior for selected LLR test rods for the power ramping portion of each test are presented in the following sections. Predictions are provided for Rods 345-1 and 345-2 for centerline temperature versus fuel rod power. The calculations were obtained from the FRAP-T5 code, with the thermal boundary conditions derived from the data (that is, from fuel rod power and coolant conditions).

The preconditioning power history conditions prior to each LOCE are shown in Appendix B. The fuel rod analyses were performed in sequence following the LLR test procedure. For each test, the fuel was subjected to power ramps through preconditioning, then exposed to the LOCA blowdown conditions, and finally, to reflood conditions.

The objective of the steady state analyses was twofold: first, to determine whether cladding deformation could be detected by monitoring the centerline temperature; and second, to evaluate the capability of FRAP-T5 to calculate centerline temperatures on deformed cladding.

Figures 27 and 28 present the centerline temperature versus fuel rod power data and the FRAP-T5 calculations for the preconditioning portions of Tests LLR-5, -4, and -4A for Rods 345-1 and 345-2. The calculated data were obtained using FRAP-T5 in a quasi-steady-state mode. The power was ramped to various levels and held for several minutes to obtain steady state results. Coolant conditions measured during the ramps were input to the FRAP-T5 program. Nominal, beginning-of-life fuel rod dimensions were used for fresh fuel calculations, whereas the appropriate end-of-test conditions calculated for the previous transient were used for irradiated fuel. This method of analysis attempted to consider the effect of loss of gap width, which occurred in the tests due to cladding deformation, and the initial rod condition for the following test.

The centerline temperature versus fuel rod power data obtained from Rod 345-1 during

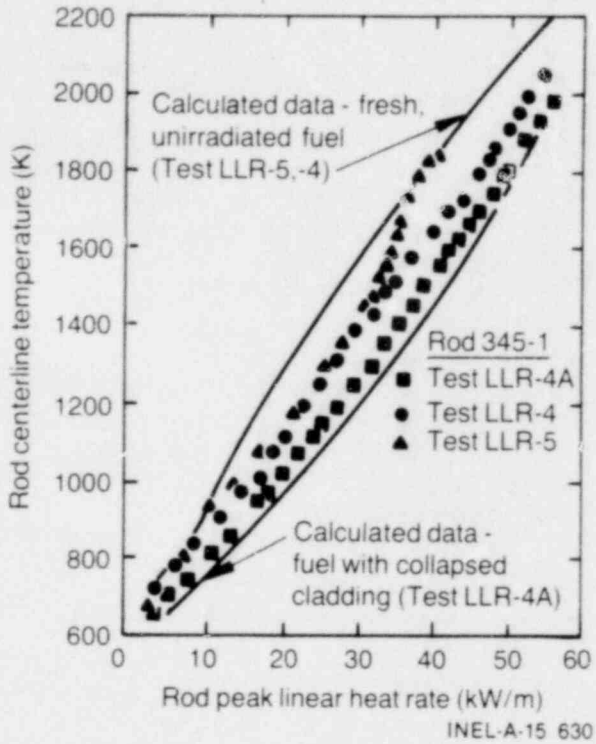

Figure 27. Comparison of steady state response of Rod 345-1 with FRAP-T5 calculations during Tests LLR-5, -4, and -4A.

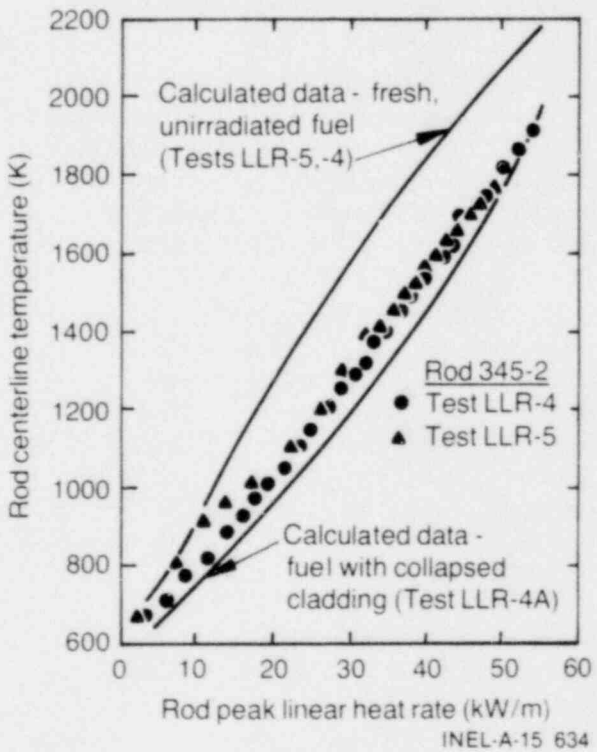

Figure 28. Comparison of steady state response of Rod 345-2 with FRAP-T5 calculations during Tests LLR-5 and -4.

Tests LLR-5, -4, and -4A are illustrated in Figure 27 with the corresponding FRAP predictions. For linear heating rates less than 30 kW/m, the measured centerline temperatures for Tests LLR-5 and -4 agree closely. At heating rates of about 30 kW/m, the data for the two tests begin to diverge. This temperature divergence is not attributed to significant cladding deformation occurring during Test LLR-5, since Olsen's criteria indicated that only buckling occurred at the thermocouple locations. The difference may be due to significant pellet relocation during Test LLR-5 that resulted in an increase in the radial thermal resistance across the fuel rod, or to measurement error. The centerline temperature data for Rod 345-2, shown in Figure 28, does not show this divergent trend.

Comparison of the steady state centerline temperature data from Tests LLR-4 and -4A for Rod 345-1 indicates that Test LLR-4A data are consistently lower than Test LLR-4 data. Since waisting was verifed on Rod 312-1 after Test LLR-4, cladding collapse probably occurred on portions of all of the fuel rods during this test. The lower centerline temperatures during the steady state portion of Test LLR-4A are probably an indication of collapsed cladding and a higher gap conductance for Rod 345-1 prior to the Test LLR-4A blowdown transient.

In general, the FRAP-T5 calculations shown in Figure 27 indicate that the code slightly overpredicts the centerline temperature for a fresh rod and slightly underpredicts the temperature for a collapsed fuel rod.

The centerline temperature versus fuel rod power data obtained from Rod 345-2 during Tests LLR-5 and -4 are illustrated in Figure 28. Rod powers were not calculated for Test LLR-4A, since the coolant differential thermocouple for Rod 345-2 failed early in the nonnuclear startup. Generally, the centerline temperature data obtained for Rod 345-2 are lower than the data obtained for Rod 345-1. The measured centerline temperatures for Rod 345-2 agree closely for Tests LLR-5 and -4 for all rod powers, but are relatively low, indicating that collapse did not occur during Test LLR-5, or the effects of cladding collapse were obscured by pellet cracking and relocation. The FRAP-T5 calculations for Rod 345-2 follow the trends evidenced for Rod 345-1.

In conclusion, FRAP-T can be used to estimate the centerline temperature response of LOFT-type fuel rods before and after being subjected to LOCA conditions. However, the effects of fuel pellet cracking and relocation (and possibly measurement error) may prevent the detection of cladding collapse with fuel centerline thermocouples during steady state operation before and after the LOCA transient.

4.3 The Critical Heat Flux Phenomenon in the LLR Tests

The critical heat flux condition is characterized by a sharp reduction of the local heat transfer coefficient, which results from the replacement of liquid by vapor adjacent to the heat transfer surface. For the case in which the surface heat flux is the independent variable, the CHF condition is manifested by a sharp increase in surface temperature as the critical heat flux value is reached.

Table 8 presents the measured times to saturated departure from nucleate boiling for the LLR fuel rods based on thermocouple and cladding elongation sensor (LVDT) readings. This table indicates the time at which the nucleate boiling heat flux rapidly decreased into a film boiling mode of heat transfer. At the point of critical heat flux, the steam formed a local insulating layer over the rod surface, resulting in a rapid increase in surface temperature. This blanket of vapor gradually propagated up (and possibly down) the fuel rod, starting at elevations below the thermocouple locations. The range of incipient time to CHF at the thermocouple locations (near the axial location of peak power) for the 41- and 46-kW/m tests was from 1.8 to 2.6 s, whereas the time to CHF in the 57- and 56-kW/m tests ranged from 1.6 to 2.0 s. The cladding elongation sensors indicated that CHF occurred at an axial elevation probably below the surface thermocouples at about 0.25 s during Tests LLR-4 and LLR-4A, and at about 0.4 to 0.5 s during Test LLR-5 (46 kW/m), excluding Rod 345-1.[a] The responses

a. Rod 345-1 behavior was influenced by a malfunctioning check valve above the rod, which allowed upper plenum coolant to leak into the shroud flow channel, resulting in a premature quench for Tests LLR-5 and LLR-4A.

TABLE 8. MEASURED TIME[a] (seconds) TO SATURATED DEPARTURE FROM NUCLEATE BOILING

Rod	Test LLR-3 (41 kW/m)	Test LLR-5 (46 kW/m)	Test LLR-4 (57 kW/m)	Test LLR-4A (56 kW/m)
312-1				
TC[b]--0°, 0.533 m[c]	2.4	1.8	1.7	
TC--180°, 0.533 m	2.8	2.0	1.7	--
LVDT	2.8	0.5/1.5	0.25/1.5	
312-2				
TC--0°, 0.457 m	2.6	2.0	1.6	1.9
TC--180°, 0.533 m	4.5	2.3/3.3	2.0	2.1
LVDT	2.0	--	--	0.25/0.8/1.5
312-3				
TC--0°, 0.533 m	2.5			
TC--180°, 0.533 m	2.5	--	--	--
LVDT	2.0			
312-4				
TC--0°, 0.533 m	2.4			
TC--180°, 0.533 m	2.4	--	--	--
LVDT	1.8			
345-1				
TC--0°, 0.533 m		1.8/3.9/4.7	1.7/4.0	2.0
TC--180°, 0.533 m	--	1.9/3.9/5.0	1.7/3.6	2.0
LVDT		1.4/2.1/3.8	0.25/1.4/2.6	0.25/1.5
345-2				
LVDT	--	0.40	0.25	0.25/1.5
399-2				
TC--0°, 0.314 m				1.6
TC--180°, 0.457 m	--	--	--	1.8
LVDT				0.25/1.5

a. Multiple times denote successive indications of departure from nucleate boiling. (The LVDT is probably indicating DNB at different locations on the fuel rod. The thermocouples are indicating successive rewets and dryouts.)

b. TC = thermocouple.

c. Distance in meters is elevation above bottom of rod heated length.

of the cladding elongation sensors during Test LLR-3 (41 kW/m) ranged from 1.8 to 2.8 s. Since the elongation sensor detects CHF at any location along the length of the rod, and the surface thermocouples only indicate the time when the thermocouple junction experiences CHF, the only time when the two measurements should coincide is when the initial CHF condition occurs close to a thermocouple junction. Since the locations of the thermocouples were chosen to correspond to high power elevations, and the cladding elongation sensors indicated CHF at 0.5 and 0.25 s rather than at 2.6 to 1.6 s, the surface thermocouples possibly delayed CHF in the instrumented portion of the fuel rods because of fin cooling, thus, subsequently affecting the local temperature measurement during Tests LLR-5, -4, and -4A. However, the effect of the centerline thermocouple on the flux profile must also be considered. The centerline thermocouples used for the LLR tests may have depressed the heat flux by as much as 5% in the upper half of the test rods.

The time to CHF for the RELAP4 pretest calculations was in the vicinity of 0.5 s. Critical heat flux was calculated to occur when the shroud flow rate decreased to a magnitude at which the code logic switched from the high flow saturated departure from nucleate boiling (DNB) correlation of Hsu and Beckner[2] to an interpolation between Hsu-Beckner and Zuber's[2] low flow CHF correlation. The Hsu-Beckner correlation is normally evaluated for mass fluxes greater than 1356 kg/m^2·s, whereas the modified Zuber correlation is applicable for mass fluxes less than 271 kg/m^2·s. The calculated mass flux at the time of CHF was in the vicinity of 678 kg/m^2·s. The actual experimental mass flux at 0.5 s could have ranged anywhere from 475 to 950 kg/m^2·s on the basis of the shroud volumetric flow and density estimates from RELAP4 calculations. The RELAP4 heat transfer logic evaluates the local void fraction, and if it exceeds 0.96, dryout occurs. These dryout critieria arise from the Hsu-Beckner DNB correlation. The underprediction of the measured time to CHF is attributed to this code logic, since at 0.5 s the hot spot quality was approximately 0.4, which resulted in a corresponding void fraction greater than 0.96. This underprediction of time to CHF would contribute to higher predicted cladding temperatures than measured.

In posttest studies, several analyses were attempted to delay CHF by delaying the development of high void fraction. These included reducing the code transition mass flux, changing the slip velocity in-core, modifying pre-CHF heat transfer modes, and using various other CHF correlations. Reducing the transition mass flux between the two correlations from 271 to 68 kg/m^2·s had little effect. It was postulated that phase separation would be inhibited and that the fluid state would possess a lower quality by applying a multiplier to the slip velocity. This application resulted in a small effect on the time to CHF, but not enough to warrant its usage. Modification of pre-CHF heat transfer only changed the film temperature distribution. The use of the General Electric Company transient CHF correlation[2] resulted in a slight (0.2 s) delay in CHF, but not enough to be significant. The Biasi correlation, as used in the TRAC[13] code, offered no potential for the low flow conditions in the LLR analyses, because the Zuber correlation was used in the low flow mode. Finally, for posttest analysis, CHF was forced to occur at the times witnessed in the tests in an attempt to more closely match the data, but cladding temperatures were again substantially higher than the data.

For the period from 1.5 to 2.5 s, the mass flux estimates in the flow shrouds ranged from 203 to 271 kg/m^2·s. These calculations are based on the predicted density shown in Figure 23. Thus, the modified Zuber correlation, which applies for mass fluxes less than 271 kg/m^2·s, would be most applicable for the prediction of CHF in the LLR tests. In Section 3.6 an annular flow regime was postulated to exist within the LLR flow shrouds during the first 6.5 to 7 s of the transients. At the point of critical heat flux, the steam formed a local insulating layer under the liquid film over the rod surface, resulting in a rapid increase in surface temperature. This blanket of vapor gradually propagated up (and possibly down) the fuel rod, starting at elevations other than the thermocouple locations. The boiling crisis mechanism for the LLR tests could possssibly have been an annular flow dryout, as suggested by Tong.[14] In this case, a liquid film covers and cools the heating surface. The boiling crisis occurs when the liquid film becomes too thin, and breaks into dry patches due to disruption of the annular liquid film from the high velocity vapor core. The characteristic of this crisis is a retarded wall temperature excursion, which was evidenced in the LLR tests at the cladding surface thermocouple locations. As noted by Tong, several parametric effects, which were evidenced in the LLR tests, can contribute to a

decrease in CHF. These effects include high pressures which reduce bubble diameter, high mass fluxes which induce downstream dryouts, and cold wall effects.

In summary, the difference between the calculated and measured times to CHF for the pretest calculations can be attributed partially to the underprediction of volumetric flow, as shown in Figure 22, and a corresponding void fraction overprediction in the period from 1.5 to 3 s, which results in the use of hydrodynamic mechanisms that govern the RELAP4 CHF calculation. This combination forces the code logic to change from a high flow correlation to an interpolation between the high flow and low flow correlations. The code assumption of homogeneity in-core, when an annular flow regime quite possibly exists, further complicates the situation. The RELAP4 code is not capable of predicting an annular flow regime dryout. Finally, the use of steady state CHF correlations to define the transient CHF situation evidenced in the LLR tests may not be valid.

4.4 Transient Thermal and Mechanical Response of LLR Fuel Rods

The transient response of the fuel rods is described with respect to the transient thermal and mechanical behavior during the LLR tests. The transient thermal response of the fuel rods is defined by the cladding surface temperature and fuel centerline temperature behavior. The cladding temperature history, in combination with the pressure differential across the cladding, controls the type and degree of cladding deformation. The fuel centerline temperature indicates the stored energy redistribution throughout the transient. The mechanical response of the fuel rods is discussed with respect to the cladding axial elongation and the posttest diameter measurements. The cladding axial elongation provides a direct indication of CHF and the total axial strain incurred by the fuel rod cladding. At the elevated temperatures attained during the transients, the unpressurized rods experienced cladding collapse and waisting. The details of these observations are discussed subsequently.

During the transients, centerline temperatures decreased immediately after reactor scram as the nucleate boiling environment removed the internal stored energy until CHF. The temperatures then continued to decrease during the transient as the stored energy was redistributed toward the periphery of the fuel pellet. Selected results of fuel centerline temperature responses are presented in subsequent subsections. Several of the centerline temperature responses have been categorized as trend[a] information. Qualified[b] data are compared with FRAP-T5 calculations.

Measured cladding temperatures followed the coolant saturation temperature until CHF occurred. After CHF, measured cladding temperatures rose rapidly, reaching maximums in the period from 8 to 20 s. After the maximum values were reached, the measured cladding temperatures decreased slowly until test termination. During steady state operation, heat transfer was by forced convection to the coolant, resulting in a coolant temperature increase of approximately 10 K from shroud inlet to shroud outlet. After initiation of blowdown, measured coolant temperatures followed the coolant saturation temperature until approximately 6.5 s, at which time the coolant quality was approximately unity and the rod was surrounded by superheated steam. The fuel rod surface heat transfer during this period can be derived from the coolant conditions described in Section 3 and the RELAP4 pretest calculations. Prior to CHF, a nucleate boiling environment was experienced. After CHF, film boiling conditions were established and cladding temperatures rapidly increased. As the coolant quality approached unity, the mode of surface heat transfer changed to a combination of forced convection to steam and radiation to the flow shroud, which was maintained for the remainder of the blowdown transient. This change in the heat transfer mode resulted in gradually decreasing cladding temperatures for the remainder of the blowdown transient. The RELAP4 predicted range of the heat transfer coefficient during this period is from 50 to 100 $W/m^2 \cdot K$. After 15 s, radiation heat transfer was dominant, as the decreased coolant mass in the shrouds resulted in a reduction in convective heat transfer. RELAP4 predicted that radiation would come into

a. Trend data—suitable only for illustrative purposes and not for numerical analysis.

b. Qualified data—represents the variable being measured within specified uncertainty limits.

dominance at approximately 5 s into the transient, equalling the convective heat transfer coefficient for the remainder of the transient. The decay heat contribution to the stored energy amounted to approximately 3% of the initial power, which helped maintain the elevated cladding temperatures.

The pre- and posttest data and the cladding temperature responses calculated by RELAP4 are presented for each fuel rod in subsequent subsections. The cladding temperatures at the thermocouple locations were overpredicted in all cases. RELAP4 predictions of cladding temperature ranged from 170 K (for Test LLR-3) to 305 K (for Test LLR-4A) higher than measured. Since CHF was predicted to occur at the thermocouple locations at approximately 0.5 s for all cases, the code predicted a more rapid initial temperature rise rate than measured. For posttest calculations, although CHF was forced to occur at the times witnessed in the tests, cladding temperatures were again overpredicted. For these calculations, the rise rates were comparable, but the maximum predicted temperatures ranged from 120 K (for Test LLR-3) to 310 K (for Test LLR-4A) higher than the measured values. Since the cladding temperature response was overpredicted in both the pre- and posttest calculations, either the stored energy model or the post-CHF heat transfer models, or both, are considered inadequate for LLR test analysis purposes. Also, the decay heat history used in the calculation may be too high, or the rod power may be overestimated due to the centerline thermocouple depressing the heat flux, both of which would contribute to the overcalculation of cladding temperature. For the calculated and observed cladding thermal responses to coincide, the magnitude and response of the surface heat transfer coefficient must be in close agreement with the actual surface heat transfer. Since the stored energy model causes the centerline temperature data to be underpredicted, post-CHF heat transfer models are not dissipating enough energy during the nucleate and film boiling modes of operation. Increased heat transfer during this time interval would cause lower peak cladding temperatures, after which time the radiation heat transfer mode would dominate, resulting in gradually decreasing temperatures for the remainder of the blowdown transient.

The effect of fin cooling by the surface mounted thermocouples is a major concern in evaluating LOCA-type experiments. Since the LLR tests did not positively determine the effects of external thermocouples on fuel rod response, an investigation is currently in progress in the Thermal Fuels Behavior Program to quantify these thermocouple effects. A series of five experiments, designated the Thermocouple Effects Test Program, has been conducted with nuclear fuel rods to evaluate fin cooling effects during the blowdown and reflood portions of a LOCA. These effects were evaluated by using four test rods per test with either surface mounted (LOFT technique) or embedded thermocouples located at the same elevation. The thermocouple responses were then compared and correlated to the test thermal-hydraulic conditions. On the basis of the results of these tests, the conclusion reached was that surface thermocouples do influence fuel rod thermal response during a LOCA. As blowdown was initiated, rods with embedded thermocouples exceeded CHF within 1 s, whereas rods with surface thermocouples reached CHF within 1 to 5 s. The measured cladding temperatures achieved during blowdown were generally 100 K lower for the surface instrumented fuel rods than the fuel rods with embedded thermocouples for each second of delay in CHF. During reflood, fuel rods with the surface mounted thermocouples quenched significantly before rods with embedded thermocouples.

During the postirradiation examination of the LLR fuel rods, several permanent changes were found to have occurred to the cladding. Visual appearance, which provides an indication of the severity of the transients, was examined. All the rods were found to be uniformly covered with a black layer of zirconium dioxide. Figure 29 is an example of the posttest rod appearance of the LLR fuel rods. There was no visual indication of the axial extent of film boiling. In addition, the fuel rods did not exhibit any visually discernible deformation (bowing or loss of diameter). Cladding temperatures that result in the deformation and oxidation of the cladding were evaluated. Temperature profiles approximated from metallurgical samples (including the azimuthal and longitudinal temperature gradients around the thermocouples) were tabulated. Collapse of the unpressurized fuel rods was also analyzed. The posttest diameter measurements indicated that the cladding of all the rods (except Rods 312-3 and 312-4 from Test LLR-3) had collapsed onto the fuel stack nominally from 30 to 60 cm from the bottom of the heated length. These results are discussed in the following subsections for each fuel rod.

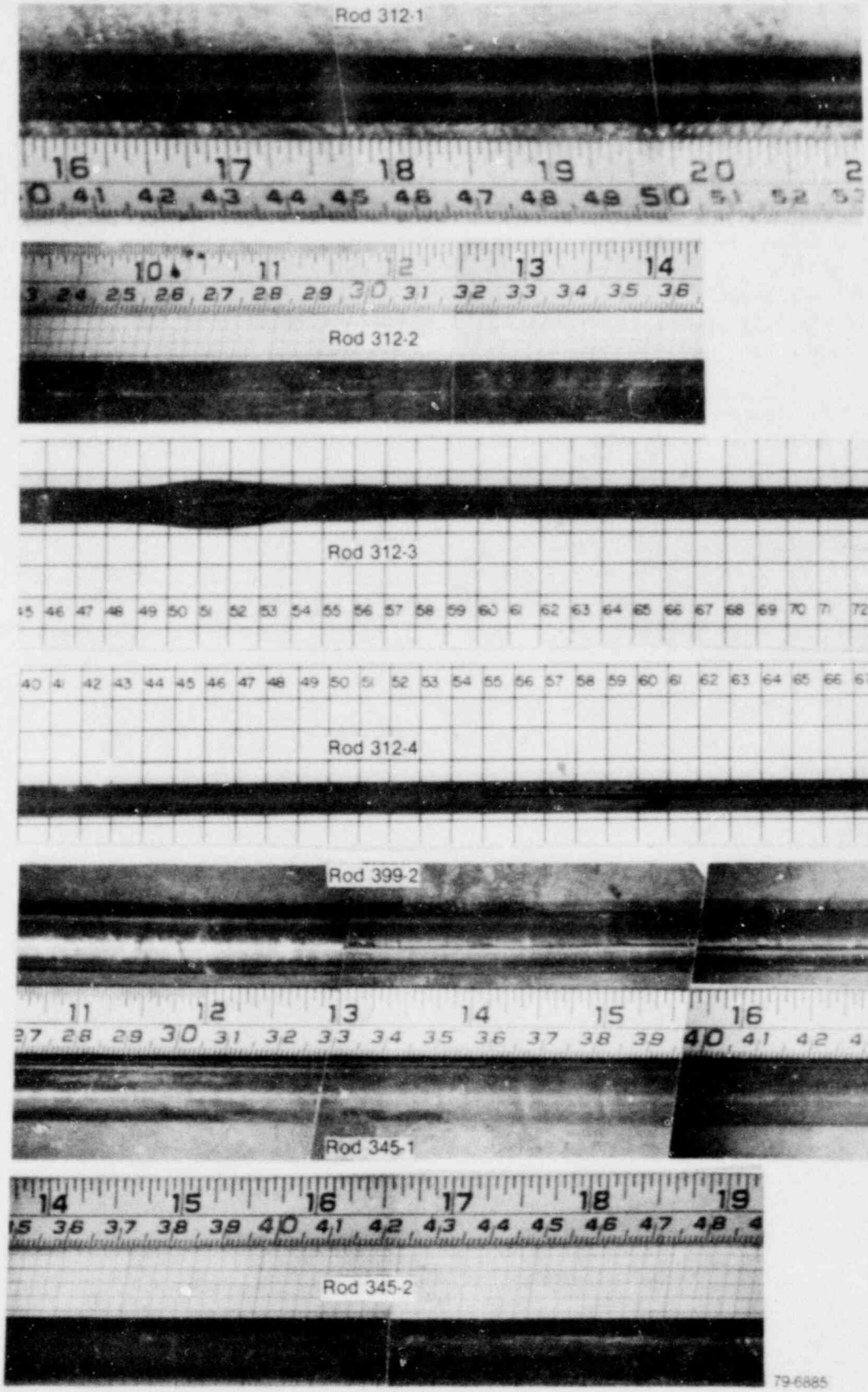

Figure 29. Posttest photographs of LLR fuel rods.

4.4.1 Fuel Rod 312-1. Rod 312-1 was used for Tests LLR-3, -5, and -4. A maximum temperature of 1125 K was recorded for this rod during Test LLR-4. Removal of the rod after this test for postirradiation examination provided the opportunity to study the effects of three successive transients on the LLR fuel rods. The rod exhibited collapse with some waisting as a result of Test LLR-4. On the basis of microstructural evidence, temperatures were estimated to be in the range of 1100 to 1150 K at the thermocouple locations. Details of the response of Rod 312-1 during the three transients and postirradiation results are presented in the following subsections.

4.4.1.1 Test LLR-3, Rod 312-1—Figure 30 illustrates the cladding temperature, cladding elongation, and coolant midplane temperature response of Rod 312-1 during Test LLR-3, for a 30-s duration. The peak power was calculated from test data to be 40.3 kW/m just prior to blowdown. During the first 2.4 s, the measured cladding temperatures decreased approximately 15 and 20 K, at the 0- and 180-degree locations, respectively, essentially following the coolant saturation temperature. A decrease in cladding length, as indicated by the cladding elongation sensor, coincided with the cladding temperature response for this time interval. The cladding temperature data indicate that the rod achieved DNB at approximately 2.4 s at the 0-degree, 0.533-m thermocouple location, whereas the 180-degree, 0.533-m thermocouple indicated DNB at 2.8 s. The cladding elongation transducer indicated a sharp expansion at 2.8 s, which suggests that CHF occurred over a significant length of the fuel rod surface and indicates that the surface thermocouples probably did not affect the transient response of the rods during Test LLR-3.

The temperature measurements at the two azimuthal locations on the fuel rod indicate that CHF occurred within 0.4 s. The calculated difference in rod power between the two orientations was approximately 5%, with the 0-degree quadrant (facing the center hanger rod) at the highest power; thus, the temperature at 0 degrees should have been slightly higher for the LLR tests if the fuel rod geometry and surface boundary conditions were axisymmetric. A small circumferential variation in cladding temperature was also measured. The 0-degree thermocouple measured a maximum cladding temperature of 950 K at 10 s, whereas the 180-degree thermocouple measured 930 K at 20 s. These variations are attributed to the initial rod power distribution and, possibly, coolant thermal-hydraulics.

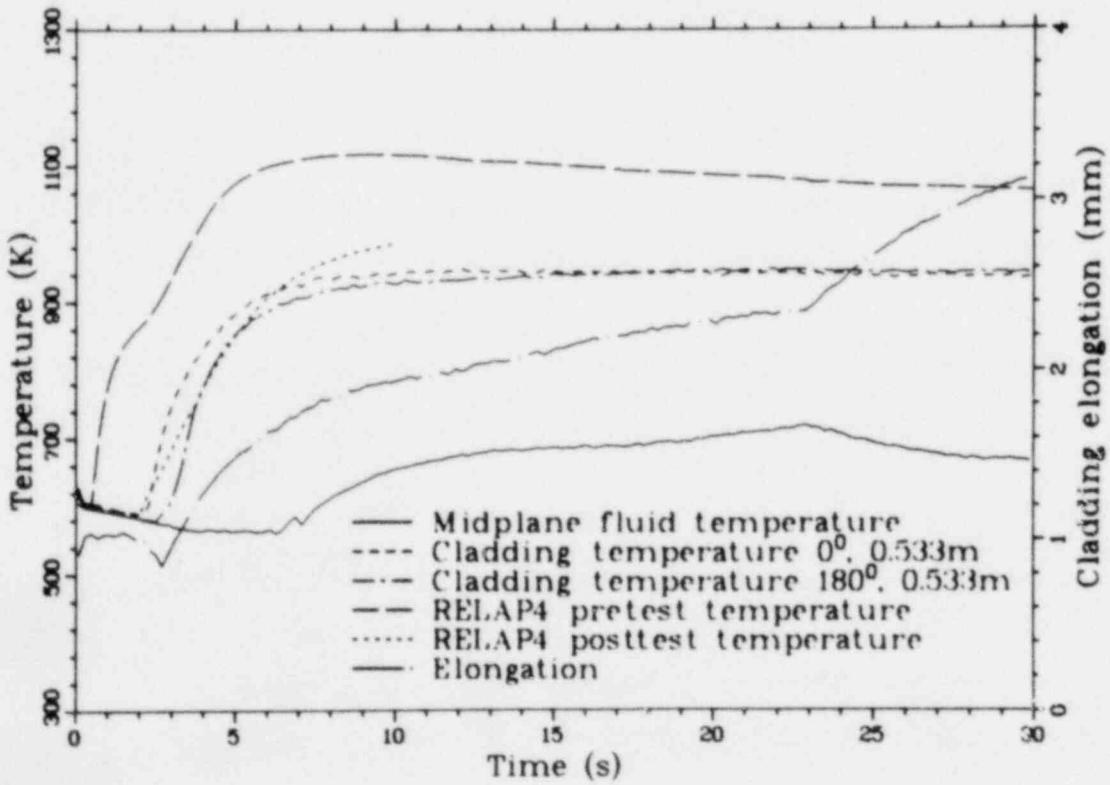

Figure 30. Thermal and mechanical behavior of Rod 312-1 during Test LLR-3.

Since the fuel rod elongation sensor is biased by attachment to the flow shroud, it can only measure relative changes in length of the flow shroud and fuel rod. For instance, an increase in the length of the fuel rod produces a proportional increase in output voltage of the sensor; however, an increase in the flow shroud length produces a decrease in the sensor response. That is, a decrease in the length of the flow shroud produces the same sensor response as if the fuel rod length increased by a corresponding amount. As shown in Figure 29, when the transient was initiated with the reactor scram, the rod experienced a slight increase and then a slight axial contraction during the first 2.8 s until CHF. The contraction was probably due to a relaxation of the fuel-cladding interfacial contact, which resulted during the final preconditioning prior to blowdown. This relaxation is attributed to the decrease in power and the increase in heat transfer during the nucleate boiling mode of operation. During the rapid temperature increase following DNB, the rod experienced an axial strain to approximately 1.8 mm. The rod continued to elongate to 3.2 mm at 30 s.

The fluid thermocouple response, which is the typical coolant response witnessed during all of the LLR tests, follows the depressurization saturation line until approximately 6.5 s, after which a superheated environment is indicated for the remainder of the blowdown transient.

The maximum measured cladding temperature is plotted as a function of fuel rod differential pressure in Figure 31. The measured temperature-pressure history falls below the cladding buckling region, as determined by Olsen, which indicates that no permanent cladding deformation would be expected to have occurred to Rod 312-1 during Test LLR-3.

The measured fuel centerline temperature[a] at 0.533 m for Rod 312-1 for Test LLR-3 is shown in Figure 32. The initial centerline temperature was 2030 K. The temperature decreased to 1160 K at 10 s when the stored energy was finally redistributed toward the periphery of the fuel pellet. After this time, the centerline temperature increased gradually until fuel rod quenching occurred at 37 s. After quenching occured, the cladding temperatures decreased to 440 K for the remainder of the experiment.

a. Categorized as trend information.

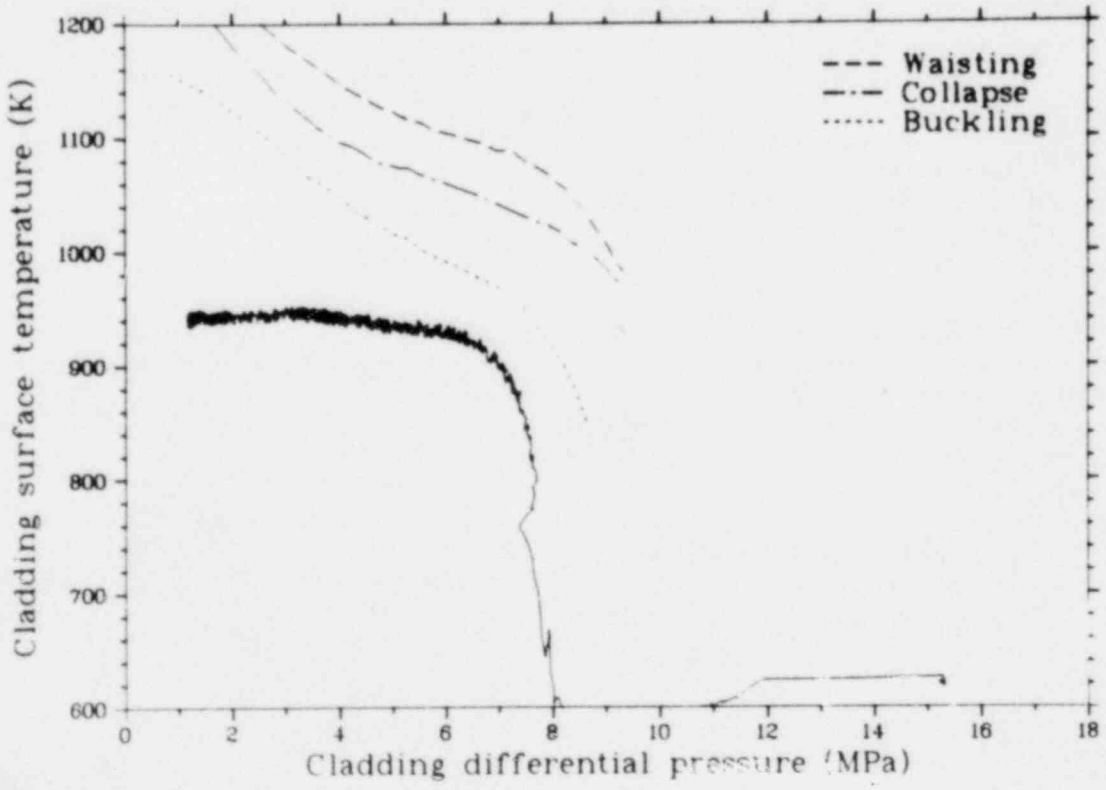

Figure 31. Surface temperature versus fuel rod differential pressure of Rod 312-1 during Test LLR-3.

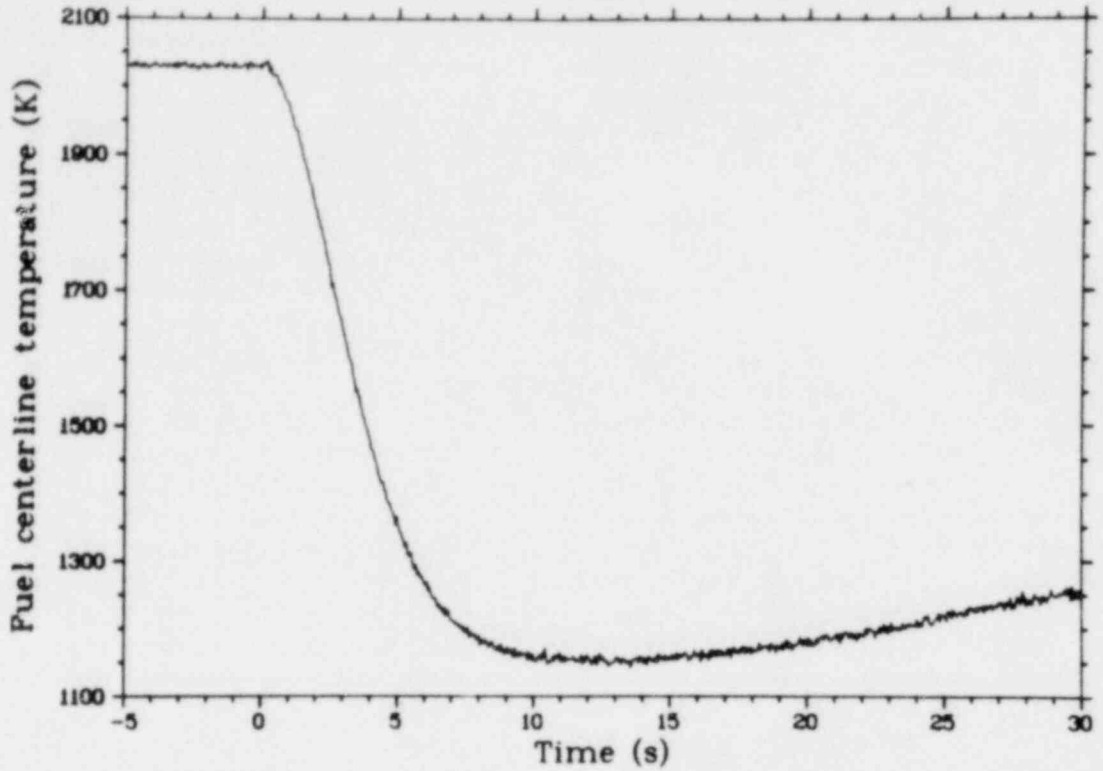

Figure 32. Fuel centerline temperature of Rod 312-1 during Test LLR-3.

4.4.1.2 Test LLR-5, Rod 312-1—Figure 33 illustrates the cladding temperature and elongation response of Rod 312-1 during Test LLR-5, for a 30-s duration. The rod peak power of Rod 312-1 was calculated from test data to be 47.3 kW/m just prior to blowdown. The cladding surface thermocouple data at the 0-degree, 0.533-m thermocouple location indicated that the rod achieved DNB at 1.8 s and reached a maximum surface temperature of 1000 K at 10 s. The 180-degree, 0.533-m thermocouple indicated DNB at 2.0 s and a maximum surface temperature of 990 K at 10 s. The elongation sensor first indicated a moderate increase in cladding length at 0.5 s, and then a stronger indication at 1.5 s as DNB started at an elevation probably lower than the cladding thermocouples and propagated up the rod. The discrepency between the thermocouple measurements and the elongation sensor indicates that the surface thermocouples may have affected the transient response of the rods by delaying CHF.

As shown in Figure 34, based on Olsen's criteria, the cladding surface temperature versus differential fuel rod pressure indicates cladding buckling probably occurred at the thermocouple locations for Rod 312-1 for Test LLR-5. However, since DNB was probably achieved earlier at lower elevations than the thermocouples, estimates of higher temperatures at lower elevations have been made. On the basis of the response of Rod 399-2 cladding surface thermocouples (Subsection 4.4.7) during Test LLR-4A, which measured cladding temperatures of 1260 and 1205 K at the 0.314- and 0.457-m locations, respectively, and the response of the fuel rods of Tests LLR-5 and -4, the temperature was estimated to be 1030 K at the 0.314-m location for Rod 312-1. This temperature would also result in local buckling of the fuel rod at the 0.314-m axial elevation.

The measured fuel centerline temperature at 0.533 m for Rod 312-1 for Test LLR-5 is illustrated in Figure 35. The measured temperature was 1950 K at steady state conditions prior to blowdown.

4.4.1.3 Test LLR-4, Rod 312-1—Figure 36 illustrates the cladding temperature and elongation response of Rod 312-1 during Test LLR-4, for a 30-s duration. The rod peak power for Rod 312-1 was calculated from test data to be 56.6 kW/m just

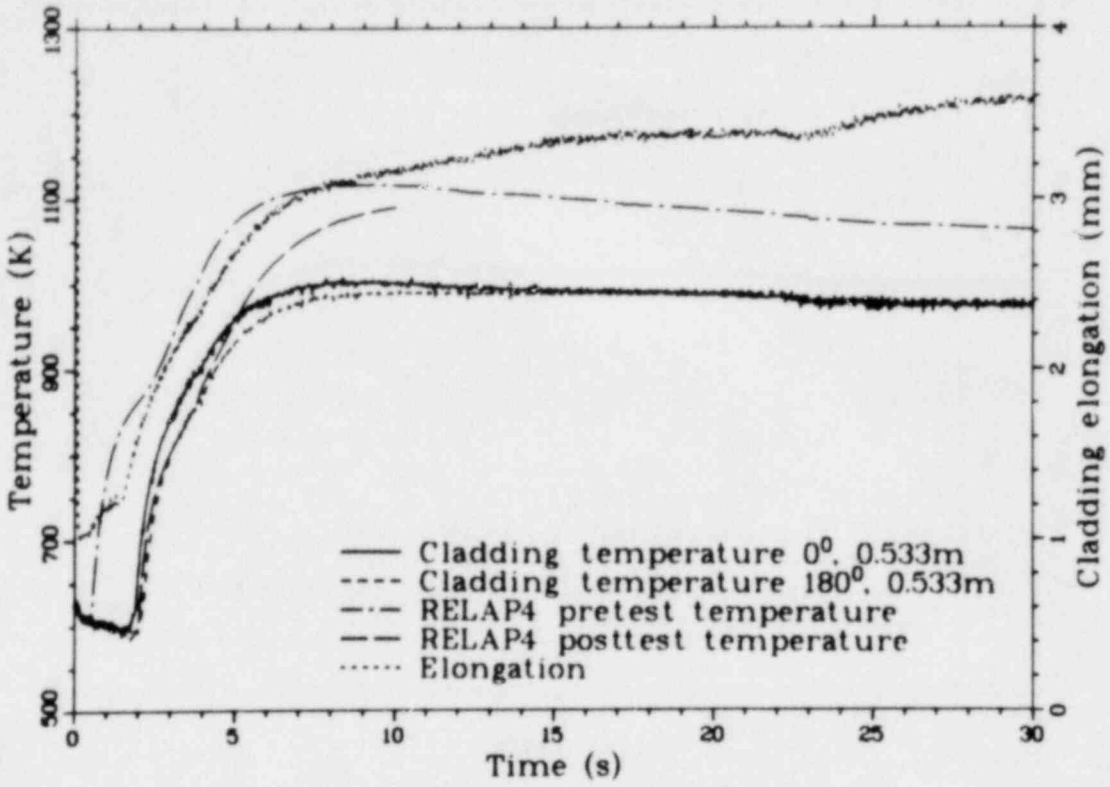

Figure 33. Thermal and mechanical behavior of Rod 312-1 during Test LLR-5.

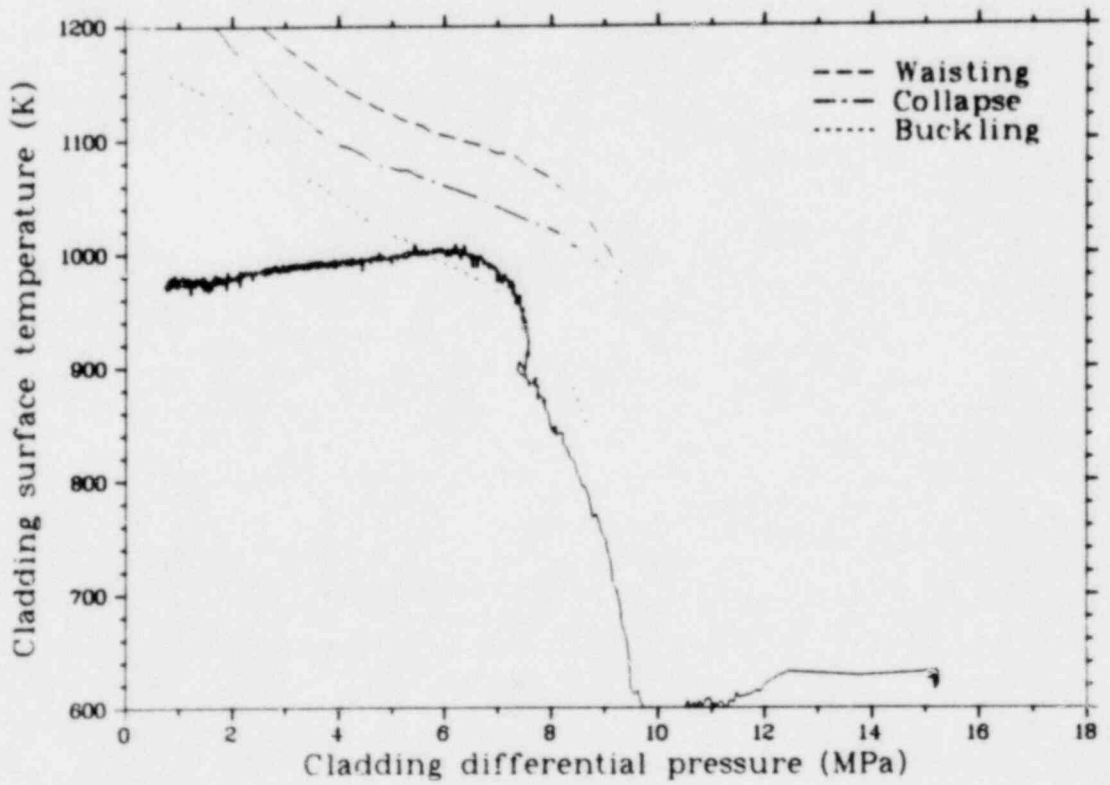

Figure 34. Surface temperature versus fuel rod differential pressure of Rod 312-1 during Test LLR-5.

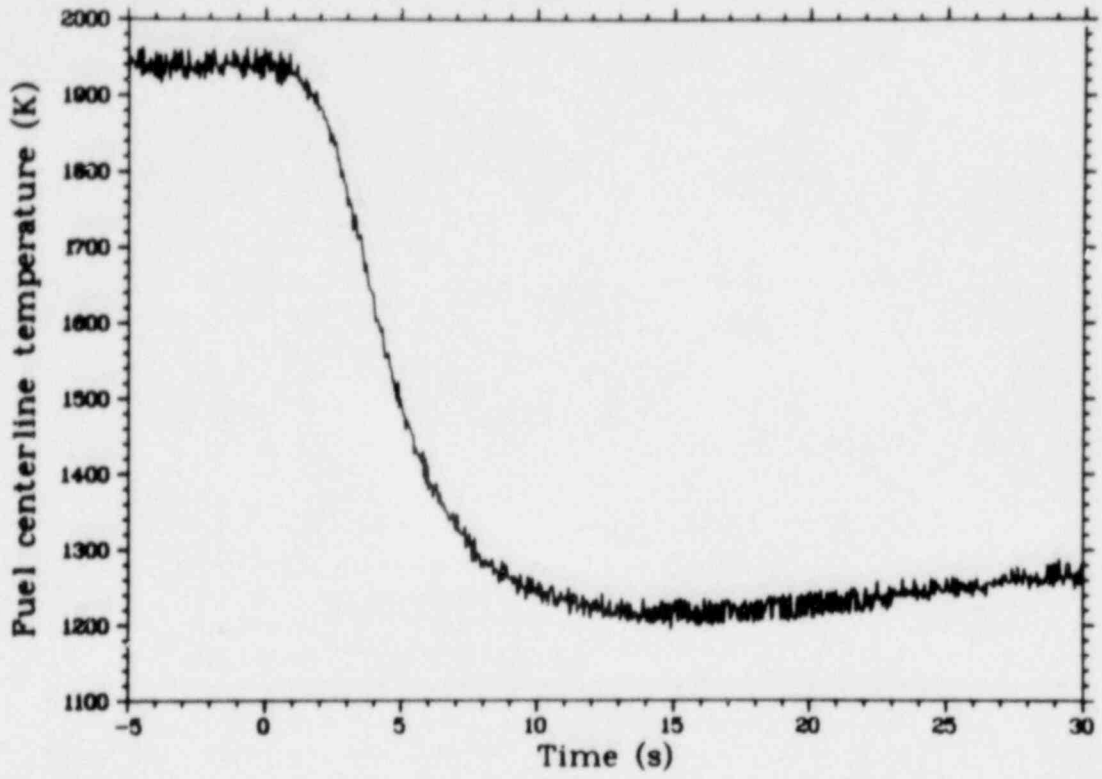

Figure 35. Fuel centerline temperature of Rod 312-1 during Test LLR-3.

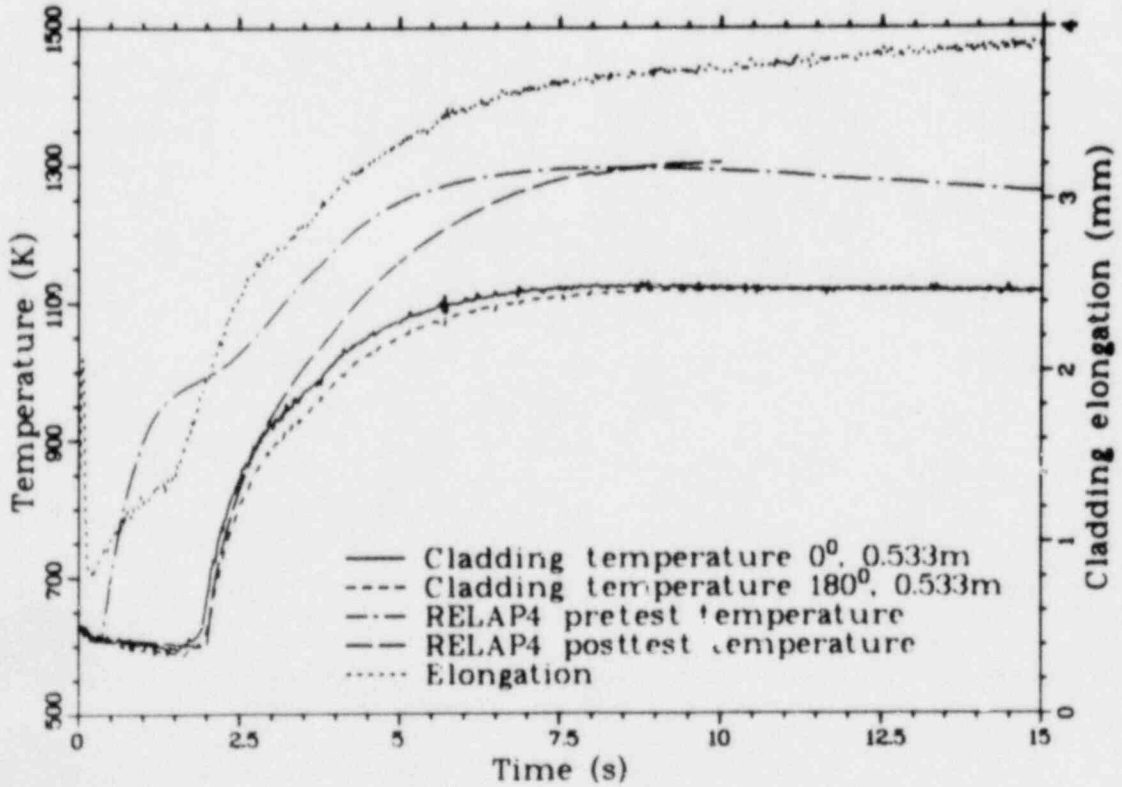

Figure 36. Thermal and mechanical behavior of Rod 312-1 during Test LLR-4.

prior to blowdown. The cladding surface thermocouple data at the 0-degree, 0.533-m thermocouple location indicated that the rod achieved DNB at 1.7 s and reached a maximum surface temperature of 1125 K at 7 s. The 180-degree, 0.533-m thermocouple indicated DNB at 1.7 s and reached a maximum surface temperature of 1120 K at 10 s. The elongation sensor first indicated a moderate increase in cladding length at 0.25 s, then a stronger indication at 1.5 s as DNB started at an elevation probably lower than the cladding thermocouples and propagated up the rod. Again, a possible thermocouple effect on fuel rod response is indicated.

As shown in Figure 37, based on Olsen's criteria, the cladding surface temperature versus fuel rod differential pressure indicates that the cladding at the thermocouple locations was subjected to temperatures slightly above those required to cause waisting at the thermocouple locations. This was confirmed in the postirradiation examination. On the basis of the response of Rod 399-2 during Test LLR-4A, cladding temperatures as high as 1195 K may have been achieved at the 0.314-m location. These temperatures would result in collapse along the lower portion of the fuel rod. This deformation was also confirmed in the postirradiation examination.

The measured fuel centerline temperature at 0.533 m for Rod 312-1 for Test LLR-4 is illustrated in Figure 38. The measured temperature was 2330 K at steady state conditions prior to blowdown.

4.4.1.4 Postirradiation Examination of Rod 312-1—Permanent changes to the cladding of Rod 312-1 occurred as a result of the three successive blowdowns. The visual examination revealed cladding waisting 35 to 55 cm from the bottom of the fuel stack.

A maximum temperature of 1125 K was measured for Rod 312-1 at the 0.533-m location. The cladding microstructure that corresponds to this temperature is the $\alpha + \beta$ transformation regime, which exists in the temperature range of 1100 to 1270 K. Figure 39 presents the cladding microstructure (transverse Section M1-2) at the thermocouple junctions located 0.533 m above the bottom of the fuel stack. Recrystallized, equiaxed α-zircaloy structure is present throughout the entire cladding thickness, including some β precipitates at the grain boundaries, which indicates temperatures in the range of 1100 to 1150 K. A longitudinal section (Section M1-1) was prepared from 0.50 to 0.511 m above the bottom of the heated length in the 0- to 180-degree plane to

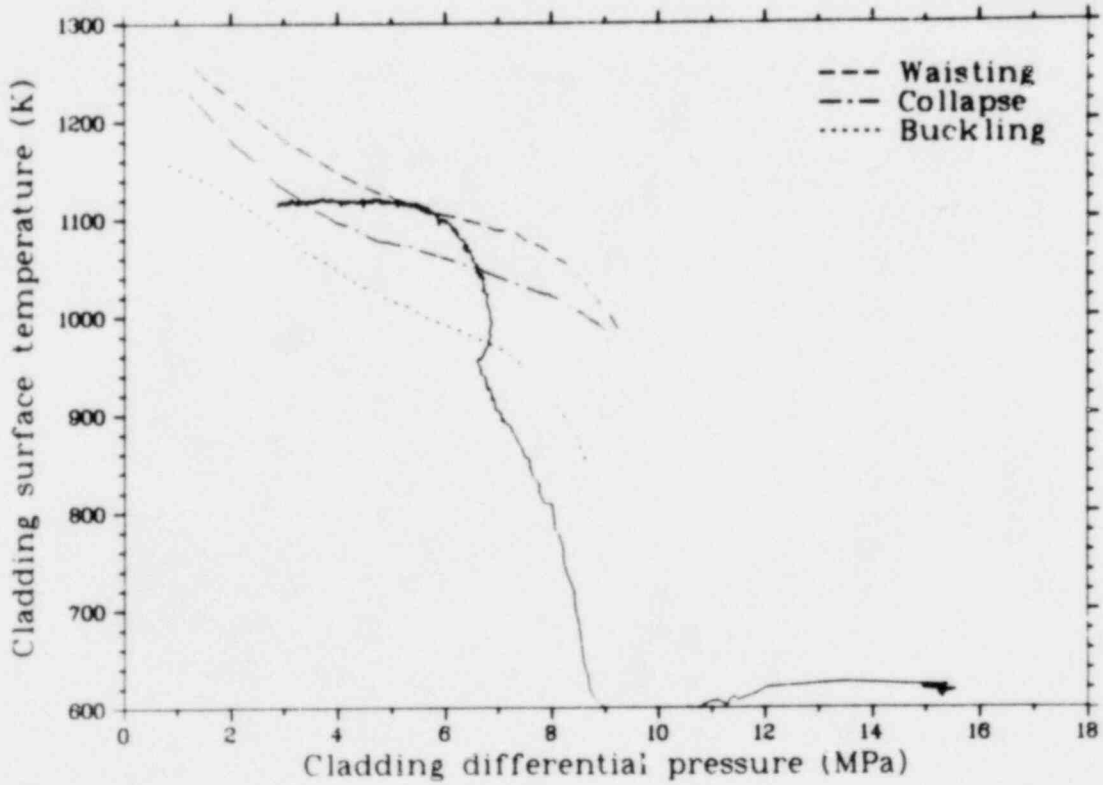

Figure 37. Surface temperature versus fuel rod differential pressure of Rod 312-1 during Test LLR-4.

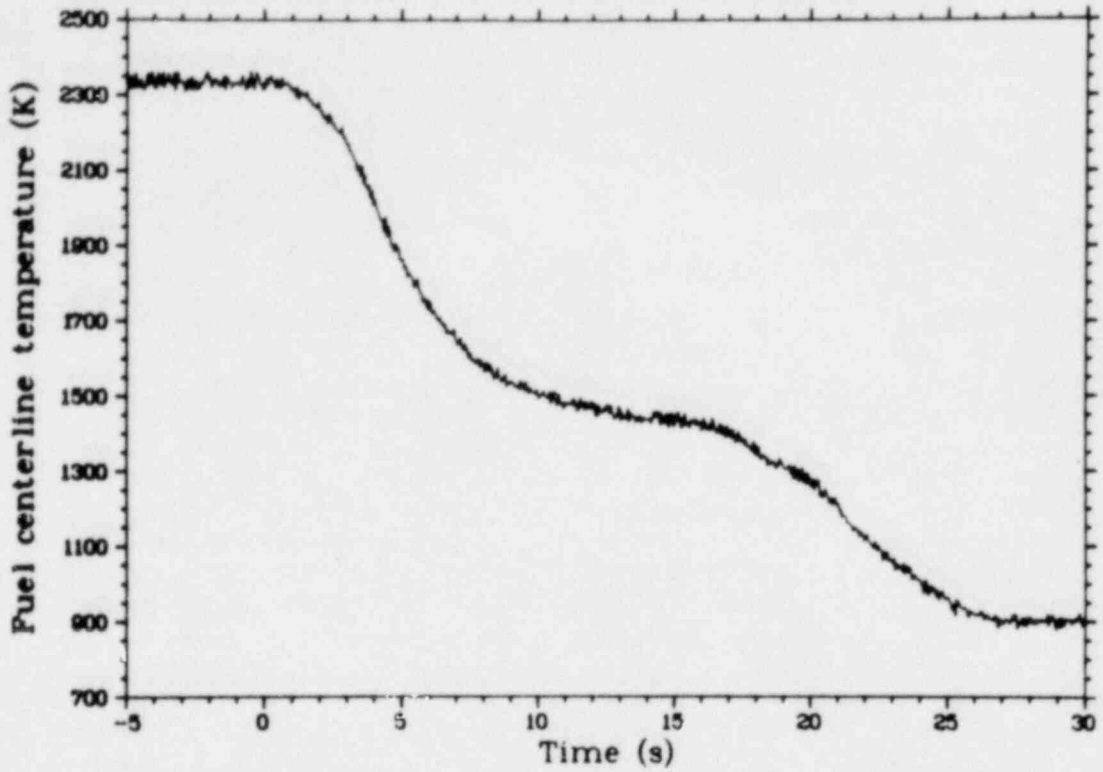

Figure 38. Fuel centerline temperature of Rod 312-1 during Test LLR-4.

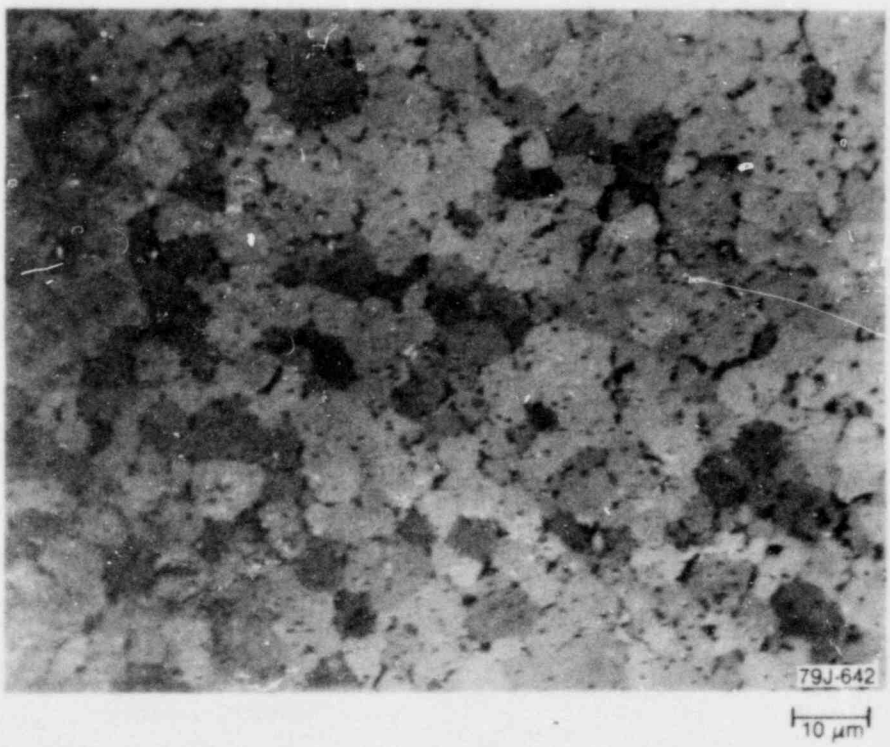

Figure 39. Rod 312-1 transverse cladding microstructure (Sample M1-2) from 0.53 to 0.55 m.

characterize the axial temperature profile of the rod. A microstructure similar to that witnessed on transverse Section M1-2 was observed at 0.50 to 0.511 m.

The measurement of oxide layer thickness, in conjunction with applicable oxide layer growth kinetics, provides an independent estimate of cladding temperatures during testing. The oxide layer on the LLR fuel rods was evaluated to determine the extent of oxide layer growth due to steady state operation and to the increased temperatures during the successive LLR transients. Rod 312-1 was at reactor operating temperatures (600 K) for approximately 241 h. A calculation was performed to determine how much of the observed oxide thickness resulted from this exposure. By using oxidation kinetics, a zirconium dioxide thickness of 0.7 μm was obtained for oxidation during the entire 241 h of preconditioning. A total thickness of 3 μm was measured after the three transients for Rod 312-1. Zirconium dioxide and oxygen-stabilized alpha zirconium layers due to the steam-zircaloy reaction were measured on the external surface of the cladding, and an oxygen stabilized alpha zirconium layer due to the UO_2-zircaloy reaction was measured on the inside surface of the cladding for all the LLR fuel rods. These measurements were made using photomicrographs of the fuel rod. Cladding temperatures were determined from these layers by using the BUILD5[a] computer code, which relates the time at temperature to the thickness of the respective layer, and Leistikow's[a] out-of-pile experiment data. These temperatures are tabulated in Table 9. As shown, the maximum estimated temperatures, T_{ξ},[b] are in the range of 1140 to 1145 K, which are consistent with the maximum measured temperature of 1125 K.

Posttest diametral measurements were made at one orientation along the length of each LLR fuel rod. The data for Rod 312-1 are plotted versus the fuel stack axial length in Figure 40. The rod exhibited collapse, with the maximum diametral decrease of 0.06 mm from 57.1 to 63.7 cm, and a nominal decrease of 0.05 mm from 29.1 to 57.1 cm from the bottom of the active fuel stack. The location of maximum collapse did not correspond to the axial peak power location (45.7 cm), which corresponded to the maximum pretest RELAP4 cladding temperatures. However, the decrease in diameter at this point was only slightly less than the maximum decrease.

An analysis of measured cladding deformation and cladding microstructure was performed and a comparison of these quantities with calculated values for cladding strain was made for all the LLR fuel rods. Permanent plastic radial engineering strains of 0.001 to 0.006, were calculated by the relationship

$$E_r = \frac{D_{pre} - D_{post}}{D_{pre}} \quad (9)$$

where

D_{pre} = pretest rod diameter

D_{post} = posttest rod diameter.

The strain was 0.006 at 0.603 m and 0.0046 at the peak power location (0.457 m), as shown in Figure 41. At the ends of the collapse zones, at 2 and 88.3 cm, the radial strains were zero.

4.4.2 Fuel Rod 312-2. Rod 312-2 was the only fuel rod used for all four LLR tests. A maximum temperature of 1165 K was recorded for this rod during Test LLR-4. Slightly lower cladding temperatures were recorded for Test LLR-4A. On the basis of Olsen's deformation criteria, the rod probably experienced waisting during the Test LLR-4 transient, and thus probably entered the power ramping portion of Test LRR-4A with the maximum deformation expected to occur to any of the LOFT rods during the Power Ascension Tests. During the postirradiation examination, the rod exhibited collapse with some waisting. On the basis of microstructure analysis, temperatures were estimated to be in the range of 1200 to 1270 K at lower (29 cm) elevations on the fuel rod, whereas at the thermocouple locations, temperatures ranged from 1150 to 1200 K. Details of the response of Rod 312-2 during the four transients and postirradiation examination results are presented in the following subsections.

4.4.2.1 Test LLR-3, Rod 312-2—Figure 42 illustrates the cladding temperature, cladding elongation, and coolant midplane temperature response of

a. A detailed explanation of the BUILD5 code and Leistikow's method is included in Reference 3.

b. Combined layers of ZrO_2 and oxygen-stabilized alpha — ξ-layer.

TABLE 9. OXIDATION THICKNESSES AND CORRESPONDING MAXIMUM CLADDING TEMPERATURES

Rod	Specimen	Location[a] (cm)	Orientation[b] (degrees)	Maximum Thickness (μm)			Approximate Maximum Temperature[e] (K)			
				ZrO_2	O[c]	I[d]	ZrO_2	O[b]	T_ζ[f]	Microstructure
312-1	M1-1	50.0 to 51.1 L	0, 180	3.0	2.0	2.5	1115 to 1120	1175 to 1180	1140 to 1145	1100 to 1150
312-1	M1-2	53.3 T	0 to 360	3.0	2.0	2.5	1115 to 1120	1175 to 1180	1140 to 1145	1100 to 1150
312-2	M2-1	27.5 to 29.0 L	90, 270	5.0	5.0	6.0 to 7.0	1150 to 1210	1245 to 1315	1195 to 1260	1200 to 1270
312-2	M2-2	42.0 to 43.5 L	0, 180	4.5	4.0	4.0	1135 to 1200	1220 to 1290	1175 to 1245	1150 to 1200
312-2	M2-3	45.0 to 46.5 L	0, 180	3.5 to 4.0	2.5 to 3.0	Not clear	1105 to 1165	1175 to 1245	1135 to 1200	1150 to 1200
312-2	M2-4	53.3 T	0 to 360	2.5	2.5	>3.0	1040 to 1100	1160 to 1235	1095 to 1155	1050 to 1100
312-3	M3-1	48.4 T	0 to 360	<1.0	None	None	--	--	--	920 to 1100
312-3	M3-2	54.2 T	0 to 360	<1.0	None	None	--	--	--	920 to 1100
312-4	M4-1	27.2 to 29.2 L	90, 270	<1.0	None	None	--	--	--	866 to 920
312-4	M4-2	51.8 T	0 to 360	<1.0	None	None	--	--	--	866 to 920
312-4	M4-3	53.3 T	0 to 360	1.5 to 3.0	Not clear	None	--	--	--	866 to 920
345-1	M5-1	25.4 to 26.9 L	90, 270	4.0	4.0	Not clear	1105 to 1110	1210 to 1215	1155	1150 to 1200
345-1	M5-2	45.7 T	0 to 360	3.5 to 4.0	4.0	0 to 5.0	1095 to 1100	1210 to 1215	1150	1100 to 1150
345-1	M5-3	53.3 T	0 to 360	3.0	2.0	0 to 3.0	1065 to 1070	1135	1090 to 1095	1050 to 1100
345-2	M6-1	25.4 to 26.9 L	90, 270	7.0	4.0	Not clear	1190 to 1195	1210 to 1215	1200 to 1205	1150 to 1200
345-2	M6-2	45.7 T	0 to 360	3.0 to 3.5	3.5 to 4.0	0 to 5.0	1080 to 1090	1190 to 1210	1120 to 1140	1150 to 1200
345-2	M6-3	53.3 T	0 to 360	4.5 to 5.0	2.5	Not clear	1120 to 1130	1160	1130 to 1140	1050 to 1100
399-2	M7-1	25.8 to 27.8 L	0	4.0 to 5.0	3.5 to 4.0	Not clear	1180 to 1190	1240	1205 to 1215	1200 to 1270
399-2	M7-1	25.8 to 27.8 L	180	5.0 to 6.0	4.0 to 4.5	4.0 to 5.0	1240 to 1260	1275 to 1295	1255 to 1275	>1270
399-2	M7-2	29.1 to 31.1 L	180	4.5 to 5.0	4.0 to 5.0	Not clear	1225 to 1230	1275 to 1295	1250 to 1255	1200 to 1270
399-2	M7-3	31.4 T	0	5.0 to 6.0	4.0 to 4.5	None	1240 to 1260	1275 to 1295	1255 to 1275	>1270
399-2	M7-3	31.4 T	90	4.0 to 5.0	3.5 to 4.5	Not clear	1180 to 1190	1250 to 1255	1215 to 1225	1200 to 1270
399-2	M7-3	31.4 T	180	6.0	Not clear	None	1230 to 1240	--	--	1200 to 1270
399-2	M7-3	31.4 T	270	5.0 to 6.0	5.0 to 5.5	None	1240 to 1260	1305 to 1325	1270 to 1290	>1270
399-2	M7-4	45.7 T	0 to 360	4.0	3.5	Not clear	1160 to 1175	1230 to 1235	1190 to 1200	1200 to 1270
399-2	M7-5	65.8 to 67.8 L	90, 270	<1.0	<1.0	None	--	--	--	1100 to 1150

a. Measured from bottom of heated length. T denotes transverse section. L denotes longitudinal section.

b. The 0-degree position for each fuel rod is toward the center of the test assembly, and each degree-orientation is clockwise as viewed from the top of the rod.

c. Outer oxygen-stabilized α-zircaloy phase or oxygen-rich α-zircaloy phase.

d. Inner UO_2-zircaloy reaction layer.

e. BUILD5 calculations were used to estimate temperatures greater than 1270 K from oxidation thicknesses. For temperatures less than 1270 K, a similar calculation was made using Leistikow's out-of-pile experimental data. The difference in temperatures was less than 40 K between these two calculations.

f. Combined layers of ZrO_2 and oxygen-stabilized alpha = ζ layer.

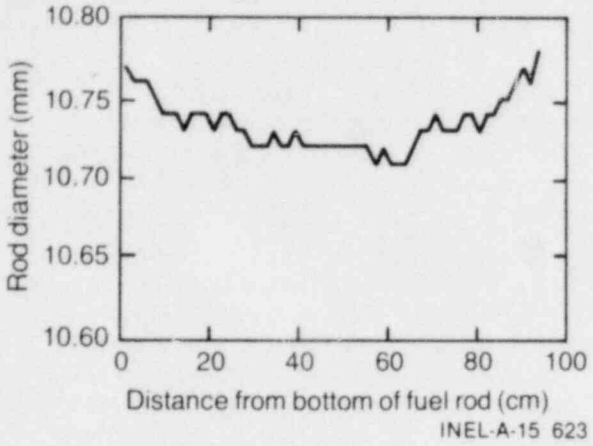

Figure 40. Postirradiation examination measurements of cladding diameter for Rod 312-1.

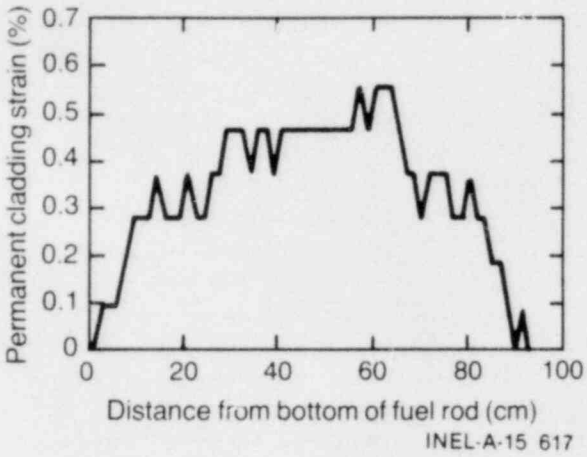

Figure 41. Circumferential strain from posttest diameter measurements of Rod 312-1.

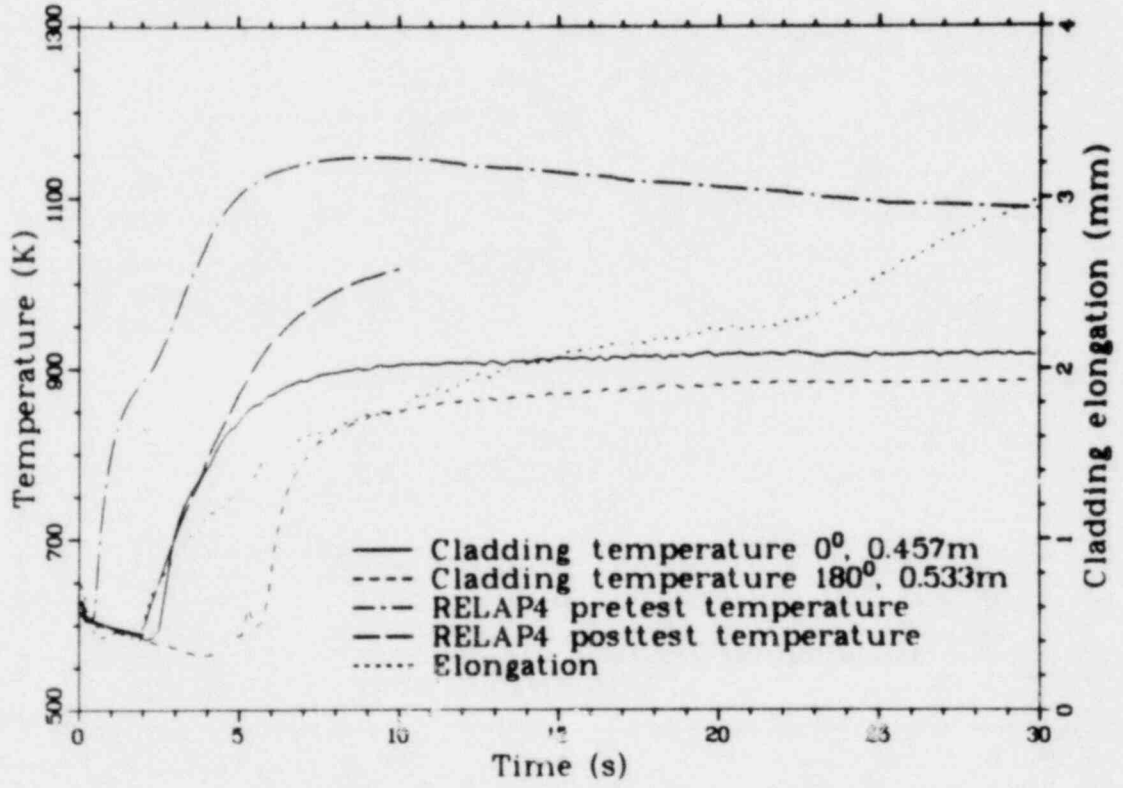

Figure 42. Thermal and mechanical behavior of Rod 312-2 during Test LLR-3.

Rod 312-2 during Test LLR-3, for a 30-s duration. Cladding surface temperature measurements were made on Rod 312-2 at 0.457 and 0.533 m from the bottom of the fuel stack at azimuthal orientations of 0 and 180 degrees, respectively. The calculated difference in rod power between these two locations was approximately 6%, with the 0.457-m location at the highest power, as calculated by RELAP4. The rod peak power for Rod 312-2 was calculated to be 40.8 kW/m just prior to blowdown. The cladding temperature data indicate that the rod achieved DNB at approximately 2.6 s at the 0-degree, 0.457-m thermocouple location, and 4.5 s at the 180-degree, 0.533-m thermocouple location. This circumferential variation in time to CHF, which also occurred for this rod during Test LLR-5, is attributed to the initial rod power distribution, and possibly coolant thermal-hydraulics. Flow channeling or circumferential variations in flow may have existed on the 180-degree side of the fuel rod, which would increase the cladding surface heat transfer coefficient from that of the 0-degree location. The 0.457-m thermocouple measured a maximum cladding temperature of 920 K at 20 s, and the 180-degree thermocouple measured 885 K at 23 s.

As shown by the elongation sensor information in Figure 42, when the transient was initiated with the reactor scram, the rod experienced an axial contraction for approximately 2.0 s until CHF. During the rapid temperature increase for the first 8 s following DNB, the rod experienced an axial elongation to approximately 1.6 mm. The rod continued to elongate to 3.0 mm at 30 s.

The maximum measured cladding temperature is plotted as a function of fuel rod differential pressure in Figure 43. The measured temperature-pressure history falls below the cladding buckling region, as determined by Olsen, which indicates that no permanent cladding deformation would be expected during Test LLR-3.

The measured[a] fuel centerline temperature at 0.457 m for Rod 312-2 for Test LLR-3 is shown in Figure 44 with the corresponding FRAP-T5 calculated centerline temperature response. The initial centerline temperature was 1870 K. The temperature decreased to 1090 K at 10 s when the stored energy was finally redistributed toward the

a. Categorized as trend information.

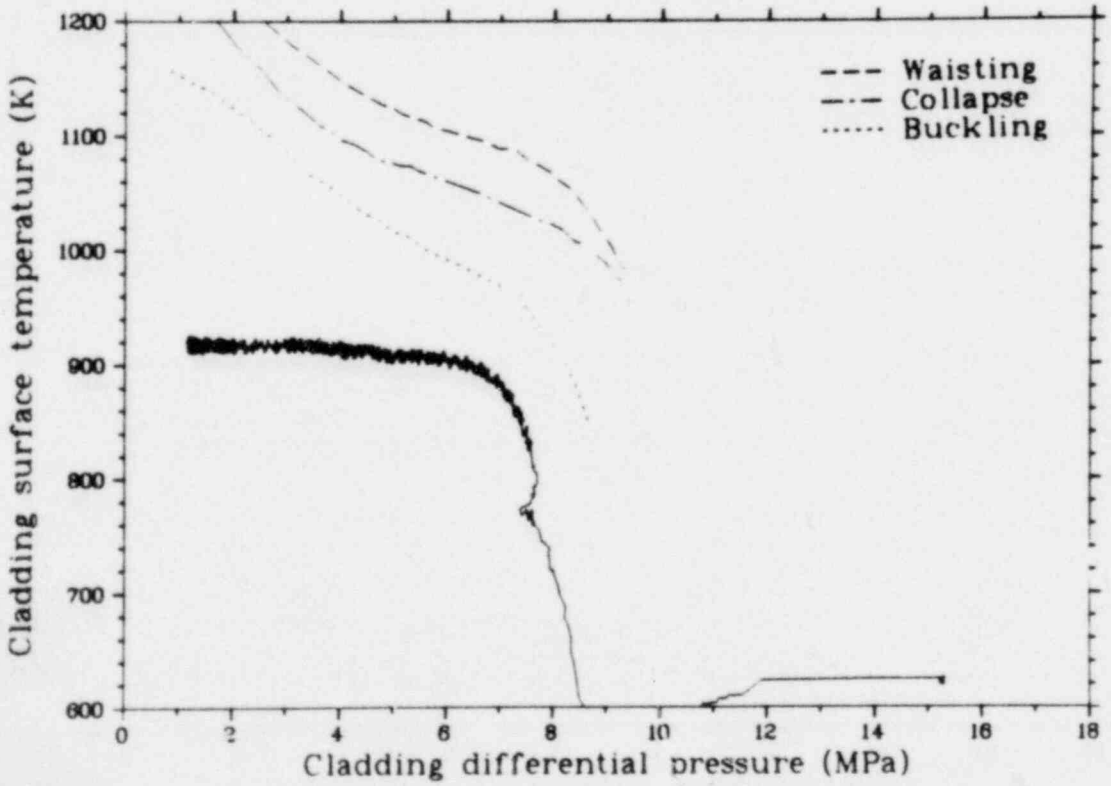

Figure 43. Surface temperature versus fuel rod differential pressure of Rod 312-2 during Test LLR-3.

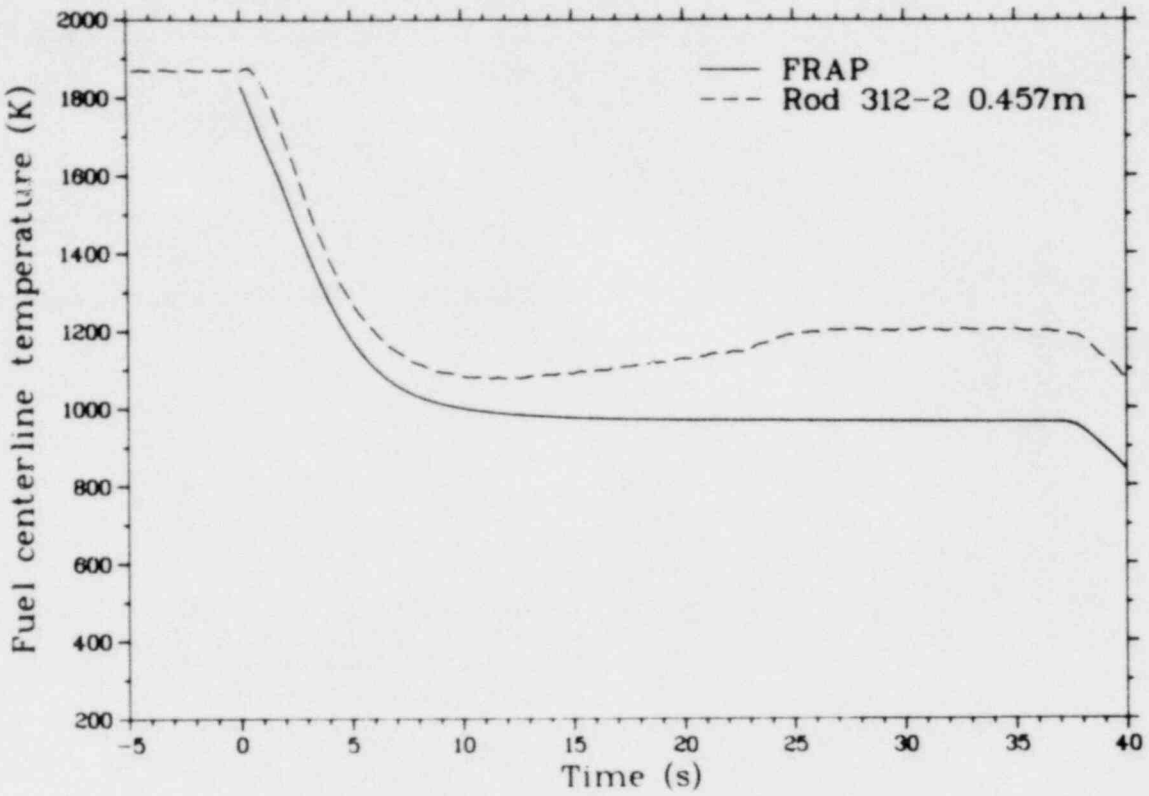

Figure 44. Comparison of measured fuel centerline temperature of Rod 312-2 with FRAP-T5 calculation for Test LLR-3.

periphery of the fuel pellet. At this point, the centerline temperature gradually increased to 1200 K at 25 s, at which time the centerline temperature stabilized and remained essentially constant until the fuel rods were rapidly quenched by the reflood system at 37 s. At quench, the cladding temperatures dropped to 440 K for the remainder of the experiment. The fuel centerline temperature was calculated with FRAP-T5, using the measured cladding temperature at the thermocouple locations as the surface boundary condition to obtain the internal rod dynamics. The modified Ross and Stoute[5] correlation was used for the unpressurized LLR fuel rods to calculate gap conductance. The fuel centerline temperature was undercalculated for the entire transient. The uncertainties that are inherent in these calculations include initial fuel rod power, fuel-to-cladding gap conductance, and UO_2 thermal conductivity.

4.4.2.2 Test LLR-5, Rod 312-2– Figure 45 illustrates the cladding temperature and elongation response of Rod 312-2 during Test LLR-5, for a 30-s duration. The rod peak power of Rod 312-1 was calculated to be 49.3 kW/m just prior to blowdown. The cladding surface thermocouple data at the 0-degree, 0.457-m thermocouple location indicated that the rod achieved DNB at 2.0 s and reached a maximum surface temperature of 1015 K at 10 s. The 180-degree, 0.533-m thermocouple indicated DNB at 2.3 s, rewetting at 2.35 s, a second DNB at 3.3 s, and a maximum surface temperature of 1005 K at 17 s. A comparison of the lower turbine flow rates for this rod with the lower turbine flow rates of the other rods did not indicate any anomalous flow behavior in this shroud. The elongation sensor for this rod failed sometime prior to the transient.

As shown in Figure 46, based on Olsen's criteria, the cladding surface temperature versus differential fuel rod pressure indicates cladding buckling probably occurred at the thermocouple locations during Test LLR-5. However, based on the response of Rod 399-2, since DNB was probably achieved earlier at lower elevations than the thermocouples, estimates of higher temperatures at lower elevations have been made. A temperature of 1030 K was estimated for the 0.314-m location of Rod 312-2. This temperature would also result in local fuel rod buckling at this elevation.

4.4.2.3 Test LLR-4, Rod 312-2– Figure 47 illustrates the cladding temperature and elongation responses of Rod 312-2 during Test LLR-4, for a

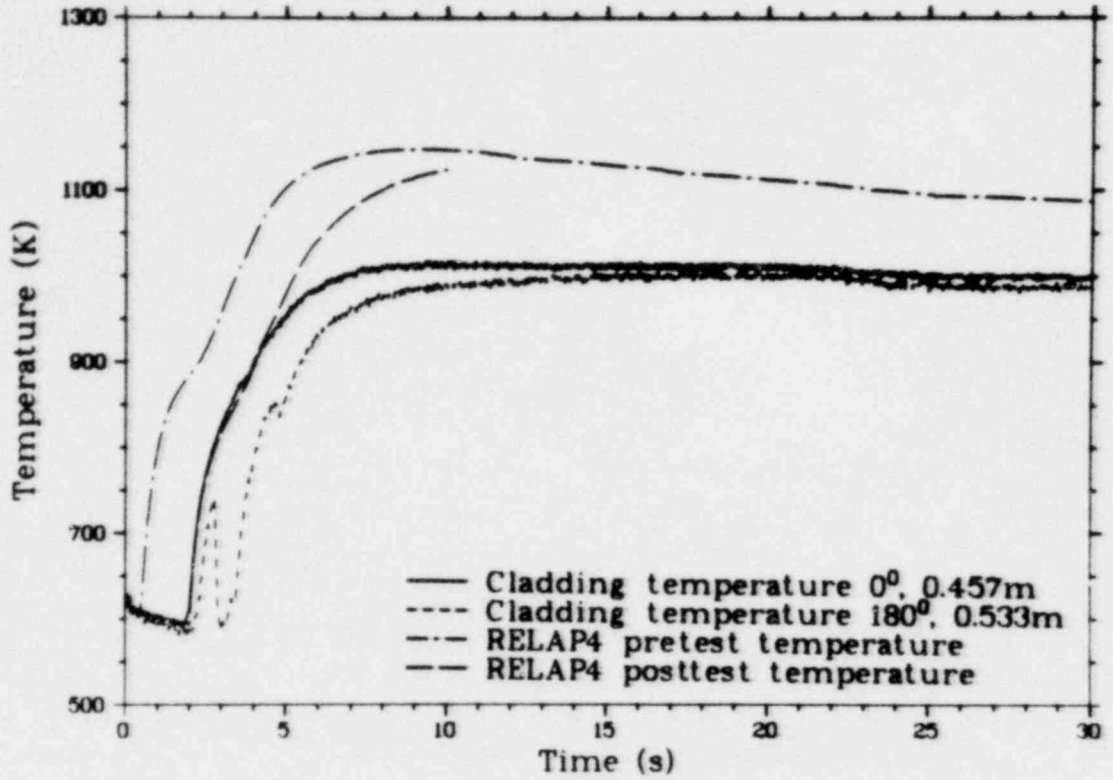

Figure 45. Thermal and mechanical behavior of Rod 312-2 during Test LLR-5.

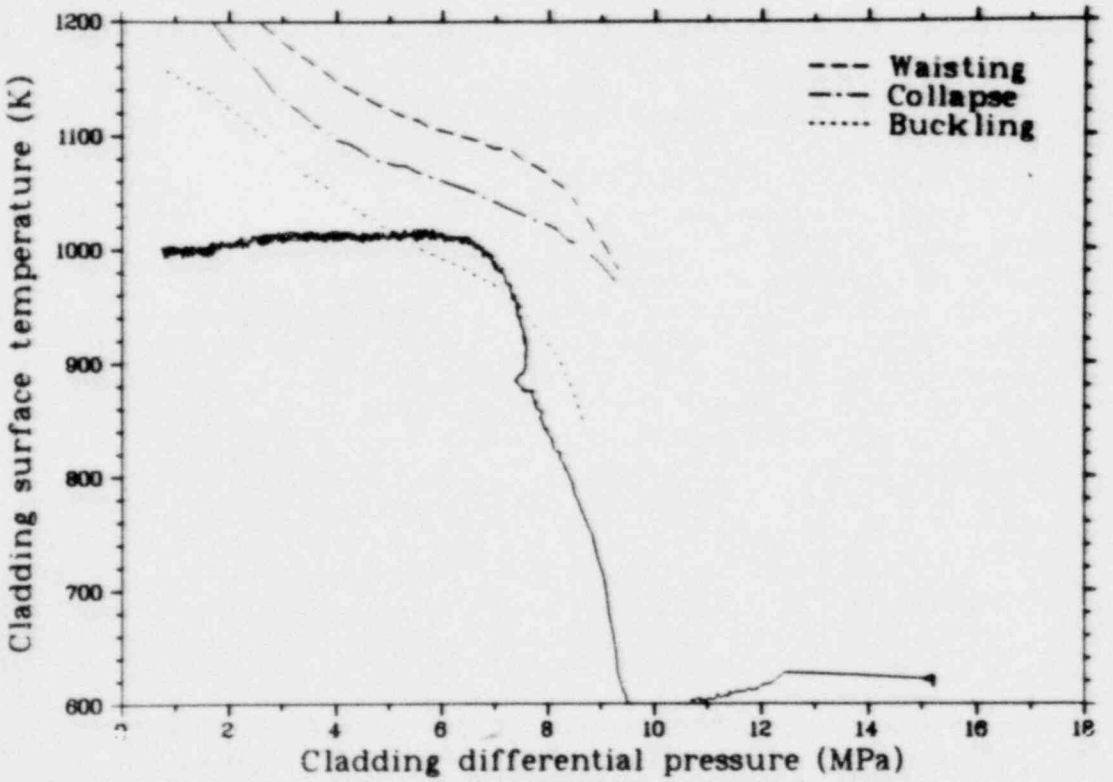

Figure 46. Surface temperature versus fuel rod differential pressure of Rod 312-2 during Test LLR-5.

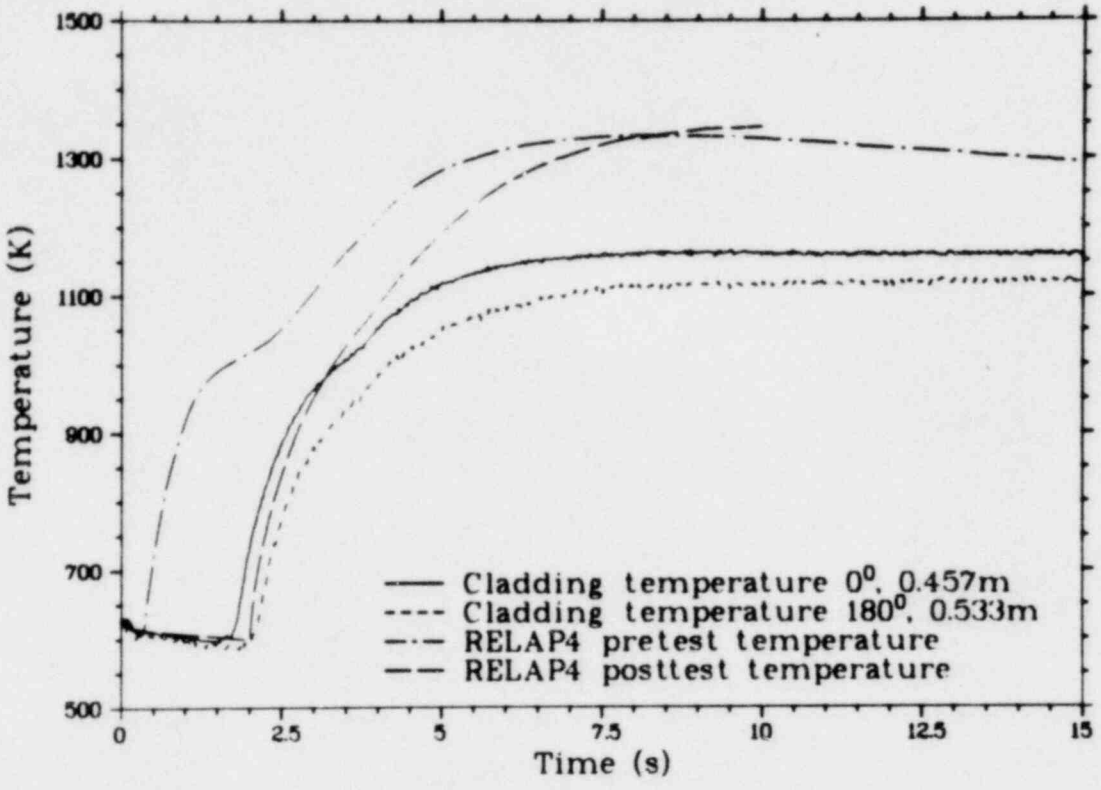

Figure 47. Thermal and mechanical behavior of Rod 312-2 during Test LLR-4.

30-s duration. The rod peak power of Rod 312-2 was calculated to be 55 kW/m just prior to blowdown. The cladding surface thermocouple data at the 0-degree, 0.457-m thermocouple location indicated that the rod achieved DNB at 1.6 s and reached a maximum surface temperature of 1165 K at 8 s. The 180-degree, 0.533-m thermocouple indicated DNB at 2.0 s and a maximum surface temperature of 1120 K at 15 s. The elongation sensor for this rod was not operable for this test.

As shown in Figure 48, based on Olsen's criteria, the cladding surface temperature versus fuel rod differential pressure indicates that the cladding was subjected to temperatures slightly above those required to cause waisting at the thermocouple locations. Cladding temperatures as high as 1205 K may have been achieved at the 0.314-m location, which would also result in waisting at this location.

4.4.2.4 Test LLR-4A, Rod 312-2—Figure 49 illustrates the cladding temperature and elongation response of Rod 312-2 during Test LLR-4A, for a 30-s duration. The rod peak power of Rod 312-2 was calculated to be 50.6 kW/m just prior to blowdown. The cladding surface thermocouple data at the 0-degree, 0.457-m thermocouple location indicated that the rod achieved DNB at 1.9 s and reached a maximum surface temperature of 1150 K at 6 s. The 180-degree, 0.533-m thermocouple indicated DNB at 2.1 s and reached a maximum surface temperature of 1065 K at 13 s. The LVDT first indicated a moderate increase in cladding length at 0.25 s, with more pronounced increases at 0.8 and 1.5 s, as DNB started at an elevation probably lower than the cladding thermocouples and propagated up the rod. This indicates a possible thermocouple effect on fuel rod response.

As shown in Figure 50, based on Olsen's criteria, the cladding surface temperature versus fuel rod differential pressure indicates that the cladding was subjected to temperatures above those required to cause waisting at the thermocouple locations. This deformation was not confirmed in the postirradiation examination (PIE), as only collapse was evident at the thermocouple locations. However, cladding temperatures as high as 1205 K may have been achieved at the 0.314-m location, which, based on Olsen's criteria, would result in waisting at this location. This deformation was confirmed in the PIE.

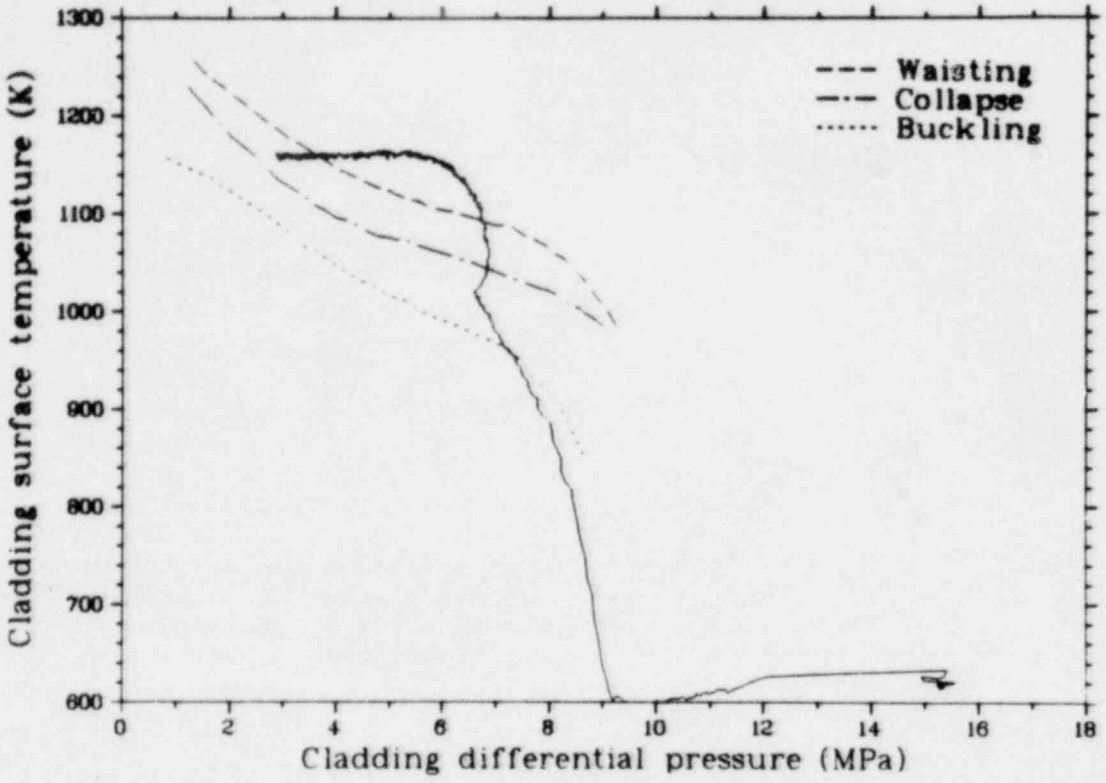

Figure 48. Surface temperature versus fuel rod differential pressure of Rod 312-2 during Test LLR-4.

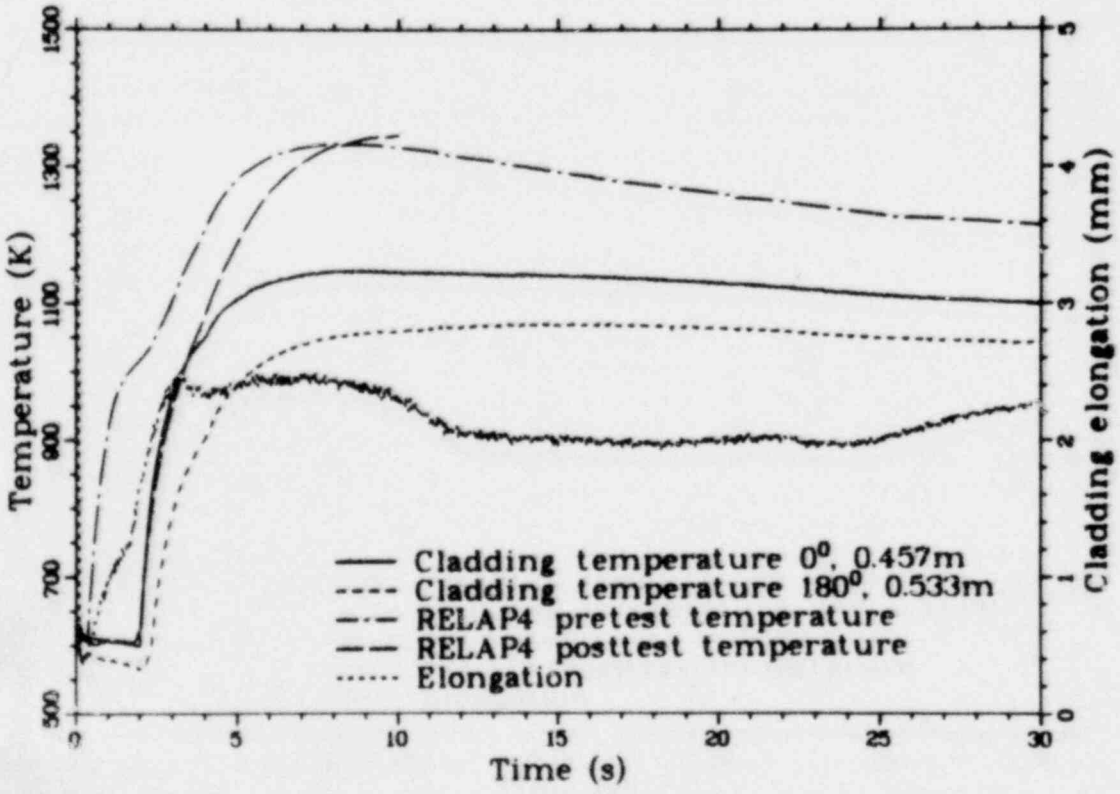

Figure 49. Thermal and mechanical behavior of Rod 312-2 during Test LLR-4A.

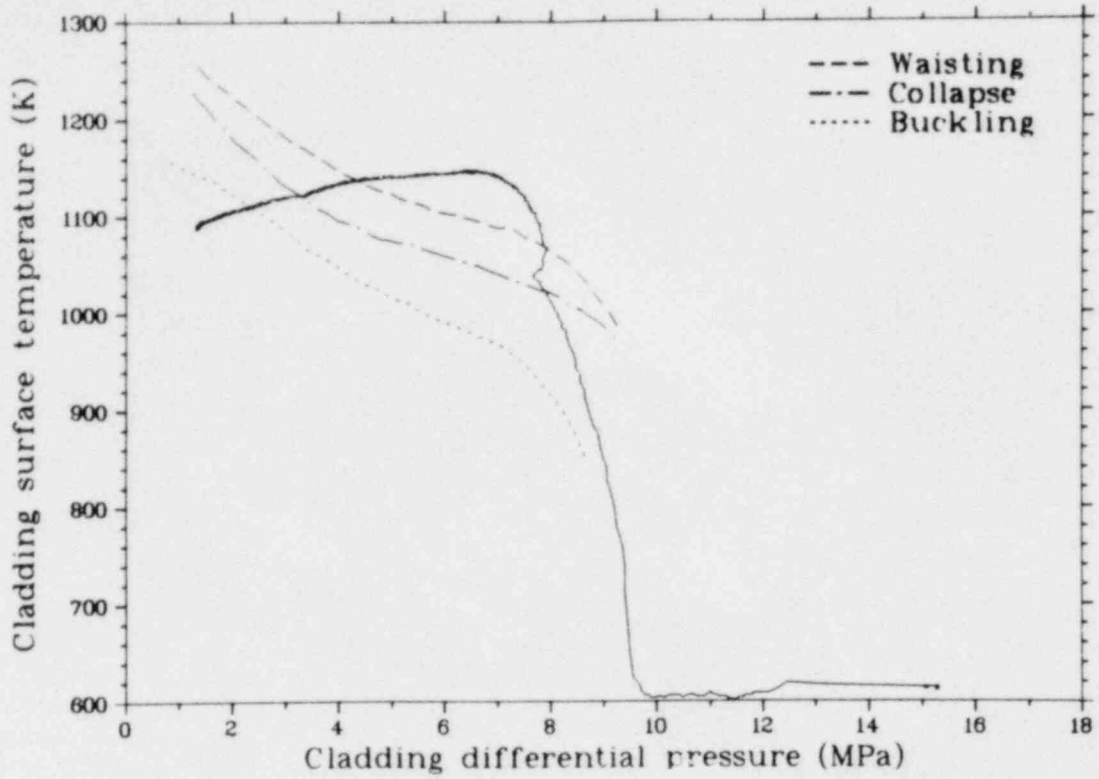

Figure 50. Surface temperature versus fuel rod differential pressure of Rod 312-2 during Test LLR-4A.

4.4.2.5 Postirradiation Examination of Rod 312-2—Permanent changes to the cladding of Rod 312-2 occurred as a result of the four successive blowdowns. During the visual examination the rod showed waisting 27 to 37 cm above the bottom of the fuel stack.

A maximum temperature of 1165 K was measured for Rod 312-2 at the 0.457-m location. The cladding microstructure that corresponds to this temperature is the $\alpha + \beta$ transformation regime, which exists in the temperature range of 1100 to 1270 K. Figure 51 presents the cladding microstructure (longitudinal Section M2-3) at the thermocouple junction located 0.457 m above the bottom of the fuel stack. The microstructure showed an $\alpha + \beta$ zircaloy structure throughout the entire cladding thickness, which indicates temperatures in the range of 1150 to 1200 K. A longitudinal section (Section M2-1) was made from 0.275 to 0.29 m above the bottom of the heated length in the 90- and 270-degree plane to characterize the axial temperature profile of the rod. The microstructure consisted of a high concentration of prior β zircaloy, with a low concentration of equiaxed α zircaloy. The approximate temperature range for this structure is 1200 to 1270 K.

Rod 312-2 was at reactor operating temperatures (600 K) for approximately 264 h. A calculation was performed to determine how much of the observed oxide thickness resulted from this exposure. By using oxidation kinetics, a zirconium dioxide thickness of 0.7 μm was obtained for oxidation during the entire 264 h of preconditioning. A total thickness of 2.5 μm was measured at the thermocouple locations after the four transients for Rod 312-2. Cladding temperatures determined from the oxide layers are tabulated in Table 9. The maximum estimated temperatures, T_ξ, are in the range of 1135 to 1200 K at the 45-cm axial level.

The posttest diametral measurements for Rod 312-2 are plotted versus the fuel stack axial length in Figure 52. The rod exhibited collapse, with a maximum diametral decrease of 0.07 mm from 59.8 to 64 cm and an azimuthal decrease of 0.06 mm from 12 to 54 cm from the bottom of the active fuel stack. The location of maximum collapse did not correspond to the axial location of maximum power (45.7 cm). The decrease in diameter at this point was somewhat lower than the maximum decrease. Rod 312-2 exhibited the permanent plastic radial engineering strains [as expressed by Equation (9)] shown in Figure 53. The strain was

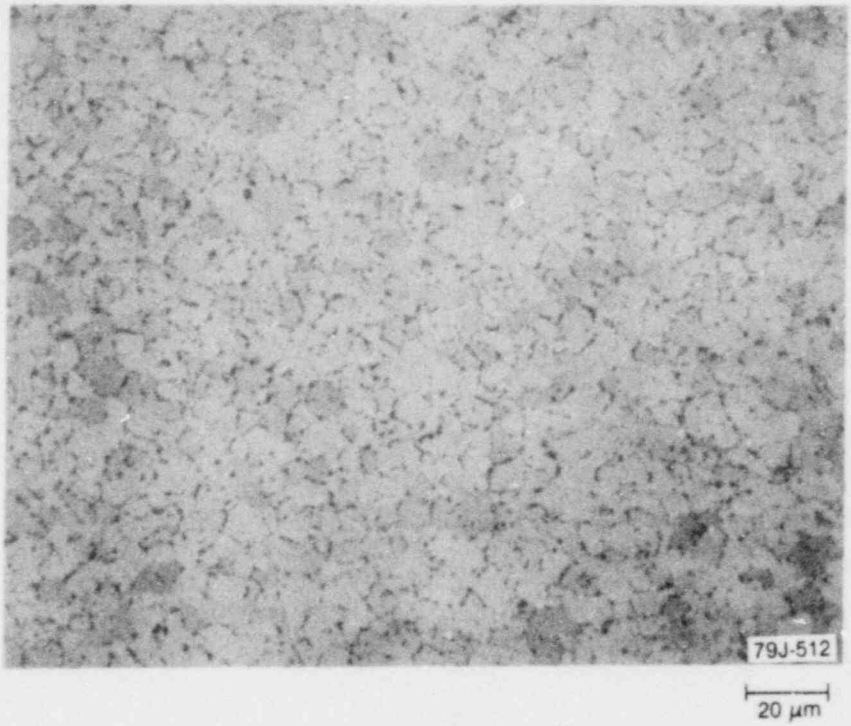

Figure 51. Rod 312-2 longitudinal cladding microstructure (Sample M2-3) at 0.457 m.

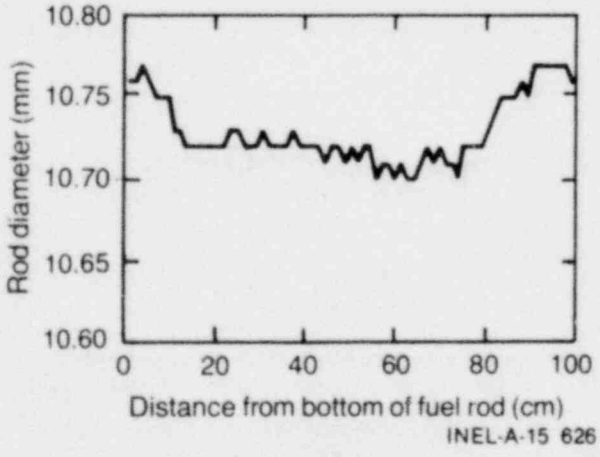

Figure 52. Postirradiation examination measurements of cladding diameter for Rod 312-2.

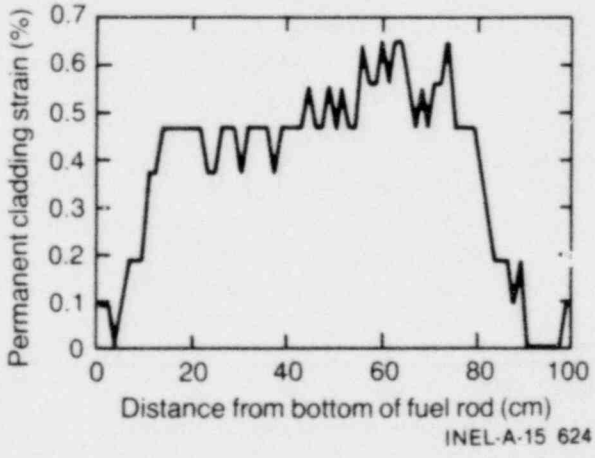

Figure 53. Circumferential strain from posttest diameter measurements of Rod 312-2.

0.0065 at 0.603 m, and 0.0055 at the peak power location (0.457 m). At the ends of the collapse zones, at 2 and 88.3 m, the radial strains were zero.

4.4.3 Fuel Rod 312-3. Rod 312-3 was used for Test LLR-3. Although only recording temperatures as high as 990 K during the test, the rod ballooned and failed during the transient due to being waterlogged sometime during the power ramping portion of the test. The rod was visibly ballooned upon removal for postirradiation examination. On the basis of microstructure analysis, temperatures were estimated to be in the range of 920 to 1100 K at the boundary of deformation. Details of the response of Rod 312-3 during Test LLR-3 and postirradiation examination results follow in the subsequent subsections.

4.4.3.1 Test LLR-3, Rod 312-3—Figure 54 illustrates the cladding temperature and cladding elongation response of Rod 312-3 during Test LLR-3, for a 30-s duration. The peak power of Rod 312-3 was calculated to be 39.5 kW/m prior to blowdown. The cladding temperature data indicate that the rod achieved DNB at both thermocouple locations at approximately 2.5 s. The cladding elongation transducer indicated a sharp increase at 2.0 s. The 0-degree thermocouple indicated a maximum cladding temperature of 965 K at 8 s, whereas the 180-degree thermocouple indicated 990 K at 12.3 s.

Rod 312-3 attained the highest measured cladding temperature of all four rods in Test LLR-3. Reactor physics pretest calculations had indicated that the use of stainless steel and zircaloy shrouded rods would provide a power tilt between the rods of 0.87 and 1.0, respectively. During the preconditioning portion of the test, the calculated figure-of-merit for this stainless steel shrouded rod had consistently indicated rod powers comparable to the high power (zircaloy shrouded) rods. Following the test, a high level of radiation was detected in the blowdown tank, indicating possible failure of one or more of the test rods. Rod 312-3 was found to have failed during the blowdown transient due to waterlogging, resulting in subsequent ballooning (up to 50% diameter increase) and rupture at the 180-degree plane. The plenum pressure in Rod 312-3, which had consistently indicated a high value (saturation of the sensor at 7.2 MPa), followed the system depressurization quite closely after the rod apparently

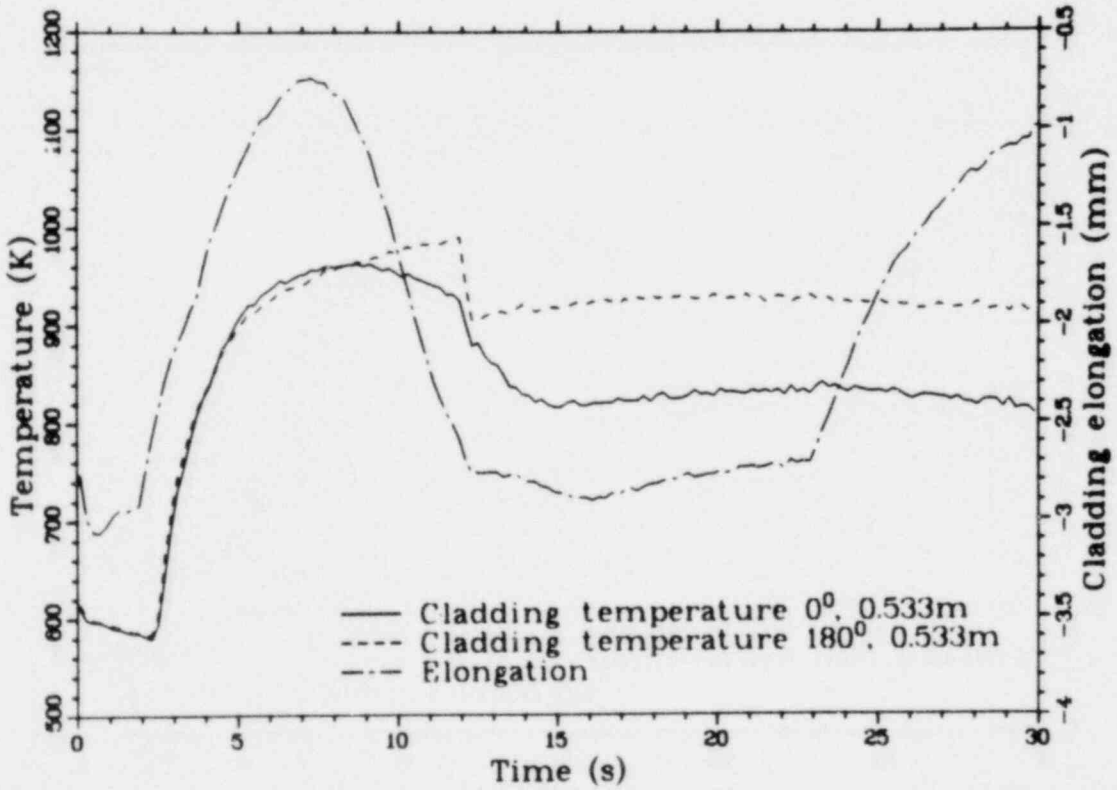

Figure 54. Thermal and mechanical behavior of Rod 312-3 during Test LLR-3.

burst at 12.3 s. A comparison of the Rod 312-3 plenum pressure response with the svtem pressure is shown in Figure 55. The response of the pressure transducer in Rod 312-3 indicated that the rod apparently failed when the system pressure reached approximately 5 MPa. Apparently, Rod 312-3 had a small leak in the cladding throughout the test, which would account for the saturated (7.2 MPa) indication by the plenum pressure transducer and would permit waterlogging, which resulted in ballooning and rupture during the blowdown. Upon ballooning at 12.3 s, the gap conductance was significantly reduced, resulting in a sudden decrease in cladding temperature. Figure 29 presents a photograph of Rod 312-3 that shows the ballooned region.

When the transient was initiated with the reactor scram, the rod experienced a rapid axial contraction for approximately 0.7 s. The fuel rod length then increased slightly until 2.0 s, when a dramatic increase in cladding length was recorded until 7.5 s. At this time, the elongation sensor indicated a contraction until 12.3 s. This is attributed to the differential pressure across the rod causing ever increasing ballooning and, thus, relaxation of the fuel-cladding interfacial contact. The elongation sensor also indicated a subsequent increase at 22 s with the opening of the second cold leg blowdown valve.

The fuel centerline thermocouple at 0.533 m on Rod 312-3 failed prior to the transient.

4.4.3.2 Postirradiation Examination of Rod 312-3– Rod 312-3 was visibly ballooned from 0.46 to 0.54 m from the bottom of the rod.

A maximum temperature of 990 K was measured for Rod 312-3 at the 180-degree, 0.533-m location. The cladding microstructure that corresponds to this temperature is the high α-zircaloy regime, which exists in the temperature range of 920 to 1100 K. Figure 56 presents the cladding microstructure (transverse Section M3-2) at 0.54 m from the bottom of the heated length. Equiaxed α-zircaloy structure is present throughout the entire cladding thickness. The oxide layer on Rod 312-3 was not evaluated since the oxide thickness was extremely small. The posttest diametral measurements for Rod 312-3 are plotted versus the fuel stack axial length in Figure 57. The rod exhibited ballooning, with the maximum diametral increase of 5.7 mm along the rod midsection at 50 cm from the bottom of the active fuel

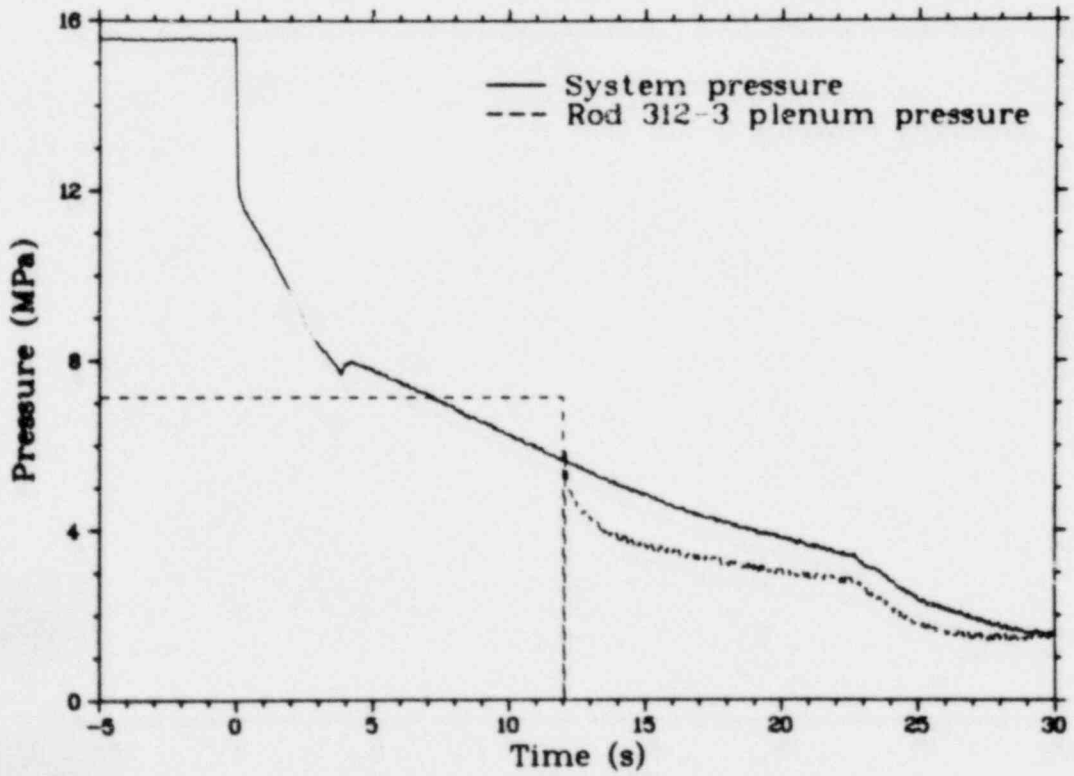

Figure 55. Rod 312-3 plenum pressure and system pressure versus time during Test LLR-3.

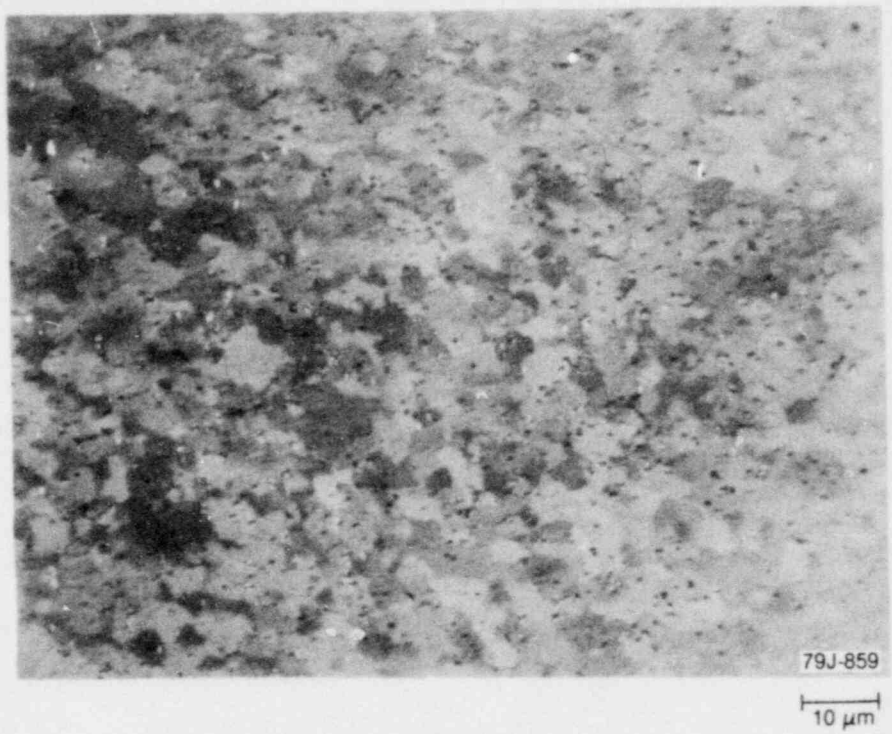

Figure 56. Rod 312-3 transverse cladding microstructure (Sample M3-2) from 0.48 to 0.50 m.

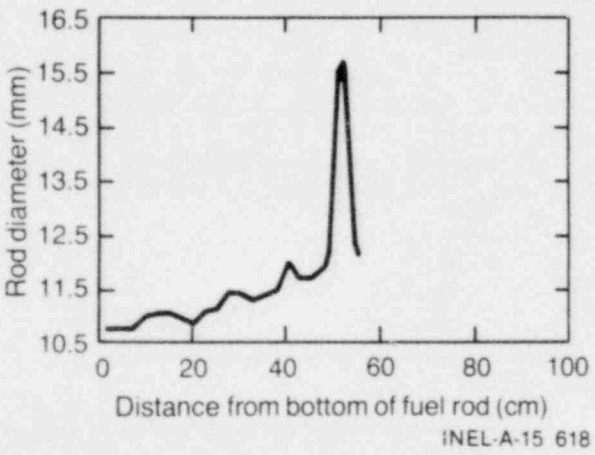

Figure 57. Postirradiation examination measurements of cladding diameter for Rod 312-3.

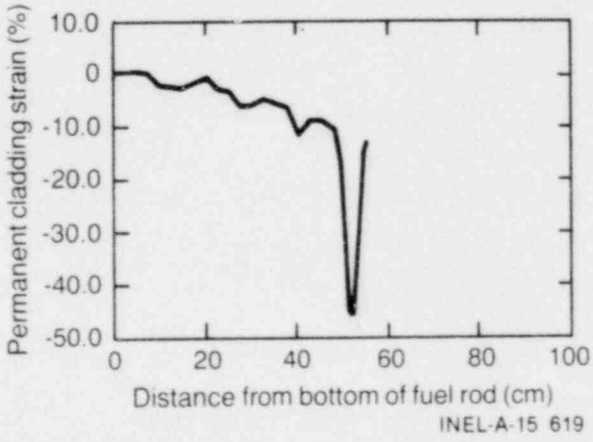

Figure 58. Circumferential strain from posttest diameter measurements of Rod 312-3.

stack. Permanent plastic radial engineering strains as expressed by Equation (9) are shown in Figure 58. The strain was 0.006 at 0.603 m, and 0.0046 at the peak power location (0.457 m). At the ends of the ballooning zones, at 2 and 88.3 cm, the radial strains were zero.

4.4.4 Fuel Rod 312-4. Rod 312-4 was used for Test LLR-3. A maximum temperature of 880 K was recorded for this rod during the transient. Removal of the rod after this test for postirradiation examination provided the opportunity to study the effects of one low power test on LOFT-type peripheral rods. The rod exhibited minor deformation as a result of the test. On the basis of microstructure analysis, temperatures were estimated to be in the range of 866 to 920 K at the thermocouple locations and on lower portions of

the rod. Details of the response of Rod 312-4 during the test and postirradiation results follow in the subsequent subsections.

4.4.4.1 Test LLR-3, Rod 312-4—Figure 59 illustrates the cladding temperature and elongation responses of Rod 312-4 during Test LLR-3, for a 30-s duration. The peak power of Rod 312-4 was calculated to be 34.3 kW/m just prior to blowdown. The cladding temperature data indicate that the rod achieved DNB at approximately 2.4 s at both thermocouple locations. The cladding elongation transducer indicated a sharp increase at 1.8 s. The 0-degree thermocouple measured a maximum cladding temperature of 880 K at 22 s. The 180-degree thermocouple essentially followed the 0-degree thermocouple for the entire transient.

The cladding elongation sensor for this stainless steel shrouded rod was biased because of the variation in thermal expansion between the stainless steel and zircaloy interface junction. During the rapid temperature increase for the first 8 s following DNB, the rod experienced a minimal axial strain. The rod elongated a total of 3.15 mm during the blowdown transient.

The measured cladding temperature is plotted as a function of fuel rod differential pressure in Figure 60. The measured temperature-pressure history falls below the cladding buckling region, as determined by Olsen, which indicates that no permanent cladding deformation would be expected to have occurred to Rod 312-4 during Test LLR-3.

The fuel centerline thermocouple for Rod 312-4 failed prior to Test LLR-3.

4.4.4.2 Postirradiation Examination of Rod 312-4—Rod 312-4 showed no observable deformation. A maximum temperature of 880 K was measured for Rod 312-4 at the 0.533-m location. The cladding microstructure that corresponds to this temperature is the mixed stress-relieved and preequiaxed α-phase, which exists in the temperature range of 866 to 920 K. Figure 61 presents the cladding microstructure (transverse Section M4-3) in the plane of the 0- and 180-degree thermocouple junctions located 0.533 m above the bottom of the fuel stack. Mixed stress-relieved and preequiaxed α-zircaloy structure is present throughout the entire cladding thickness. A longitudinal section (Section M4-1)

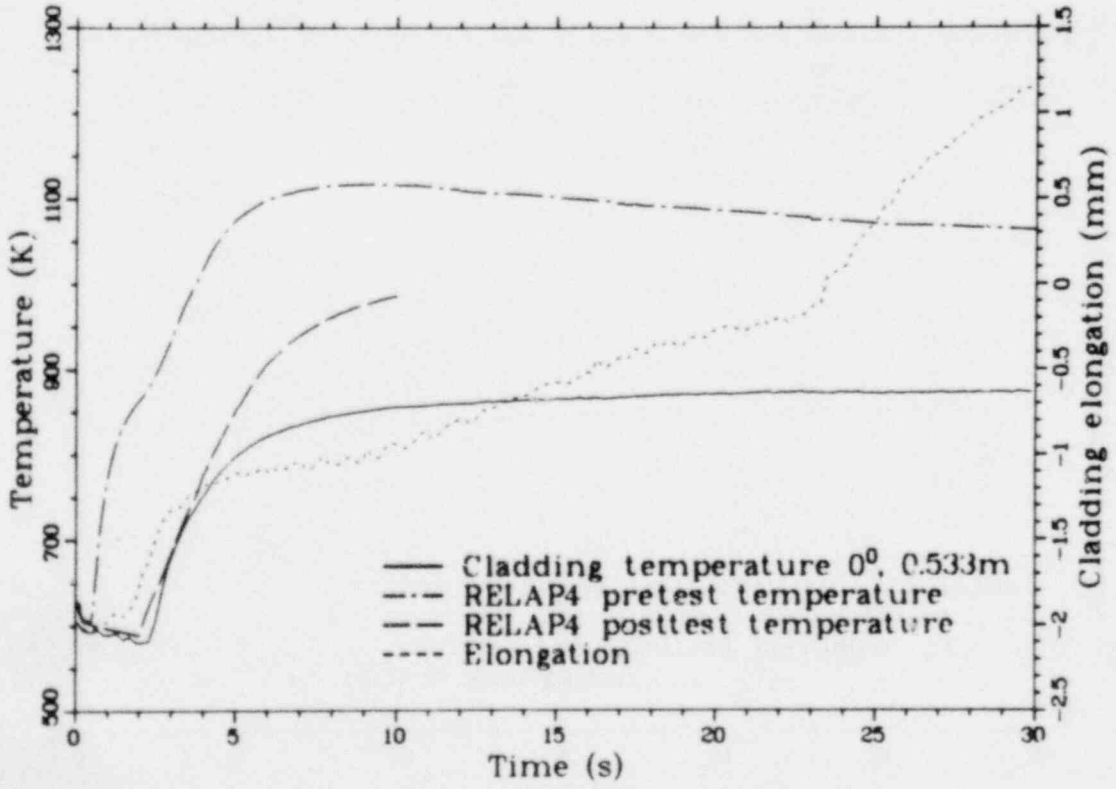

Figure 59. Thermal and mechanical behavior of Rod 312-4 during Test LLR-3.

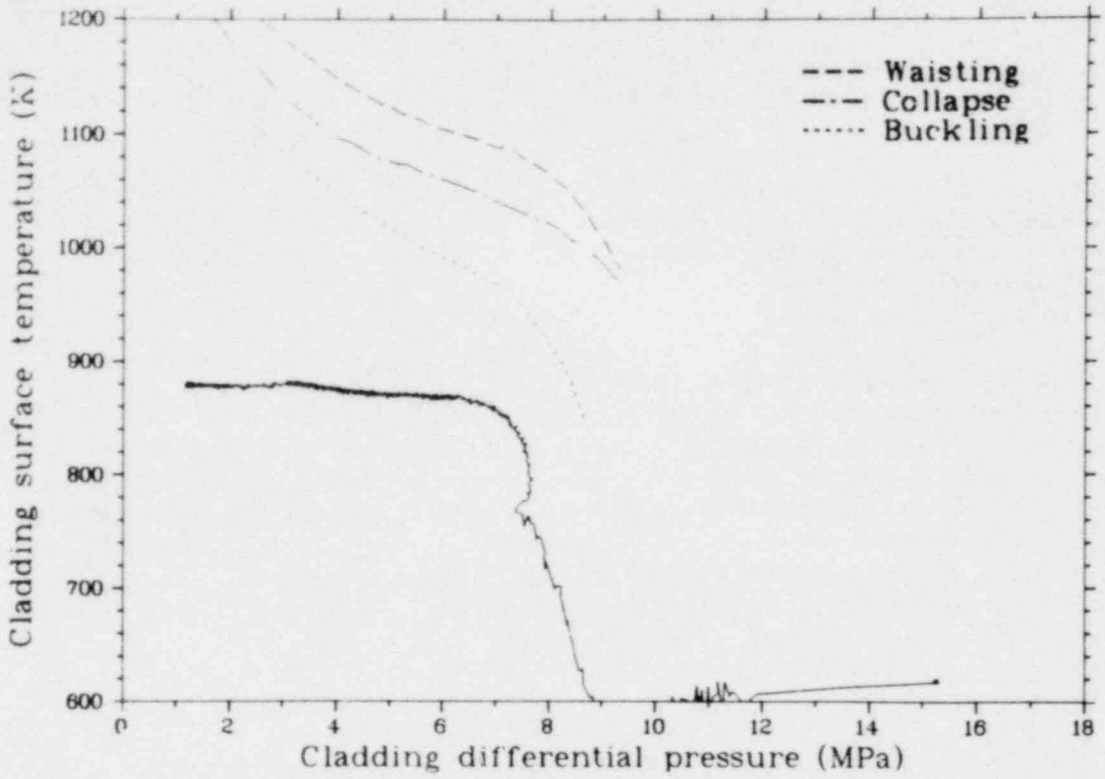

Figure 60. Surface temperature versus fuel rod differential pressure of Rod 312-4 during Test LLR-3.

Figure 61. Rod 312-4 transverse cladding microstructure (Sample M4-3) from 0.53 to 0.55 m.

from 0.27 to 0.29 m in the 90- and 270-degree plane above the bottom of the heated length was used to characterize the axial temperature profile of the rod at the most severely damaged region, anticipated to be below the thermocouples. The microstructure consisted of mixed stress-relieved and preequiaxed α-zircaloy. The approximate temperature range for this structure is also 866 to 920 K. The oxide layer on Rod 312-4 was not visible, and therefore was not evaluated.

The posttest diametral measurements for Rod 312-4 are plotted versus the fuel stack axial length in Figure 62. The rod exhibited a slight amount of collapse, with the maximum diametral decrease of 0.08 mm along the rod midsection from 0.34 to 0.64 m from the bottom of the active fuel stack. The location of maximum collapse occurred at 40 cm. Permanent plastic engineering strains as expressed by Equation (9) are shown in Figure 63. The strain was 0.0095 at 0.40 m, and 0.007 at the peak power location (0.457 m).

4.4.5 Fuel Rod 345-1. Following Test LLR-3, the two stainless steel shrouded rods (312-3 and -4) were replaced with two fresh, unirradiated, zircaloy shrouded rods, Rods 345-1 and 345-2. Rod 345-1 was used for Tests LLR-5, -4, and -4A. A maximum temperature of 1070 K was recorded for this rod during Test LLR-4A . During the postirradiation examination, the rod exhibited collapse with some waisting. On the basis of microstructure analysis. temperatures were estimated to be in the range of 1150 to 1200 K from 25 to 45 cm from the bottom of the heated length. Details of the response of Rod 345-1 during the three transients and postirradiation results are presented in the following subsections.

4.4.5.1 Test LLR-5, Rod 345-1—Figure 64 illustrates the cladding temperature, cladding elongation, and coolant midplane temperature response of Rod 345-1 during Test LLR-5, for a 30-s duration. The peak power of Rod 345-1 was calculated to be 41.9 kW/m just prior to blowdown. The cladding temperature data indicate that the rod achieved DNB at approximately 1.8 s at the 0-degree, 0.533-m thermocouple location, whereas the 180-degree, 0.533-m thermocouple indicated DNB at 1.9 s. The cladding elongation transducer indicated a sharp increase at 1.4 s. The 0-degree thermocouple indicated a maximum cladding temperature of 1000 K at 17 s, whereas the 180-degree thermocouple indicated 985 K at 22 s.

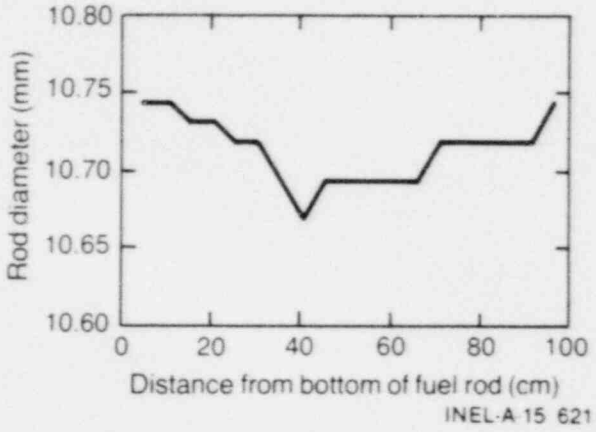

Figure 62. Postirradiation examination measurements of cladding diameter for Rod 312-4.

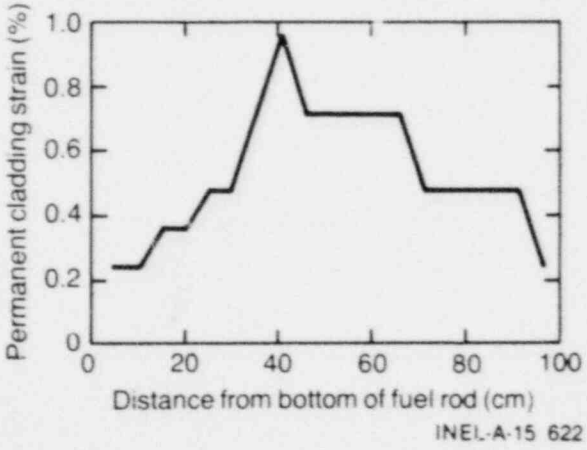

Figure 63. Circumferential strain from posttest diameter measurements of Rod 312-4.

For the first 5 s of the Test LLR-5 transient, Rod 345-1 exhibited anomalous behavior compared with the other rods in the test, rewetting at 3.8 and 4.3 s before drying out and reaching maximum cladding temperatures. Comparison of the lower turbine flowmeter for this rod with the other rod flowmeters revealed larger flows for the Rod 345-1 shroud during the first 5 s of the transient. This is attributed to a malfuctioning check valve, which allowed flow to enter from the upper plenum. Upon replacement of this check valve for Test LLR-4A, the rewet phenomenon evidenced in this test and Test LLR-4 was not witnessed.

During the rapid temperature increase for the first 8 s following DNB, the rod experienced an axial elongation of approximately 1.7 mm. The rod continued to elongate to 2.2 mm at 30 s.

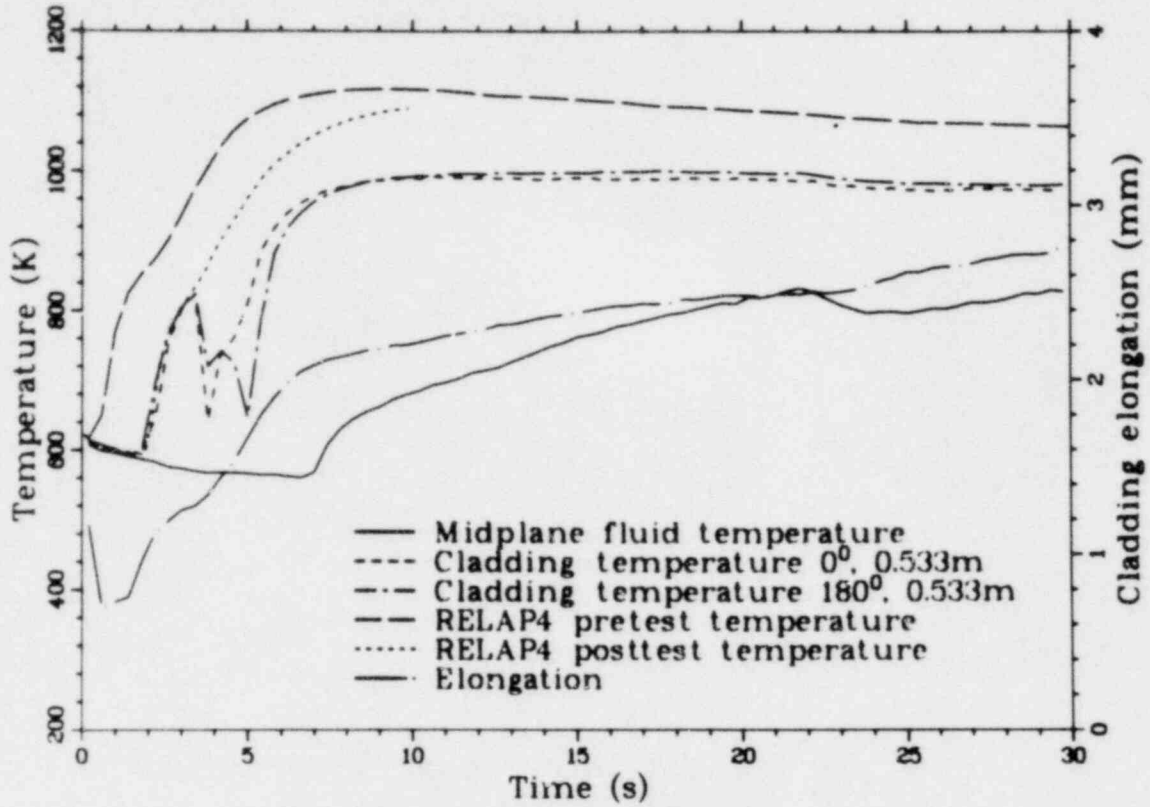

Figure 64. Thermal and mechanical behavior of Rod 345-1 during Test LLR-5.

The measured cladding temperature is plotted as a function of fuel rod differential pressure in Figure 65. The measured temperature-pressure history indicates that the cladding was subjected to incipient buckling at the thermocouple locations, as determined by Olsen.

The measured fuel centerline temperature at 0.533 m of Rod 345-1 during Test LLR-5 is shown in Figure 66 with the corresponding FRAP-T5 calculated centerline temperature response. The initial centerline temperature was 1825 K. The reactor was scrammed at 2 s during Test LLR-5. As shown in Figure 66, after blowdown was initiated, the centerline temperature slowly declined during the first 2 s, indicative of the delayed reactor scram. The fuel centerline temperature decreased immediately at 2 s and continued decreasing to 1100 K at 15 s, at which time the stored energy was finally redistributed toward the periphery of the fuel pellet. The centerline temperature then decreased gradually for the remainder of the blowdown transient.

The FRAP-T5 centerline temperature calculation for Rod 345-1 for Test LLR-5 was initiated from a complete set of input describing a fresh, unirradiated rod. The fuel centerline temperature was calculated using the measured cladding temperatures at the thermocouple locations as the surface boundary conditions to obtain the internal rod dynamics. The Ross and Stoute[5] correlation was used for the unpressurized LLR fuel rods to calculate gap conductance. The FRAP code undercalculated the initial stored energy for the fuel rods. The uncertainties that are inherent in these calculations include initial fuel rod power, fuel-to-cladding gap conductance, and UO_2 thermal conductivity. Also, the FRAP model did not include the thermocouple between the centerline thermocouple and pellet hole; thus, thermal inertia effects were excluded. The fuel centerline temperature was undercalculated for the entire blowdown. FRAP calculated that the cladding would collapse at the thermocouple location at approximately 6 s. The code also calculated the thermal gas gap to be initially closed and to remain closed throughout the blowdown transient. At the time of cladding collapse, FRAP calculated the pellet-cladding interfacial pressure to increase from 0 to 12.8 MPa with a consequent increase in the gap conductance from 24.7 to

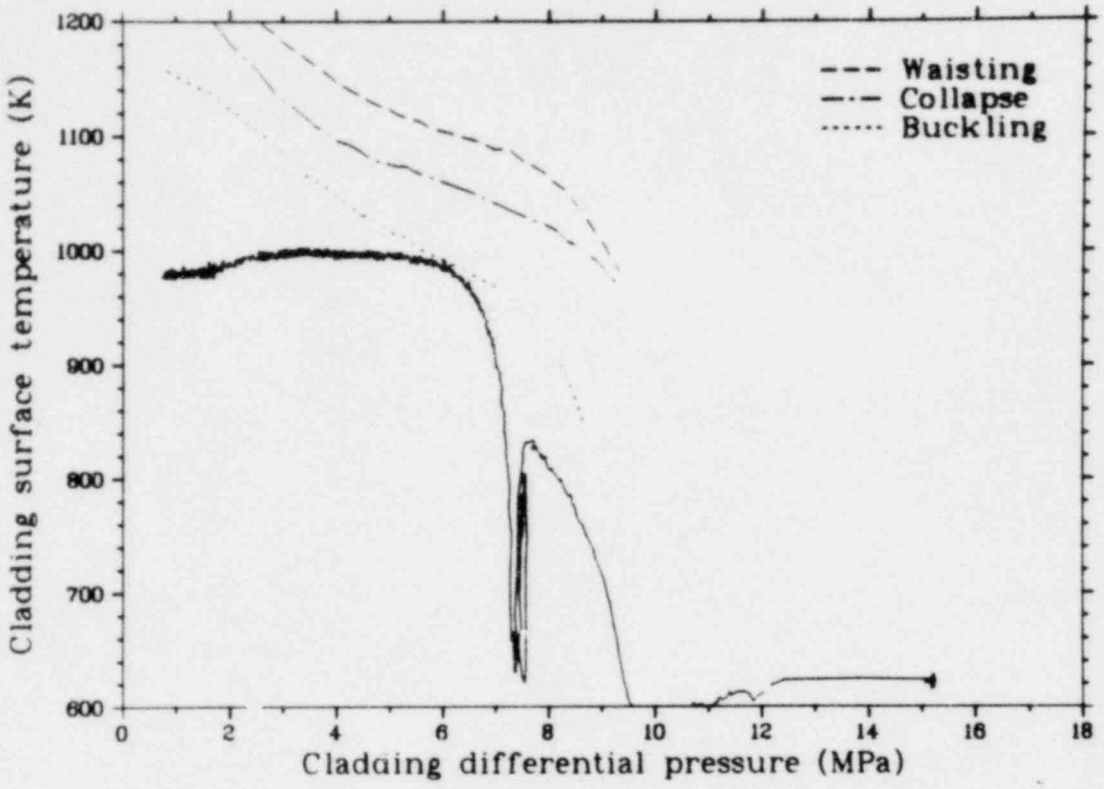

Figure 65. Surface temperature versus fuel rod differential pressure of Rod 345-1 during Test LLR-5.

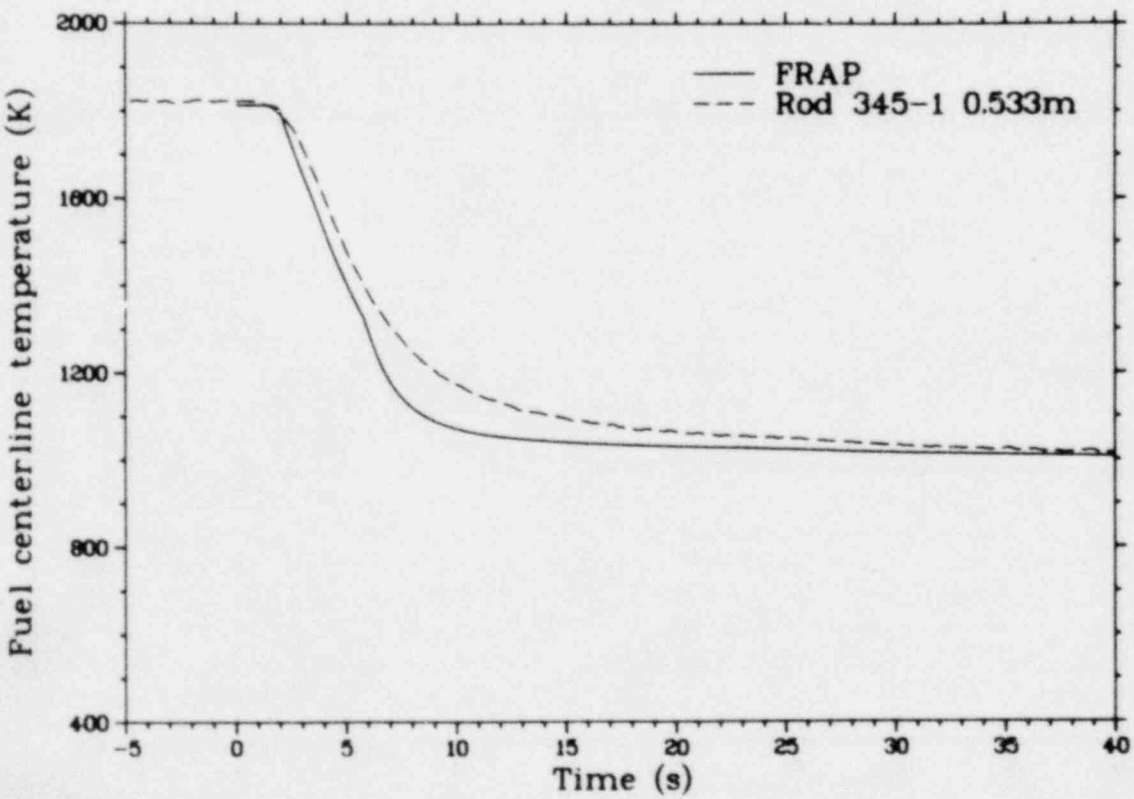

Figure 66. Comparison of fuel centerline temperature of Rod 345-1 with FRAP-T5 calculations for Test LLR-5.

61.4 kW/m^2·K. The interfacial pressure dropped rapidly to approximately 4.0 MPa within 2 s after the collapse, and approached zero at 25 s, whereas the gap conductance remained high for the greater portion of the transient.

In comparing the measured and calculated centerline temperature data in Figure 66, the time interval between 6 and 20 s brackets the time interval when significant differences (as large as 105 K) occur in the measured and calculated centerline temperatures. This difference implies that the cladding may not have collapsed at the thermocouple locations during Test LLR-5, as calculated by FRAP. As shown in Figure 65, Olsen's criteria indicated that the cladding probably experienced incipient buckling and not collapse at the thermocouple locations during Test LLR-5. The calculated gap conductance, therefore, appears to be too large. It is possible that better agreement between the measured and calculated centerline temperature would have been achieved had the cladding not collapsed in the FRAP-T5 calculation.

To confirm this assumption, a second calculation was performed with the FRAP code. To force the code to calculate lower interfacial pressures, the ambient pressure input was arbitrarily reduced from the previous calculation to assure that cladding collapse would not occur. The centerline temperature as calculated by FRAP for this instance is shown in Figure 67. The code calculated the thermal gas gap to be initially closed, but to reopen at approximately 5 s for the remainder of the transient. During the time the thermal gap was closed, FRAP calculated that no interfacial pressure existed; after the calculated gap opened the gap conductance remained below 25 kW/m^2·K for the 6- to 20-s time interval. Comparison of the measured centerline temperature data with the calculated data for the noncollapse case indicates agreement within 40 K.

On the basis of these analyses, the conclusion reached was that cladding collapse did not occur during Test LLR-5, and, on the basis of this limited data base, FRAP transient analysis may not be a reliable method for predicting cladding collapse. The cladding deformation threshold is probably predicted by FRAP, but the code requires correlations of deformation characteristics such as Olsen's data to guide it in specifying the quantity of deformation.

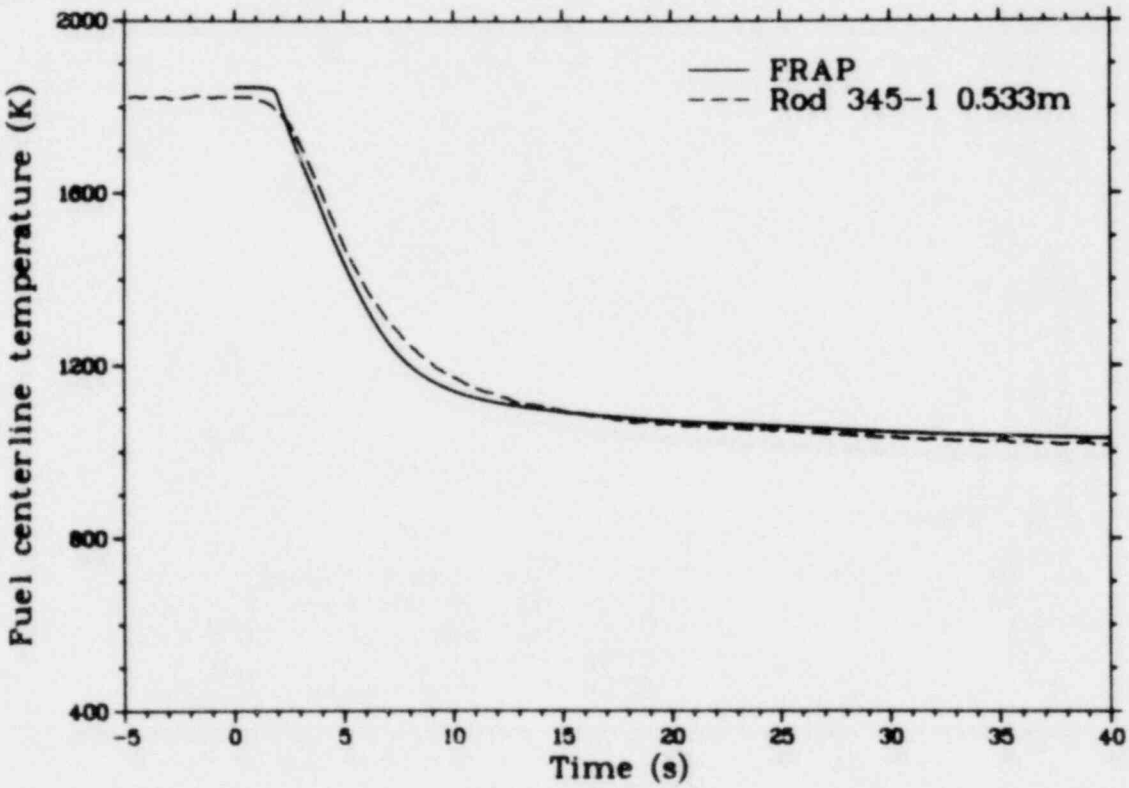

Figure 67. Comparison of fuel centerline temperature of Rod 345-1 with FRAP-T5 calculations for Test LLR-5, with modified ambient pressure boundary condition.

4.4.5.2 Test LLR-4, Rod 345-1—Figure 68 illustrates the cladding temperature and elongation responses of Rod 345-1 during Test LLR-4, for a 30-s duration. The peak power of Rod 345-1 was calculated to be 58.4 kW/m just prior to blowdown. The cladding surface thermocouple data at the 0-degree, 0.533-m thermocouple location indicated that the rod first indicated DNB at 1.7 s and reached a maximum surface temperature of 1060 K at 15 s. The 180-degree, 0.533-m thermocouple first indicated DNB at 1.7 s and reached a maximum surface temperature of 1045 K at 15 s. The cladding elongation sensor first indicated a moderate increase in cladding length at 0.25 s, and then stronger indications at 1.4 and 2.6 s, as DNB probably started at an elevation lower than the cladding thermocouples and propagated up the rod. This indicates that the surface thermocouples may have affected the transient response of the rods by delaying CHF. As with Test LLR-5, Rod 345-1 exhibited somewhat anomalous bahavior during Test LLR-4, rewetting at 2.8 s before drying out and attaining maximum cladding temperatures. This behavior is again attributed to a slight amount of leakage through the check valve during the first 4 s of the transient. The upper and lower turbine meters for this rod exhibited slightly higher flows than the other flow shroud turbines during this time period.

As shown in Figure 69, based on Olsen's criteria, the cladding surface temperature versus differential fuel rod pressure indicates that cladding buckling occurred at the thermocouple locations during Test LLR-5. However, since DNB was probably achieved earlier at elevations lower than the thermocouples (based on the cladding elongation sensor response), estimates of higher temperatures at lower elevations have been made. An estimate of 1140 K at the 0.314-m location was made for Rod 345-1 by comparison with Rod 399-2 data. This would result in waisting of the fuel rod at this lower elevation.

The measured fuel centerline temperature at 0.533 m for Rod 345-1 for Test LLR-4 is illustrated in Figure 70 with the corresponding FRAP-T5 calculated centerline temperature response. The measured temperature was 2190 K at steady state conditions prior to blowdown. When Test LLR-5 was initiated, the reactor was not scrammed until 2.65 s after initiation of blowdown. The first stages of the centerline

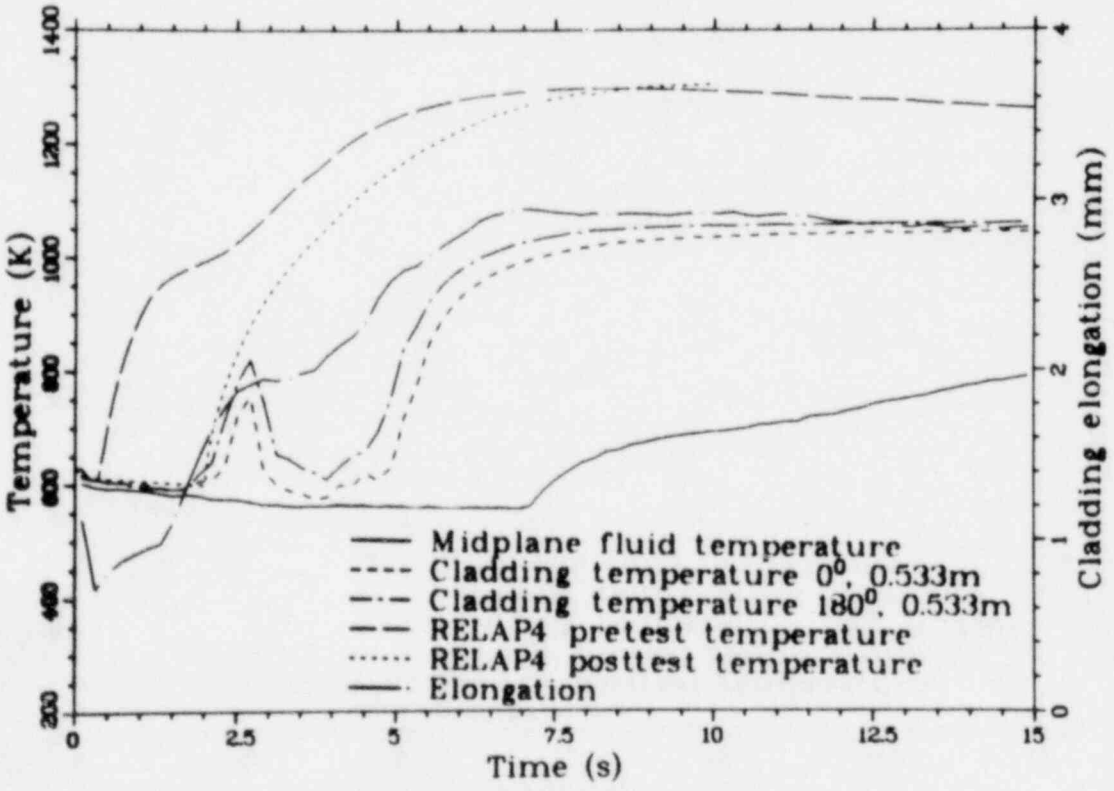

Figure 68. Thermal and mechanical behavior of Rod 345-1 during Test LLR-4.

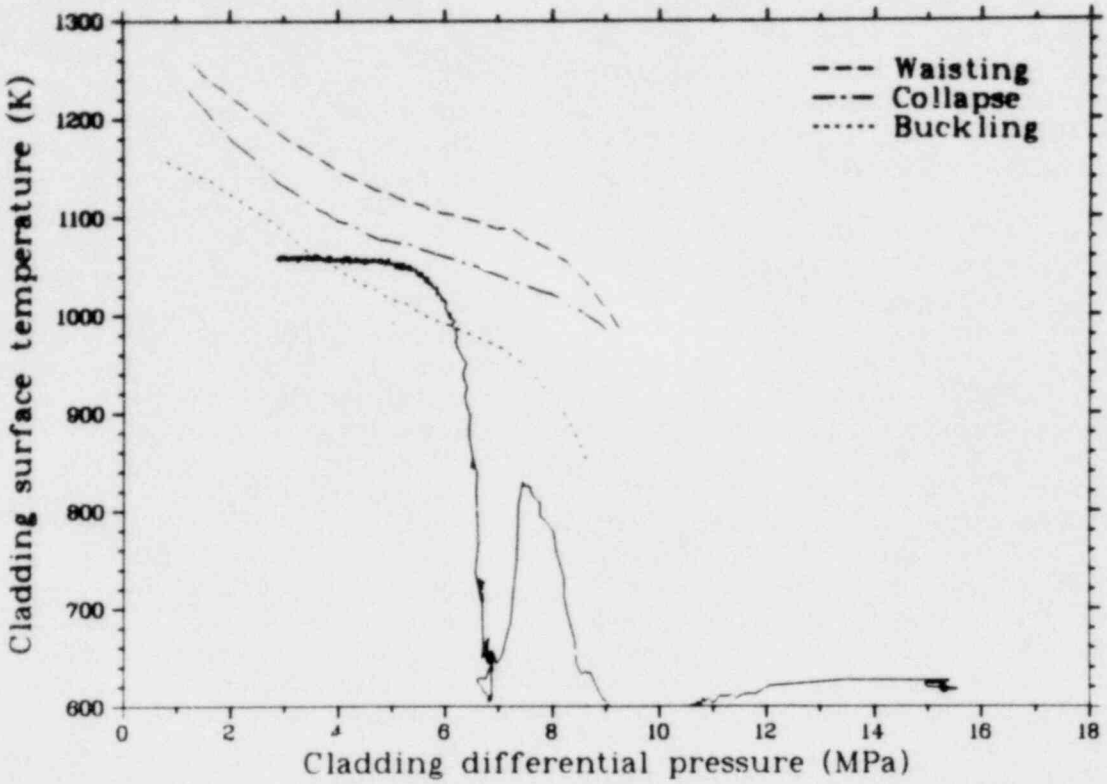

Figur 69. Surface temperature versus fuel rod differential pressure of Rod 345-1 during Test LLR-4.

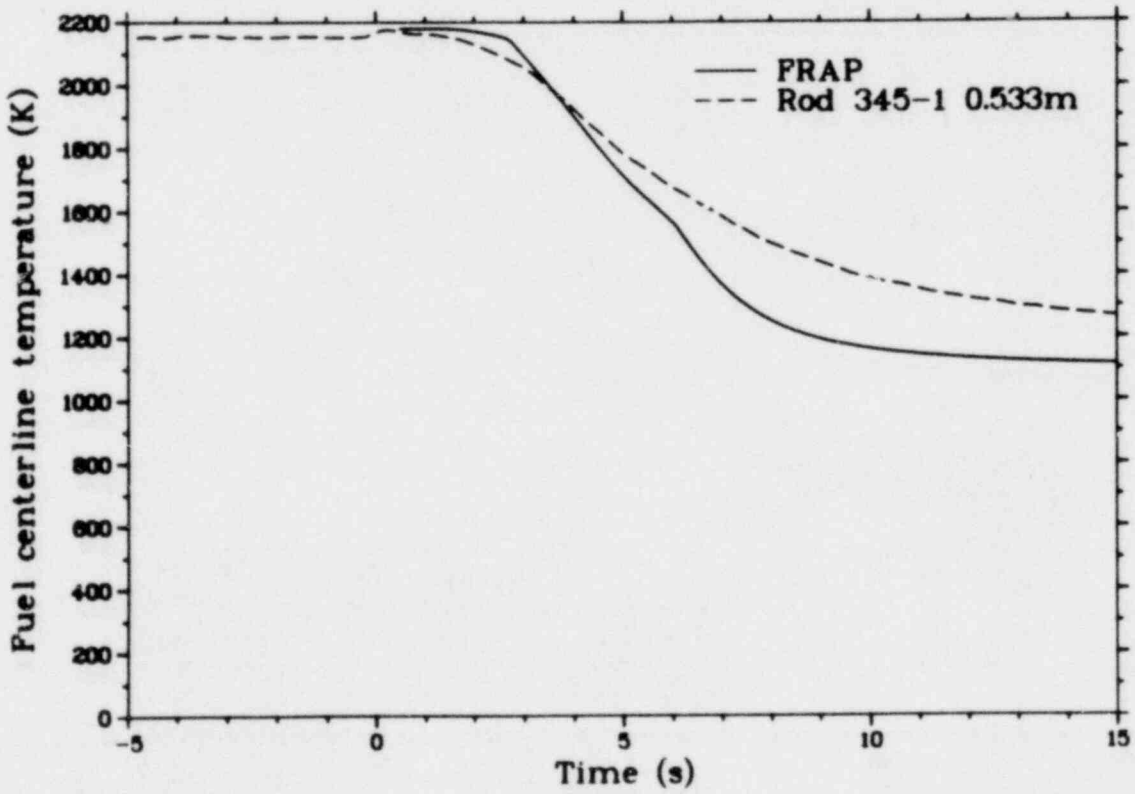

Figure 70. Comparison of fuel centerline temperature of Rod 345-1 with FRAP-T5 calculations for Test LLR-4.

temperature response are typical of that obtained from Test LLR-5. The temperature remains relatively constant until reactor scram and then decreases rapidly during the establishment of film boiling and the redistribution of stored energy.

The FRAP calculations for Test LLR-4 for Rod 345-1 were restarted from the Test LLR-5 calculation that did not result in cladding collapse. The system ambient pressure and the measured cladding surface temperature were used for the fuel rod boundary condition. FRAP calculated the cladding to collapse early in the transient, between 6 and 7 s. At the time of collapse, the interfacial pressure increased from zero to approximately 4.5 MPa, with the corresponding gap conductance increasing from 25.9 to 61.5 kW/m^2-K. A slow decline in the interfacial pressure was then calculated to occur until the first cladding rewet at approximately 15.5 s. At this time, the interfacial pressure increased to 36.8 MPa as the cladding responded to the quench.

Comparison of the measured and calculated centerline temperature data in Figure 70 indicates a significant divergence of the two curves at 6 s, with the calculations underpredicting the data. The calculation continues to diverge from the data for the next 3 s. As with the Test LLR-5 calculations, the largest discrepancies in agreement between the calculated and measured data coincided with the time interval at which FRAP calculated large values for the gap conductance. This implies that either FRAP calculates values of gap conductance that are too large when the cladding has collapsed, or that cladding collapse did not occur, or collapse was calculated before it occurred. However, in the visual postirradiation examination for Rod 312-1, the rod was observed to have achieved the waisting regime of mechanical deformation and comparable deformation probably occurred to the other rods, including Rod 345-1.

4.4.5.3 Test LLR-4A, Rod 345-1—Figure 71 illustrates the cladding temperature, cladding elongation, and coolant midplane temperature response of Rod 345-1 during Test LLR-4A, for a 30-s duration. The peak power of Rod 345-1 was calculated to be 53.3 kW/m just prior to blowdown. The 180-degree, 0.533-m thermocouple reading overlays that of the 0-degree thermocouple throughout the entire blowdown transient. The cladding surface thermocouple data indicate that the rod achieved DNB at 2.0 s at both thermocouple locations and reached a maximum surface

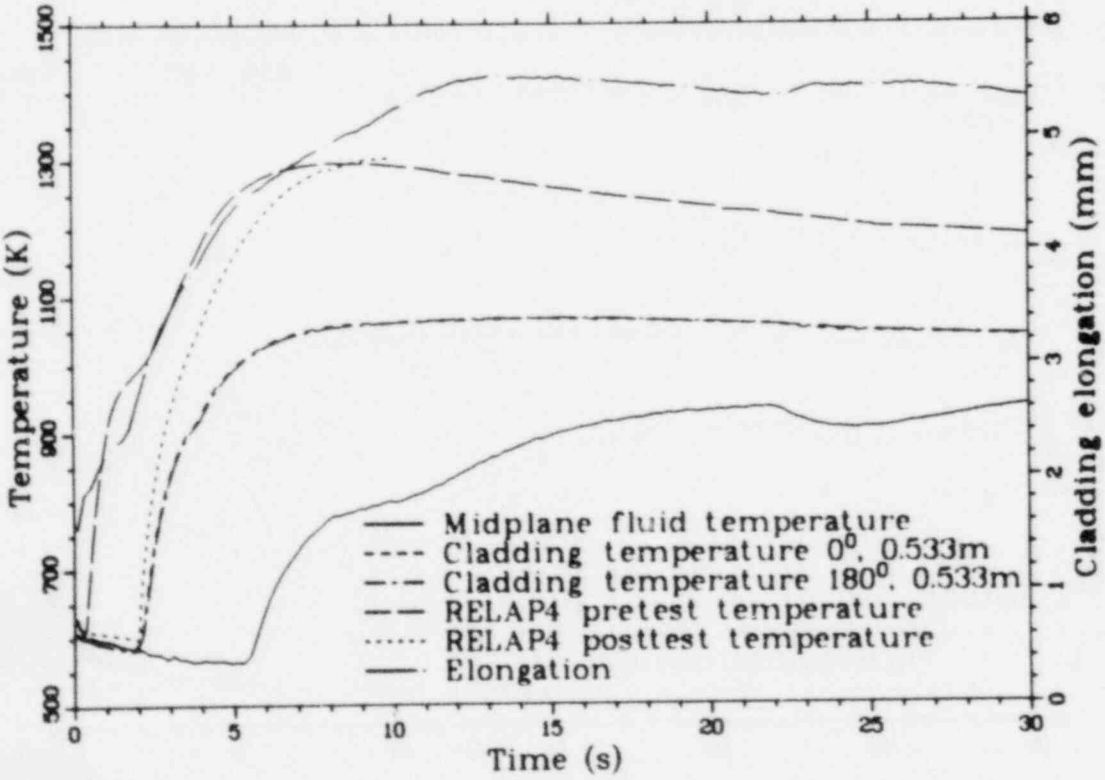

Figure 71. Thermal and mechanical behavior of Rod 345-1 during Test LLR-4A.

temperature of 1070 K at 15 s. The cladding elongation sensor first indicated a moderate increase in cladding length at 0.25 s, with a more pronounced increase at 1.5 s as DNB started at an elevation probably lower than the cladding thermocouples and propagated up the rod. This again indicates a possible thermocouple effect on fuel rod response. During the rapid temperature increase for the first 8 s following DNB, the rod experienced an axial strain of approximately 1.7 mm. The rod continued to elongate to 2.2 mm at 30 s.

The anomalous rewet behavior evidenced in Tests LLR-5 and -4 was not witnessed in Test LLR-4A for Rod 345-1. This prior behavior was attributed to a slight leakage through the Rod 345-1 check valve during the first 4 s of the transient in these tests. This check valve was replaced prior to Test LLR-4A, and the new check valve apparently eliminated the rewet condition. The upper and lower turbine meters for this rod exhibited flow responses similar to the other flow shroud turbines during this time period for this test.

The measured cladding temperature is plotted as a function of fuel rod differential pressure in Figure 72. As shown, based on Olsen's criteria, the cladding surface temperature versus fuel rod differential pressure indicates the cladding was subjected to temperatures slightly above that required to cause collapse at the thermocouple locations. This collapse was confirmed in the post-irradiation examination, and waisting was evident at the thermocouple elevation.

The measured fuel centerline temperature at 0.533 m on Rod 345-1 during Test LLR-4A is illustrated in Figure 73 with the corresponding FRAP-T5 calculated centerline temperature response. The measured temperature was 1920 K at steady state conditions prior to blowdown. When Test LLR-4A was initiated, the reactor was not scrammed until 2.85 s. The temperature decreased to 1245 K at 10 s, at which time the stored energy was finally redistributed toward the periphery of the fuel rod. After 10 s, the centerline temperature decreased gradually for the remainder of the blowdown transient until the rods were quenched.

The fuel centerline temperature as calculated with FRAP-T5 was initialized from the previous calculation for Test LLR-4, which indicated collapsed cladding. The measured cladding temperature at the thermocouple locations was used as the surface boundary condition to obtain the internal

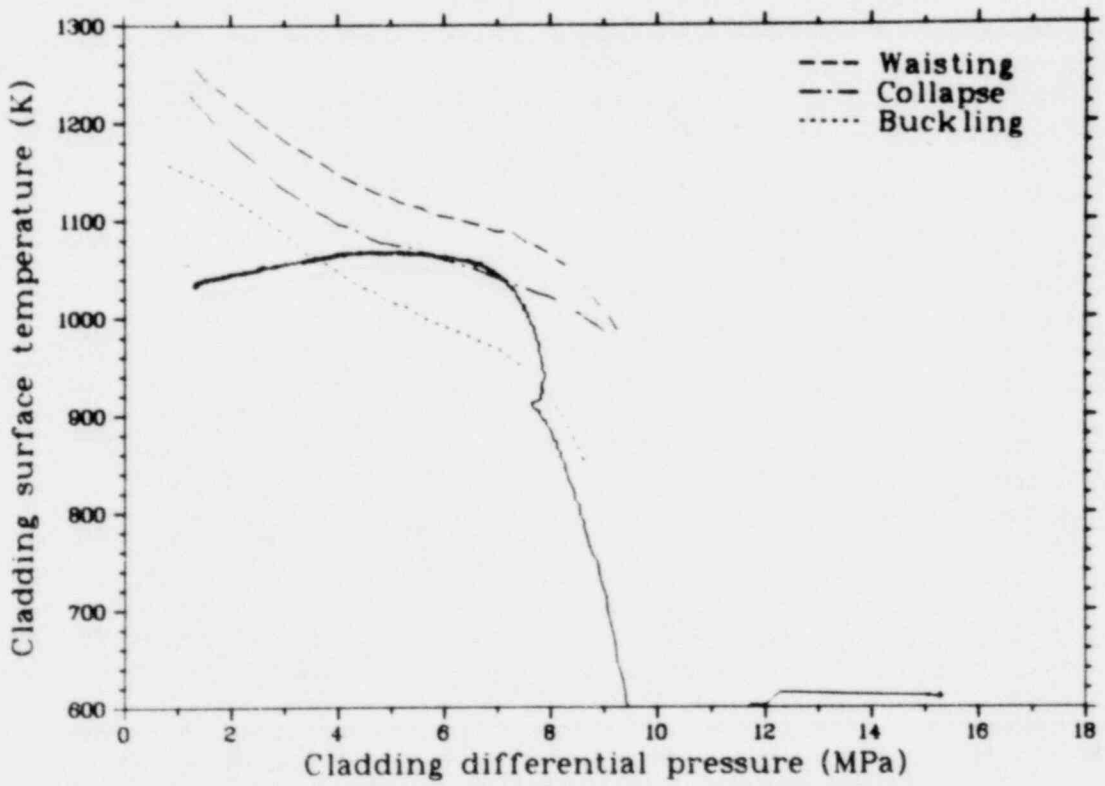

Figure 72. Surface temperature versus fuel rod differential pressure of Rod 345-1 during Test LLR-4A.

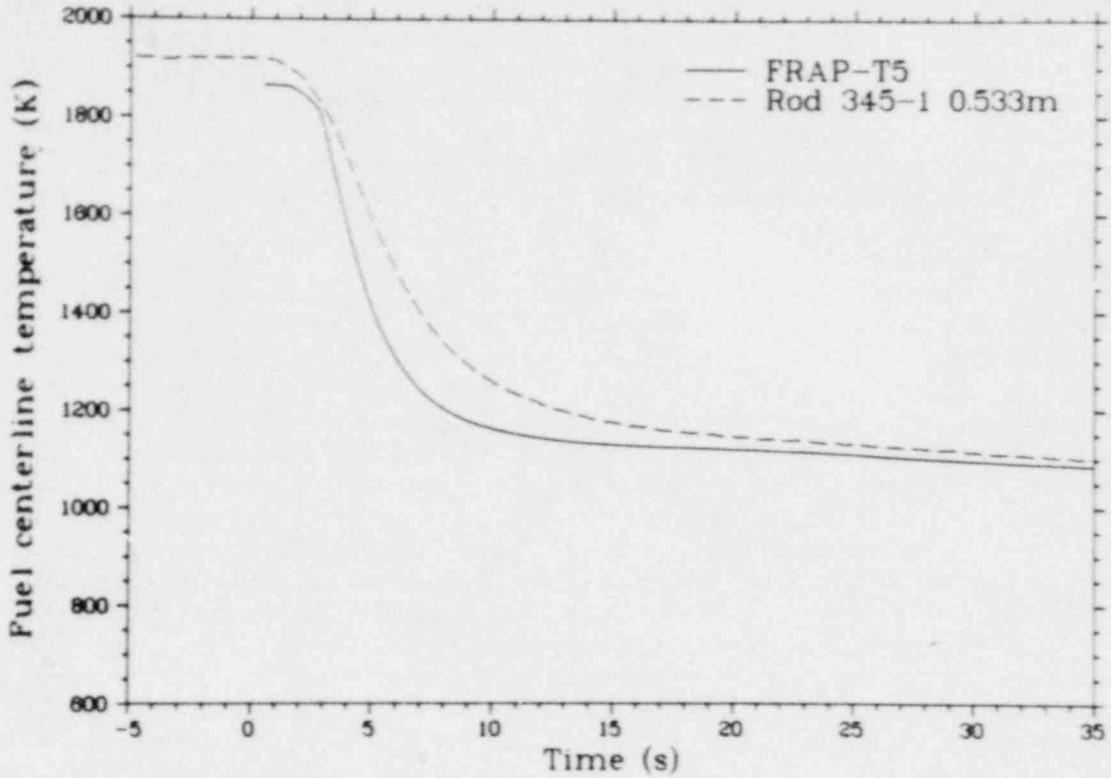

Figure 73. Comparison of fuel centerline temperature of Rod 345-1 with FRAP-T5 calculations for Test LLR-4A.

rod dynamics. The FRAP code undercalculates the centerline temperature for the fuel rod for the entire transient. The pellet-to-cladding interfacial pressure was initially calculated to be 19 MPa, which is the result of the collapsed cladding calculation from Test LLR-4. The pressure decreased rapidly to approximately 4.3 MPa at 4 s. Between 4 and 18 s, the interfacial pressure remained essentially constant in the range of 4 to 7 MPa. Past this time, the interfacial pressure decreased slowly for the remainder of the transient. The initial gap conductance as calculated by FRAP was 61.4 kW/m^2·K, which was calculated to remain constant until 37 s, at which time it gradually decreased to 33.4 kW/m^2·K at 46 s. Again, undercalculation of the measured fuel centerline temperatures suggests that FRAP is calculating gap conductances that are too large for a deformed cladding situation.

4.4.5.4 Postirradation Examination of Rod 345-1—Permanent changes to the cladding of Rod 345-1 occurred as a result of the three successive blowdowns. The rod was waisted 46 to 65 cm from the bottom of the fuel stack.

A maximum temperature of 1070 K was measured for Rod 345-1 at the 0.533-m location. The cladding microstructure that corresponds to this temperature is the recrystallized α-zircaloy regime, which exists in the temperature range of 920 to 1100 K. Figure 74 presents the cladding microstructure (transverse Section M5-3) located 0.533 m from the bottom of the heated length in the plane of the 0- and 180-degree thermocouple junctions. Only equiaxed α-zircaloy structure is present throughout the entire cladding thickness. A longitudinal section (Section M5-1) from 0.25 to 0.27 m above the bottom of the heated length was made in the 90- and 270-degree plane to characterize the axial temperature profile of the rod at the boundary of visible deformation on the fuel rod. The microstructure consisted of a high concentration of equiaxed α-zircaloy, with β precipitates mainly at the grain boundaries. The approximate temperature range for this structure is 1150 to 1200 K. On the basis of these microstructure estimates, cladding temperatures were higher below the thermocouple locations. This information supports the contention that in the higher power tests the LLR test rods first departed from nucleate boiling at a location below the thermocouples.

Rod 345-1 was at reactor operating temperatures (600 K) for approximately 89 h. A calculation was performed to determine how much of the observed oxide thickness resulted from this

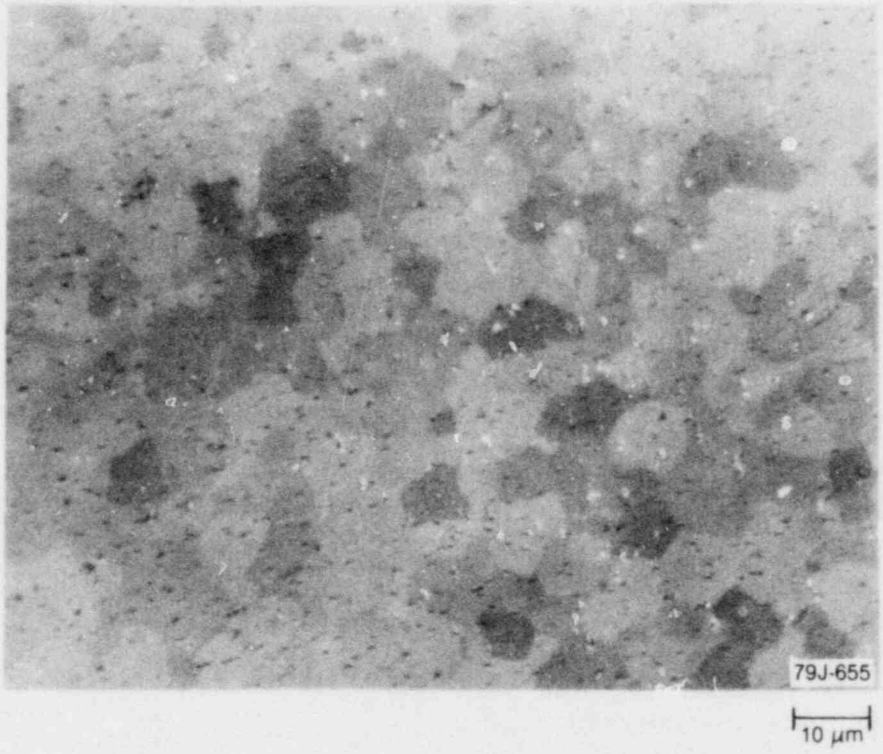

Figure 74. Rod 345-1 transverse cladding microstructure (Sample M5-3) from 0.45 to 0.47 m.

exposure. By using oxidation kinetics, a zirconium dioxide thickness of 0.5 μm was obtained for oxidation during the entire 89 h of preconditioning. A maximum total thickness of 4 μm was obtained after the three transients for Rod 345-1. Cladding temperatures determined from the oxide layers are tabulated in Table 9. As shown, the maximum estimated temperature, T_ξ, is approximately 1155 K at the 26-cm elevation.

The posttest diametral measurements of Rod 345-1 are plotted versus the fuel stack axial length in Figure 75. The rod exhibited collapse, with a maximum diametral decrease of 0.05 mm along the rod midsection from 48.3 to 65.7 cm from the bottom of the active fuel stack. The location of maximum collapse corresponded to the axial region of maximum power (45.7 cm). The calculated response of the cladding diameter to Test LLR-4A is also shown in Figure 75. FRAP-T5 calculates the fuel-cladding gap to be closed and to remain closed throughout the transient. Strong pellet-cladding interfacial pressure was calculated, indicating severe pellet-cladding contact, although only a partial UO_2-zircaloy reaction was evident from the microstructure.

Permanent plastic radial engineering strains as expressed by Equation (9) are shown in Figure 76.

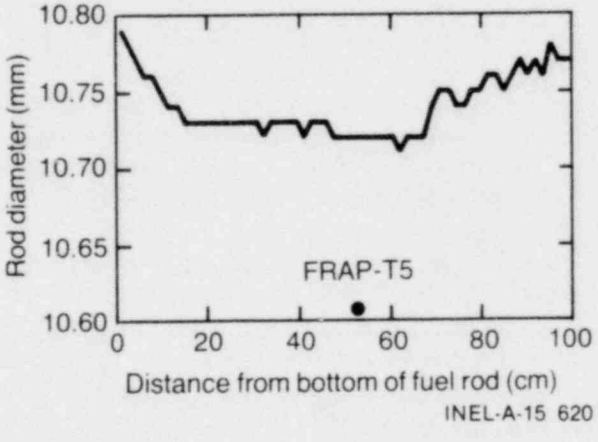

Figure 75. Postirradiation examination measurements of cladding diameter for Rod 345-1.

The strain was 0.0065 at 0.56 m, and 0.0057 at the peak power location (0.457 m). At the ends of the collapse zones, at 2 and 88.3 cm, the radial strains were zero. The same version of the FRAP code used in the centerline temperature calculations was used to calculate the strain of Rod 345-1 at the thermocouple locations. The calculated strains include the strain calculated during the steady state operation and the transients. These calculations indicate FRAP is considerably overcalculating the measured strain. The maximum calculated strain was 0.016 (1.6%).

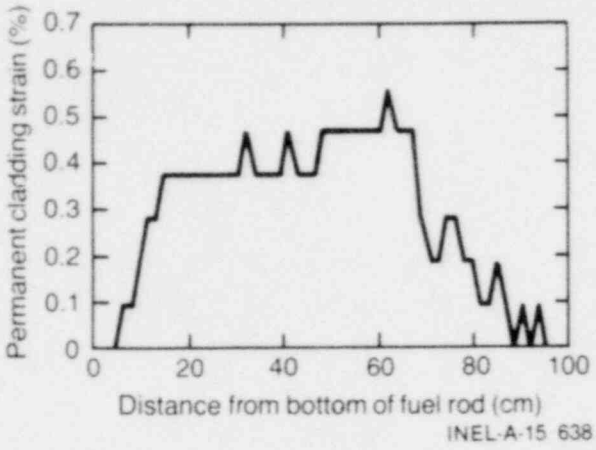

Figure 76. Circumferential strain from posttest diameter measurements of Rod 345-1.

4.4.6 Fuel Rod 345-2. One of the secondary objectives of the LLR tests was to evaluate the fin effects caused by instrumenting fuel rods with cladding thermocouples. To quantify this objective, Rod 345-2 was not instrumented with cladding thermocouples. Rod 345-2 was used for Tests LLR-5, -4, and -4A. During the postirradiation examination, the rod exhibited collapse with some waisting as a result of the three transients. Microstructure temperature estimates ranged from 1150 to 1200 K from 25 to 45 cm from the bottom of the heated length. Details of the response of Rod 345-2 during the three transients and postirradiation results are presented in the following subsections.

4.4.6.1 Test LLR-5, Rod 345-2—Figure 77 illustrates the centerline temperature and cladding elongation responses of Rod 345-2 during Test LLR-5, for a 30-s duration. The peak power of Rod 345-2 was calculated with test data to be 50.9 kW/m just prior to blowdown. The cladding elongation transducer indicated a sharp increase at 0.4 s, which compares favorably with the cladding elongation sensor response of Rod 312-1. During the rapid temperature increase for the first 7 s of the transient, the rod experienced an elongation of approximately 1.0 mm. The rod continued to elongate to 1.2 mm at 30 s.

The measured fuel centerline temperature at 0.457 m on Rod 345-2 during Test LLR-5 is also shown in Figure 77. The initial centerline temperature was 1735 K. The reactor was scrammed 2 s after Test LLR-5 was initiated. As shown in Figure 77, the fuel centerline temperature decreased immediately after scram. The temperature decreased to 1165 K at 10 s, at which time the stored energy was finally redistributed toward the periphery of the fuel rod. At this point, the centerline temperature decreased gradually for the remainder of the transient.

4.4.6.2 Test LLR-4, Rod 345-2—Figure 78 illustrates the centerline temperature and elongation response of Rod 345-2 during Test LLR-4, for a 15-s duration. The peak power of Rod 345-2 was calculated from test data to be 55.5 kW/m just prior to blowdown. The cladding elongation sensor first indicated an increase in cladding length at 0.25 s, and continued to increase for the remainder of the transient. The measured fuel centerline temperature at 0.457 m on Rod 312-1 for Test LLR-5 is also illustrated in Figure 78. The measured temperature was 1925 K at steady state conditions prior to blowdown.

4.4.6.3 Test LLR-4A, Rod 345-2—Figure 79 illustrates the centerline temperature and elongation response of Rod 345-2 during Test LLR-4A, for a 30-s duration. The peak power of Rod 345-2 was calculated to be 53.3 kW/m just prior to blowdown. The cladding elongation sensor first indicated a moderate increase in cladding length at 0.25 s, with a second increase at 1.5 s. The measured fuel centerline temperature at 0.457 m on Rod 345-2 for Test LLR-4A is also illustrated in Figure 79. The measured temperature was 2140 K at steady state conditions prior to blowdown.

4.4.6.4 Postirradiation Examination of Rod 345-2—Permanent changes to the cladding of Rod 345-2 occurred as a result of the three successive blowdowns. The rod was waisted 37 to 47 cm from the bottom of the fuel stack.

Figure 80 presents the cladding microstructure (transverse Section M6-2) located 0.45 m from the bottom of the heated length in the 210-degree plane. Mixed recrystallized α-zircaloy and limited prior β-zircaloy structures are present throughout the entire cladding thickness. This indicates temperatures in the range of 1150 to 1200 K. A longitudinal section from 0.25 to 0.27 m above the bottom of the heated length (Section M6-1) was made in the 90- and 270-degree plane to characterize the axial temperature profile on the fuel rod and to compare with the microstructure on Section M5-1. The microstructure consisted of a mixed high concentration of recrystallized

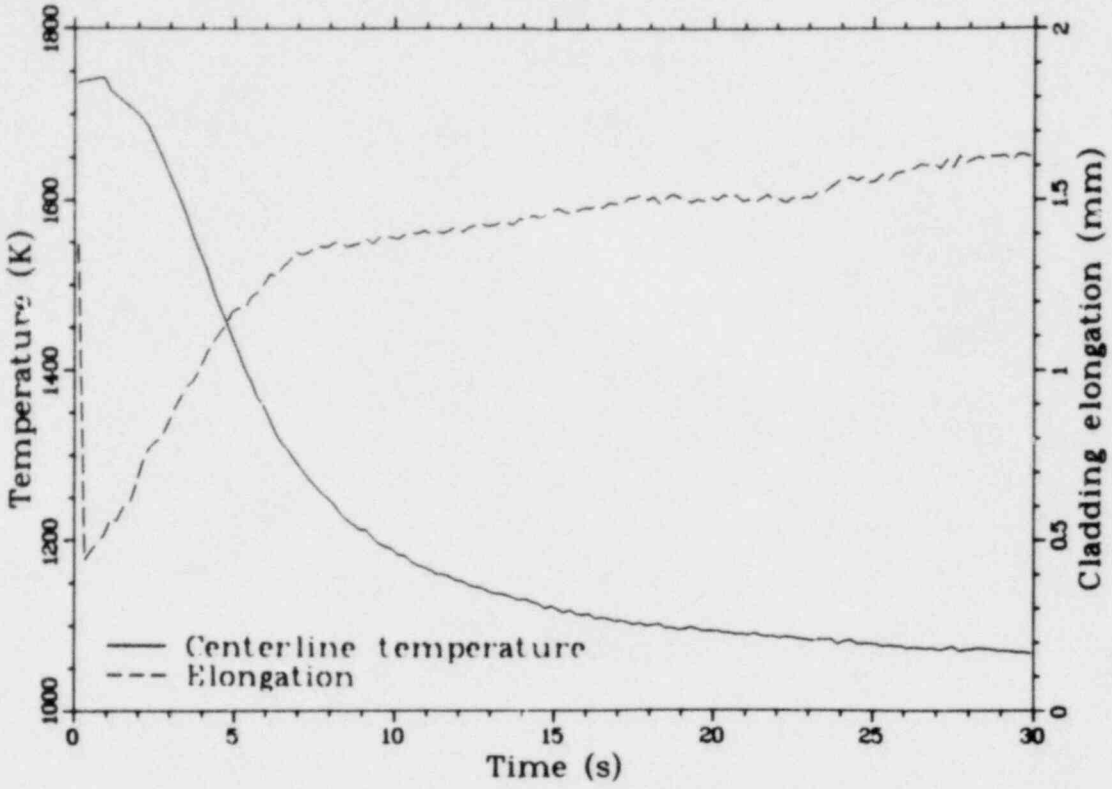

Figure 77. Thermal and mechanical behavior of Rod 345-2 during Test LLR-5.

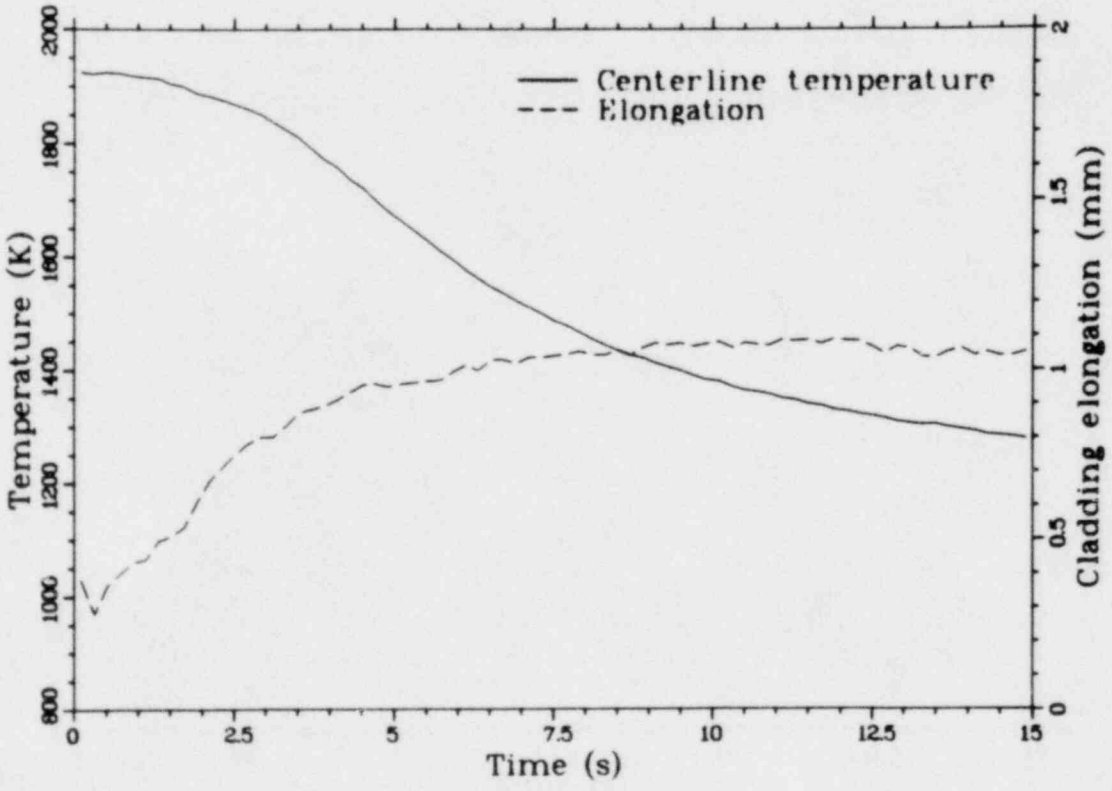

Figure 78. Thermal and mechanical behavior of Rod 345-2 during Test LLR-4.

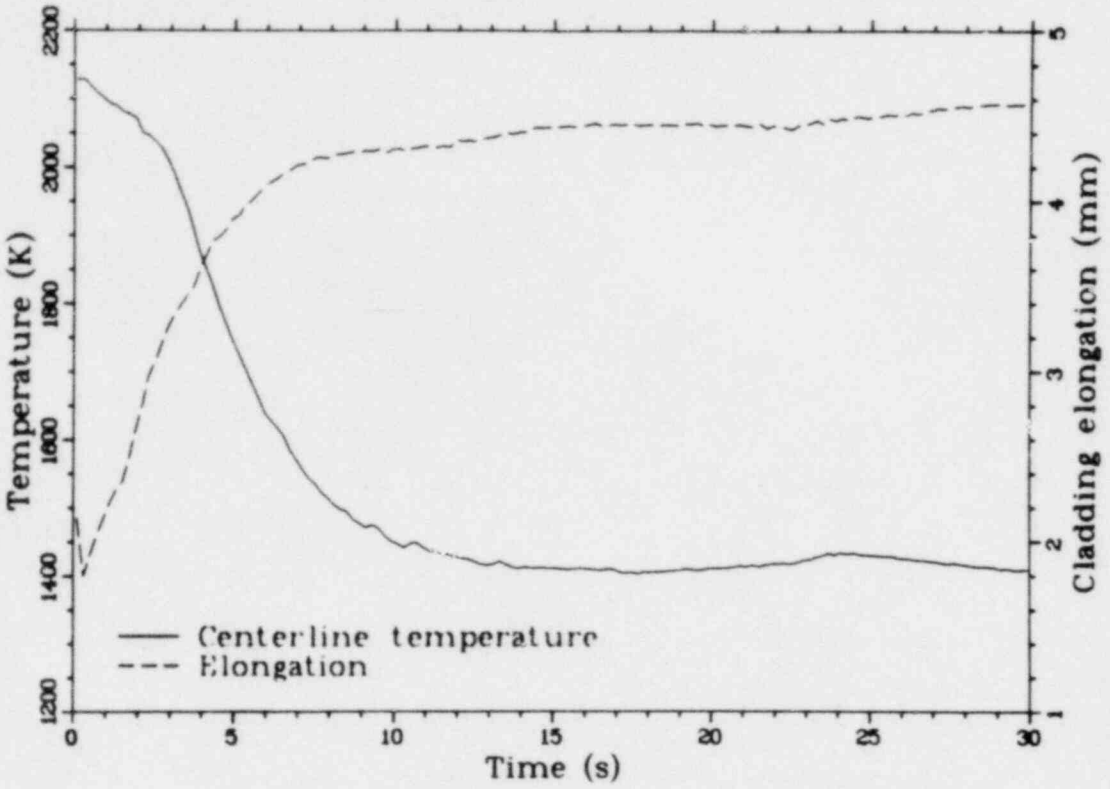

Figure 79. Thermal and mechanical behavior of Rod 345-2 during Test LLR-4A.

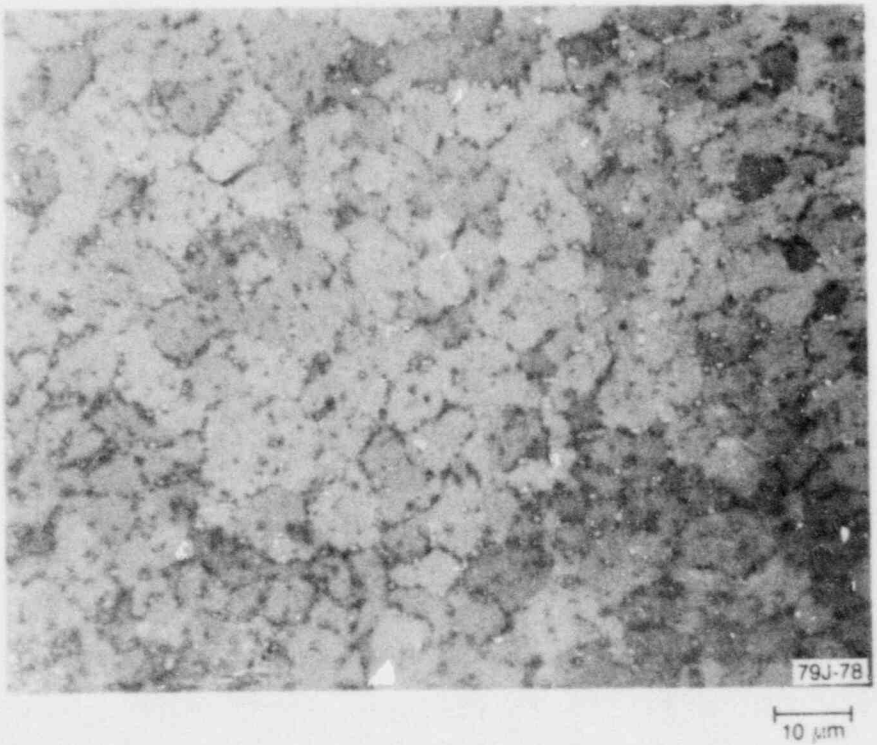

Figure 80. Rod 345-2 transverse cladding microstructure (Sample M6-2) from 0.45 to 0.47 m.

α-zircaloy and limited prior β-zircaloy. The approximate temperature range for this structure is 1150 to 1200 K.

Rod 345-2 was at reactor operating temperatures (600 K) for approximately 89 h. A calculation was performed to determine how much of the observed oxide thickness resulted from this exposure. By using oxidation kinetics, a zirconium dioxide thickness of 0.5 μm was obtained for oxidation during the entire 89 h of preconditioning. A maximum total thickness of 7 μm was obtained after the three transients for Rod 345-2. Cladding temperatures determined from the oxide layers are tabulated in Table 9. As shown, the maximum estimated temperature, T_ξ, is approximately 1205 K at the 26-cm elevation.

The posttest diametral measurements for Rod 345-2 are plotted versus the fuel stack axial length in Figure 81. The rod exhibited collapse, with a

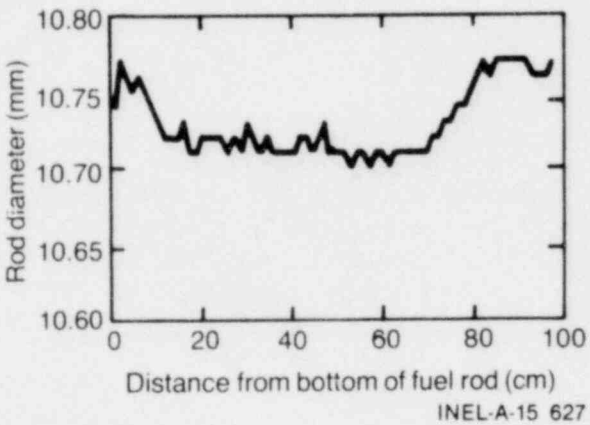

Figure 81. Postirradiation examination measurements of cladding diameter for Rod 345-2.

maximum diametral decrease of 0.06 mm from 33.2 to 69.6 cm from the bottom of the active fuel stack. Permanent plastic engineering strains as expressed by Equation (9) are shown in Figure 82. The strain was 0.0037 at 22 m. At the ends of the collapse zones, at 0.5 and 70 cm, the radial strains were zero.

Of interest is the fact that the deformation witnessed on this uninstrumented rod was greater than on its companion Rod 345-1, on the basis of visual examination, diametral measurements, and micrometer measurements.

4.4.7 Fuel Rod 399-2. Rod 399-2 was only used for Test LLR-4A, which provided the opportunity

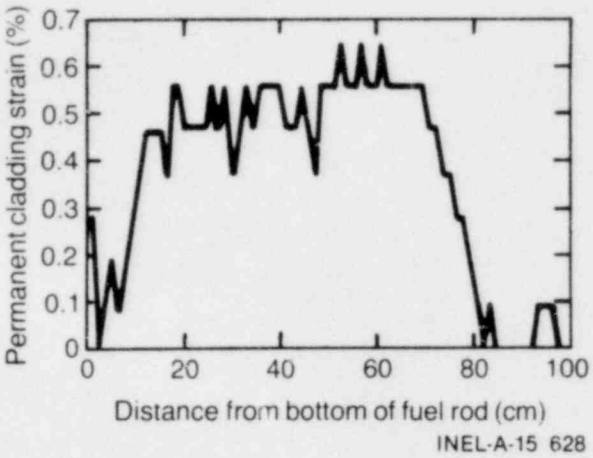

Figure 82. Circumferential strain from posttest diameter measurements of Rod 345-2.

to study the effects of one high power blowdown on LOFT-type fuel rods. A maximum temperature of 1260 K was recorded for this rod during the transient. The rod was collapsed and waisted as a result of Test LLR-4A. Microstructure temperatures were estimated to be in the range of 1200 to 1270 K at several locations on the fuel rod, including the thermocouple locations. Details of the response of Rod 399-2 during the transient and postirradiation results follow in the subsequent subsections.

4.4.7.1 Test LLR-4A, Rod 399-2. Figure 83 illustrates the cladding temperature, cladding elongation, and coolant midplane temperature response of Rod 399-2 during Test LLR-4A, for a 30-s duration. Cladding surface temperature measurements were made on Rod 399-2 at 0.314 and 0.457 m from the bottom of the fuel stack at azimuthal orientations of 0 and 180 degrees. The calculated difference in rod power between these two locations was approximately 2%, with the 180-degree, 0.457-m thermocouple at the highest power; thus, the temperature at this location should have been slightly higher for Test LLR-4A. The peak power of Rod 399-2 was calculated to be 53.2 kW/m just prior to blowdown. The cladding temperature data indicate that the rod achieved DNB at approximately 1.6 s at the 0-degree, 0.314-m thermocouple location, whereas the 180-degree, 0.457-m thermocouple indicated DNB at 1.8 s. The cladding elongation transducer indicated a sharp expansion at 0.25 s, which suggests that CHF occurred at this time over a significant length of the fuel rod surface, and a second indication at 1.5 s. This behavior indicates that the surface thermocouples may have affected the

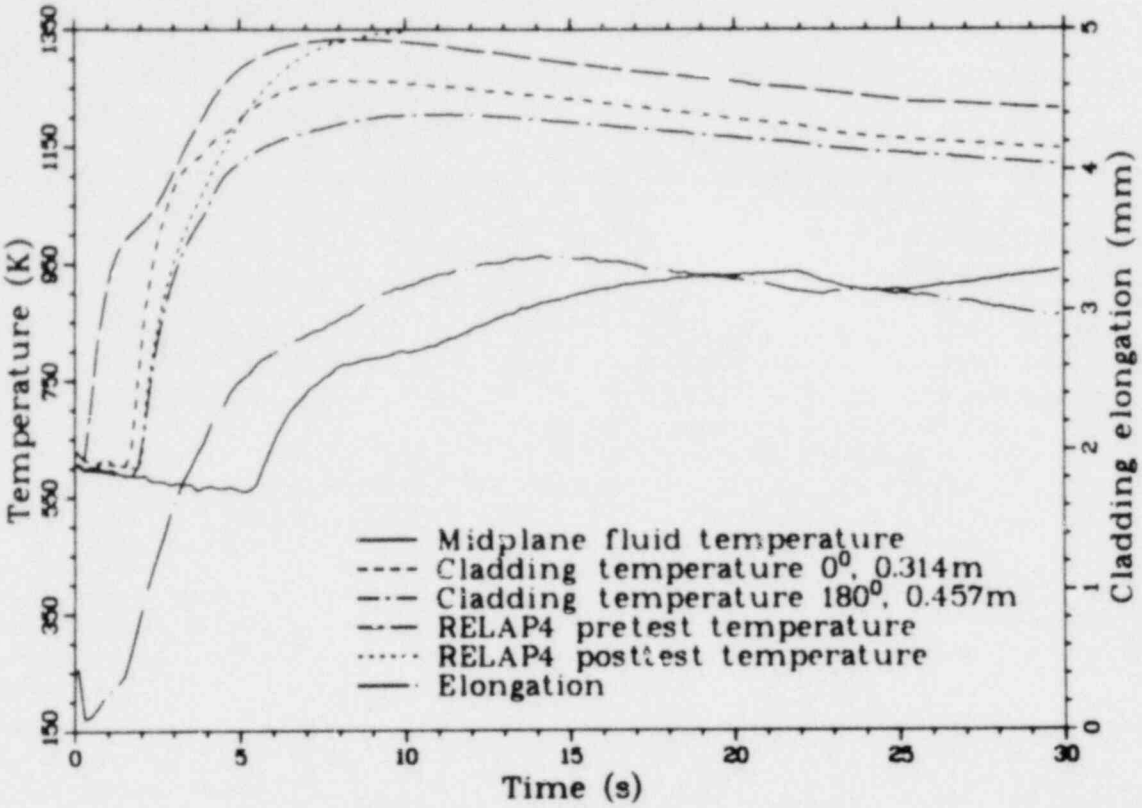

Figure 83. Thermal and mechanical behavior of Rod 399-2 during Test LLR-4A.

transient response of the rods during Test LLR-4A, as previously discussed. The 0-degree thermocouple indicated a maximum cladding temperature of 1260 K at 7.5 s, whereas the 180-degree thermocouple indicated 1205 K at 10 s. The rod experienced an elongation of approximately 3.3 mm during the first 30 s following DNB.

The measured cladding temperature is plotted as a function of fuel rod differential pressure in Figure 84. The measured temperature-pressure history is above the waisting regime, as determined by Olsen. Waisting was confirmed at both thermocouple locations during the postirradiation examination.

The fuel centerline thermocouple in Rod 399-2 failed during the preconditioning cycle prior to the transient.

4.4.7.2 Postirradiation Examination of Rod 399-2 – Permanent changes to the cladding of Rod 399-2 occurred as a result of the Test LLR-4A blowdown. The rod was waisted 32 to 52 cm above the bottom of the fuel stack.

A maximum temperature of 1260 K was measured for Rod 399-2 at the 0.314-m location. The cladding microstructure that corresponds to this temperature is the $\alpha + \beta$ transformation regime, which exists in the temperature range of 1100 to 1270 K. Figure 85 presents the cladding microstructure (transverse Section M7-3) in the plane of the 0-degree thermocouple junction located 0.314 m above the bottom of the fuel stack. Prior β-zircaloy structure is present at the 225- to 30-degree orientation, bounded by oxygen-stabilized α-zircaloy, which indicates temperatures greater than 1270 K. Circumferential temperature gradients were also observed at the 0.314-m thermocouple location.

A longitudinal section (Section M7-1) was made from 0.26 to 0.28 m above the bottom of the heated length in the 0- to 180-degree plane to characterize the axial temperature profile of the rod at a severely damaged region below the thermocouples. The maximum temperature region in the microstructure consisted of prior β-zircaloy bounded by oxygen-stabilized α-zircaloy, which indicates temperatures greater than 1270 K.

Rod 399-2 was at reactor operating temperatures (600 K) for approximately 23 h. A calculation was performed to determine how much of the

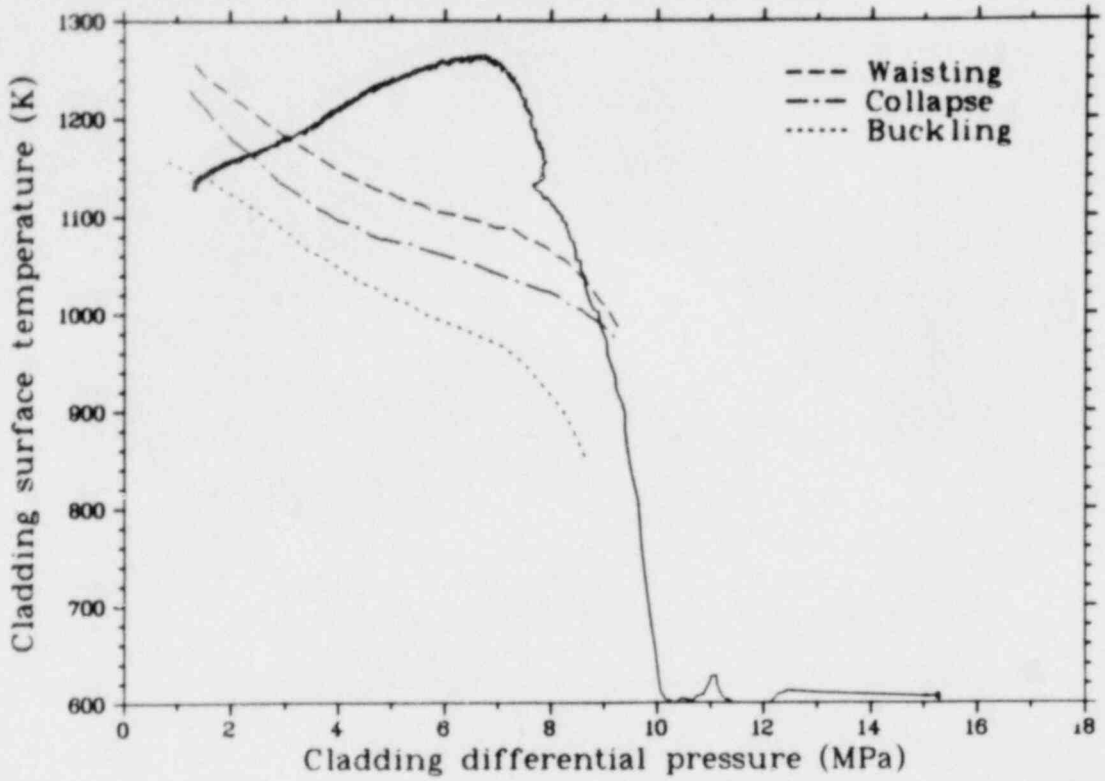

Figure 84. Surface temperature versus fuel rod differential pressure of Rod 399-2 during Test LLR-4A.

observed oxide thickness resulted from this exposure. By using oxidation kinetics, a zirconium dioxide thickness of 0.3 μm was obtained for oxidation during the entire 23 h of preconditioning. A maximum total thickness of 6 μm was measured after the Test LLR-4A transient. Cladding temperatures determined from the oxide layers are tabulated in Table 9. As shown, the maximum estimated temperature, T_ξ, is in the range of 1270 to 1290 K at the 31-cm elevation.

The posttest diametral measurements for Rod 399-2 are plotted versus the fuel stack axial length in Figure 86. The rod exhibited collapse, with a maximum diametral decrease of 0.04 mm from 15 to 46.5 cm from the bottom of the active fuel stack. Permanent plastic radial engineering strains as expressed by Equation (9) are shown in Figure 87. The strain was 0.0055 at 0.62 m, and 0.0045 at the peak temperature location (0.314 m). At the ends of the collapse zones, at 5 and 95 cm, the radial strains were zero.

The maximum estimated cladding temperature as a function of distance from the bottom of the fuel stack was obtained from the microstructure estimates from the transverse and longitudinal sections and is shown in Figure 88 for selected fuel rods. Plots of the axial temperature profile calculated by RELAP4 (posttest calculation and posttest calculation normalized to 1200 K to fit through the measured peak values at the thermocouple locations) are also included. In general, microstructure temperature estimates in the range of 1200 to 1270 K for Rods 312-2 and 399-2, and 1150 to 1200 K for Rods 345-1 and 345-2 were made from 25.8 to 31.4 cm from the bottom of the heated length. At the peak power elevation (46.5 cm), estimates ranged from 1100 to 1200 K for all the rods. The maximum measured cladding temperatures for the rods of Tests LLR-4 and -4A are also included in Figure 88.

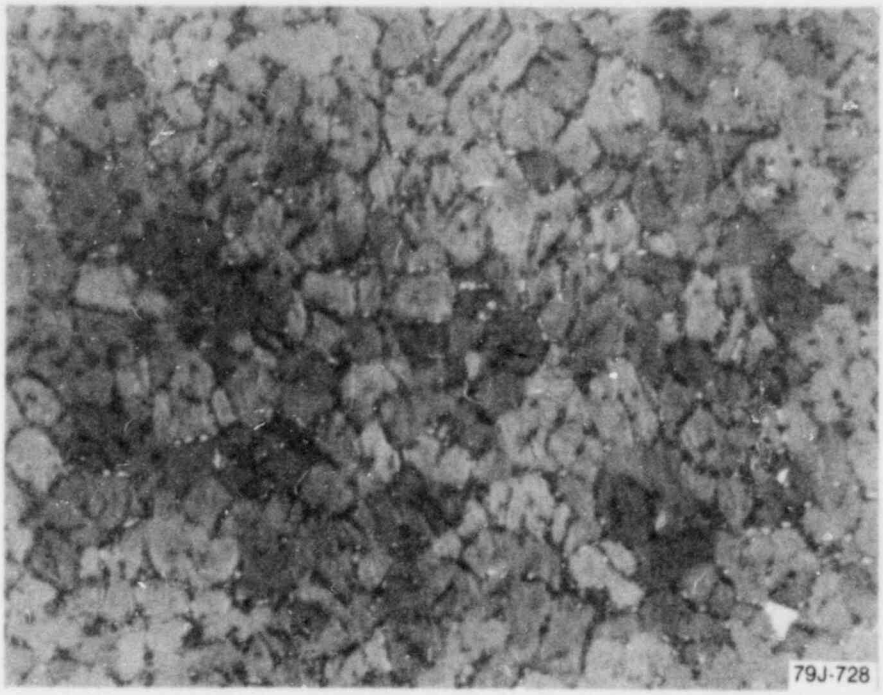

(a) 90° orientation

10 μm

(b) 270° orientation

10 μm

Figure 85. Rod 399-2 transverse cladding microstructures (Sample M7-3) from 0.31 to 0.33 m at 90 and 270 degrees.

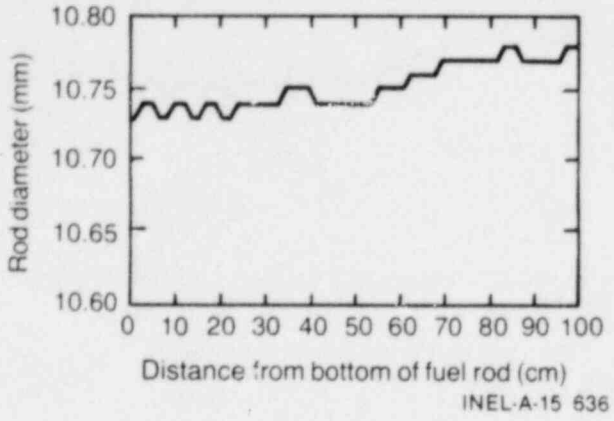

Figure 86. Postirradiation examination measurements of cladding diameter for Rod 399-2.

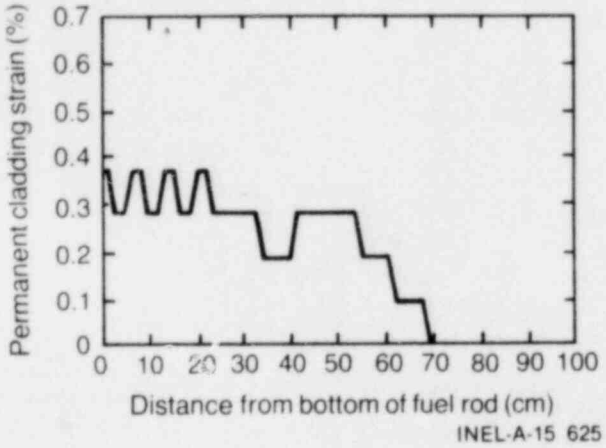

Figure 87. Circumferential strain from posttest diameter measurements of Rod 399-2.

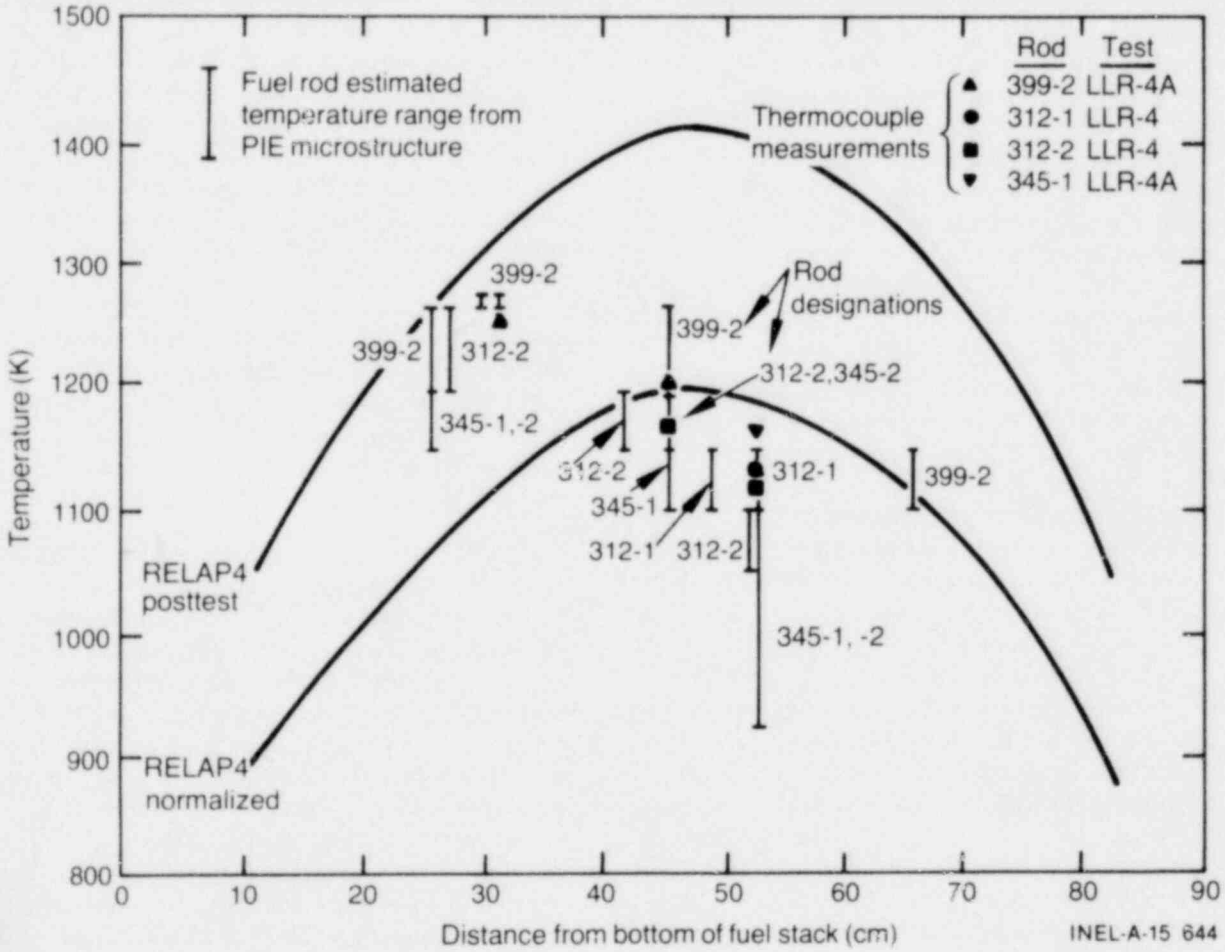

Figure 88. Comparison of maximum measured, PIE estimated (microstructure), and calculated cladding temperatures for Tests LLR-4 and -4A.

5. REFLOOD DYNAMICS EVIDENCED DURING THE LLR TESTS

One of the objectives of the PBF/LLR tests was to investigate the effects of reflood on PWR-type fuel rods subjected to previous mechanical deformation. In order to meet this objective, the PBF LOCA facility was modified to incorporate a forced feed coolant system that could model the reflood dynamics expected in a typical LOFT reflood. The controlled reflood for each test was performed by injecting coolant directly into the lower plenum of the in-pile tube to simulate a PWR reflood. The reflood coolant temperature was approximately 311 K when it entered the IPT through the upper head penetration.

The reflood phase of the LLR transients was originally to have been initiated at 35 s. The FLOOD4[a,15] code was used to predict the system reflood dynamics during the LLR tests. When a 1.58-L/s flow rate was used, the lower plenum was predicted to be filled to the bottom of the active fuel in approximately 5 s, at which time a flow rate of 0.086 L/s was to be used to simulate the LOFT temperature-time history and hot spot quench time for each test. By matching these quench times, the LLR fuel rods were expected to experience the thermal stress across the quench front that the LOFT rods are expected to experience.

A system checkout test that preceded the LLR tests showed that, in actuality, the IPT did not depressurize to 0.45 MPa, as desired, during the first 200 s of the transient. Since the reflood system was designed to operate with a positive differential pressure from the lower to upper plenum (permitting the check valves to be open), and with an IPT pressure in the range of 0.3 to 0.7 MPa, the valve sequencing for Test LLR-3 had to be modified. This involved opening the second cold leg blowdown valve at 22 s, then closing it, and opening one hot leg blowdown valve at 35 s. This sequencing was intended to modify the system hydraulic resistances and differential pressure from the lower to upper plenum, resulting in opening the check valves and permitting a flow path for the reflood water. Unfortunately, upon initiation of reflood at 35 s, the high flow water used to fill the lower plenum traversed rapidly up the active fuel length, quenching the fuel rods between 37 and 40 s. This quench was attributable to the closing of the large cold leg blowdown valve at 35 s, which modified the system hydraulic resistances and resulted in a low resistance flow path up the flow shroud for the reflood water, which rewet the rods with a low quality, two-phase mixture.

For the remaining tests, a different rationale was used to overcome the high pressure (~ 2 MPa at 35 s) problem in the IPT at reflood initiation. Examination of the pressure data from Test LLR-3 indicated that the pressure in the IPT at 120 s was in the vicinity of 0.65 MPa, whereas the differential pressure was zero. Therefore, reflood was initiated at 120 s for Tests LLR-5, -4, and -4A. Since the flow shrouds were completely voided (X = 1.0) at approximately 7 s into the transients, the heat transfer for the fuel rods past this time would be primarily controlled by radiation from the hot rod to the cooler flow shroud, as discussed previously. The cladding temperatures would decrease gradually during this period, overapproximating the time-at-temperature expected during the LOFT reflood.

By comparing the rod quench behavior indicated by the cladding elongation sensors with that indicated by the thermocouples, thermocouple fin effects can be evaluated during reflood. Table 10 lists estimates of the time to quench based on temperature and elongation measurements for all the LLR tests.

Figure 89 presents the volumetric flow indicated by the lower and upper turbine flowmeters for Rod 312-1 during Test LLR-3 for the first 60 s of the transient. The effect of opening the second cold leg blowdown valve at 22 s was rather pronounced at the lower flowmeter as the flow increased sharply to -0.3 L/s. At 36 s a significant amount of positive upflow was indicated and persisted until 44 s, at which time the volumetric flows became small for the remainder of the test and until fuel rod quench occurred at 166 s. The upper flowmeter indicated zero flow after initiation of blowdown until 37 s, at which time the volumetric flow became significant and remained so for the remainder of the transient.

Figure 90 illustrates the cladding temperature and elongation responses of Rod 312-1 during

a. FLOOD4, Idaho National Engineering Laboratory Configuration Control Number H010101B.

TABLE 10. FUEL ROD QUENCH TIMES FOR LLR TESTS

Rod	Time of Quench (s)		
	0° Thermocouple[a]	180° Thermocouple[a]	Elongation Sensor
Test LLR-3			
312-1	36.2	36.2	36.5/40.0
312-2	36.2[b]	36.2	36.5
312-3	36.0/37.5	36.0/37.5	--
312-4	36.2	36.2	36.5
Test LLR-5			
312-1	226	226	226
312-2	226[b]	226	226
345-1	226	226	226
345-2	--	--	226
Test LLR-4			
312-1	15.2	15.2	15.2
312-2	15.2[b]	15.2	--
345-1	15.2	15.2	15.1
345-2	--	--	15.2
Test LLR-4A			
399-2	244.5[c]	246.2[b]	245.0
312-2	244.6[b]	244.6	244.6
345-1	244.6	244.6	244.6
345-2	--	--	245.0

a. Thermocouples located at 0.533 m unless noted otherwise. Multiple entries indicate a more pronounced effect on rod quench for later times.

b. Located at 0.457 m.

c. Located at 0.314 m.

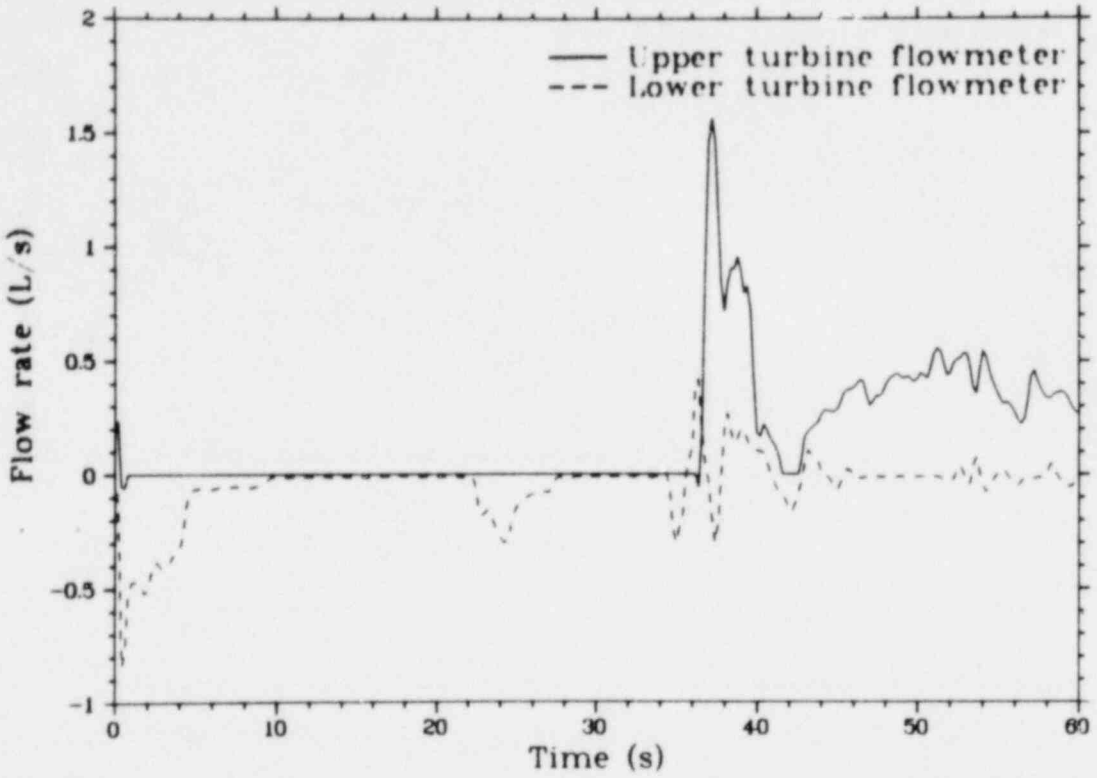

Figure 89. Volumetric flow measurements in the upper and lower portion of the Rod 312-1 flow shroud during Test LLR-3 (60-s duration).

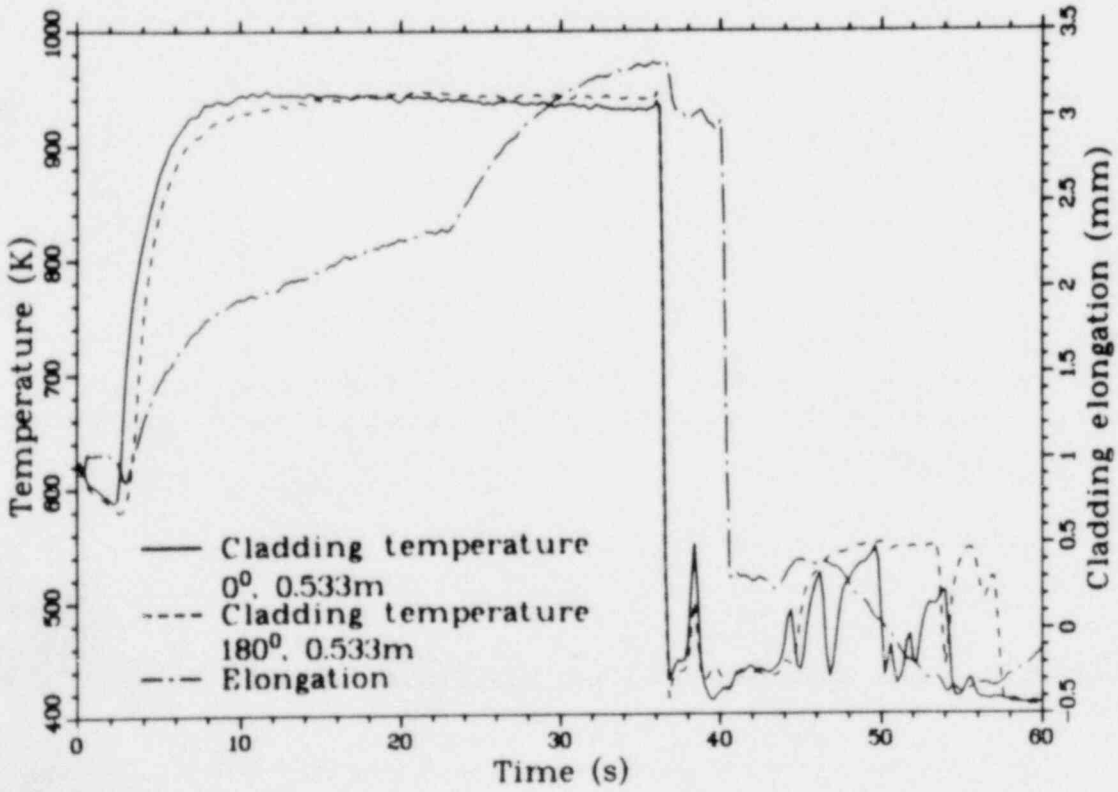

Figure 90. Long-term thermal and mechanical behavior of Rod 312-1 during Test LLR-3.

Test LLR-3 . The thermocouples indicate that the rod experienced a very rapid quench starting at 36.2 s and that the temperatures stabilized at approximately 475 K within 1 s. In contrast, the elongation sensor indicated a moderate cooling period of 3.5 s, starting at 36.5 s, followed by a rapid rod quench at 40 s. This anomaly between the two measurements indicates that the thermocouples possibly enhanced rod cooling effects or acted as fins for selective cooling of the thermocouples themselves. Comparison of the elongation response for the other rods of this test exhibits slightly different elongation sensor behavior. Although incipient cooling was indicated at 36.5 s, the other three elongation sensors used for Test LLR-3 do not indicate the pronounced quench at 40 s, but rather contract relatively moderately during this time period. Another interesting observation can be made about the thermocouple behavior of Rods 312-1, 312-2, and 312-4: shortly after the thermocouples rewet, they recorded a sudden and rapid increase in temperature at 37.5 s, essentially another DNB, before being quenched a second time at 39.2 s. This behavior may also be indicative of thermocouple fin effects.

Figure 91 presents the long-term flow behavior of the upper and lower turbine flowmeters for Rod 312-1 during Test LLR-5. The upper flowmeter indicates stagnant flow until 123 s when steam formation from the reflood water that was injected at 120 s generates the volumetric flows shown. The relatively cold reflood water condensed some of the superheated vapor in the shrouds, causing some minor flow oscillations. Since the pressure in the IPT at 120 s was in the vicinity of 0.75 MPa and the differential pressure from the lower to upper plenum was reversed (check valves closed), the reflood system was not capable of filling the lower plenum within 5 s. Therefore, when the reflood system low flow valve was activated, the coolant was prevented from flowing through the flow shrouds, and flowed directly into the downcomer annulus. The coolant continued to accumulate until the pressure in the upper plenum decayed to the point at which the pressure differential from the upper to lower plenum reversed at 174 s. The flow immediately shifted to the lower resistance flow path up the flow shrouds. At this time, the upper flowmeter indicated a significant amount of volumetric flow generated from the quench front steam formation until 240 s. (The flowmeter was apparently inoperable from 202 to 212 s.)

Figure 92 illustrates the long-term cladding temperature and elongation responses of Rod 312-1 during Test LLR-5. Pre- and posttest predictions obtained from the FLOOD4 code are also provided. A detailed description of the FLOOD4 code is provided in Appendix E. As noted in the preceding discussion, at 174 s into the transient, the reflood water reached the bottom of the 0.914-m active region of the core. With the low bottom reflooding rate (0.09 L/s) used for Test LLR-5, the coolant was characterized by a high quality mixture near the quench front and a climbing flow regime just below the quench front, as the two-phase mixture rose around the fuel rods. The hot portion of the fuel rod in front of the quench front experienced steam cooling from a dispersed flow film boiling environment. The elongation decreased slightly from 120 to 174 s. From 174 to 226 s, a significant decrease in cladding length was indicated until quench occurred at 226 s. The cladding temperature at the 0.533-m location decreased slightly during the period from 120 to 174 s. The almost adiabatic heat transfer conditions in the shrouds during this period were characterized by radiation from the rods to the shrouds, as discussed previously. The cladding temperature then decreased linearly by approximately 150 K during the time period from 174 to 226 s, after which time the rod thermocouple was quenched. As shown in Table 10, all the cladding thermocouples were quenched at approximately the same time that the rod elongation decreased sharply to its final value. This behavior could possibly be attributed to a quench front moving down the rod from the top and meeting the bottom quench front at the thermocouple junctions, or perhaps a fin effect, which implies enhanced cooling of the upper portion of the fuel rods.

The pre- and posttest calculations for the temperature history are also shown in Figure 92. Quench at the 0.533-m location was predicted by FLOOD4 to occur at 253 s for the pretest calculation and 246 s for the posttest calculations. Figure 93 presents the FLOOD4 water level pretest calculations. Once the reflood water reached the active section of the fuel, the water level rose almost linearly with the 0.086-L/s flow until the rod was quenched. No noticeable flow instabilities or large manometer-type oscillations were predicted. The quench front was predicted to move at almost a constant velocity by cooling the surface ahead of it. Behind the quench front, the surface was partially wetted and heat was removed

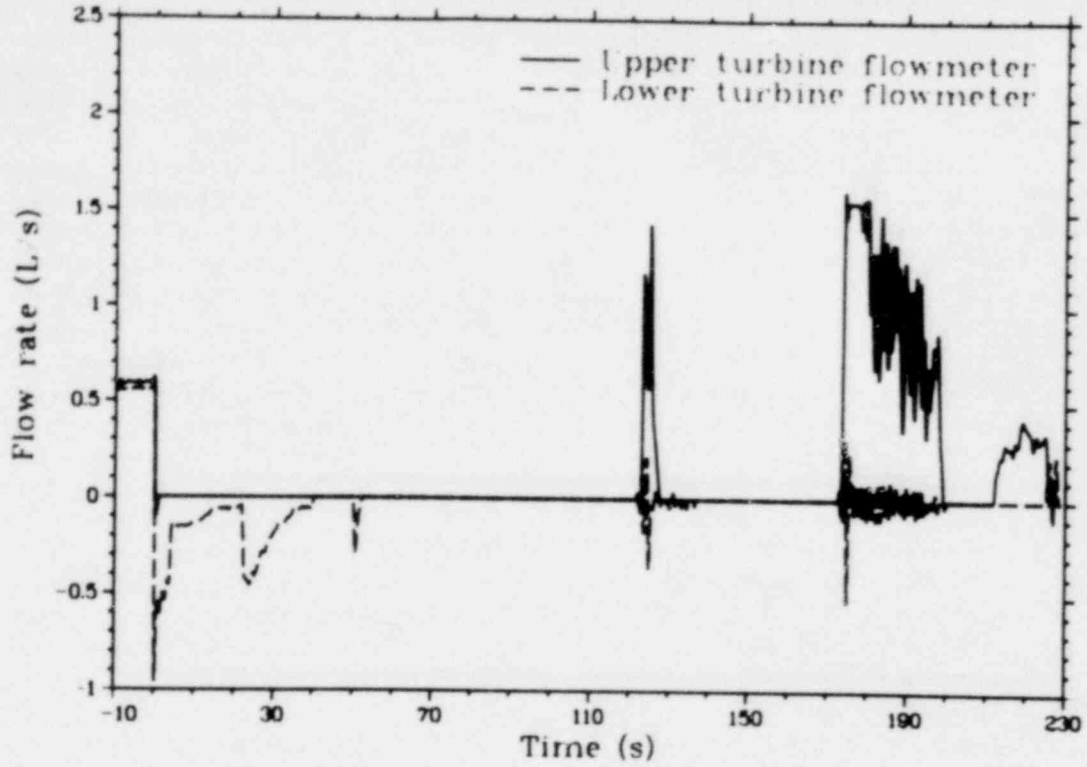

Figure 91. Volumetric flow measurements in the upper and lower portion of the Rod 312-1 flow shroud during Test LLR-3 (240-s duration).

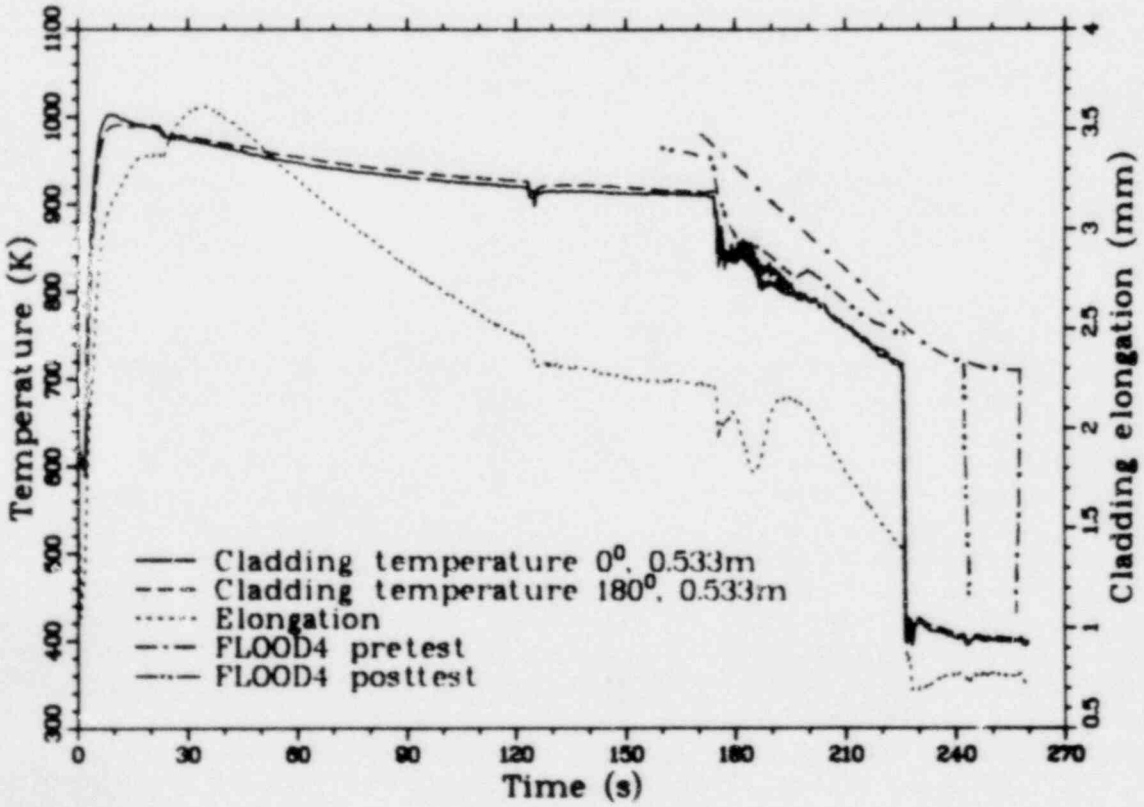

Figure 92. Long-term thermal and mechanical behavior of Rod 312-1 during Test LLR-5.

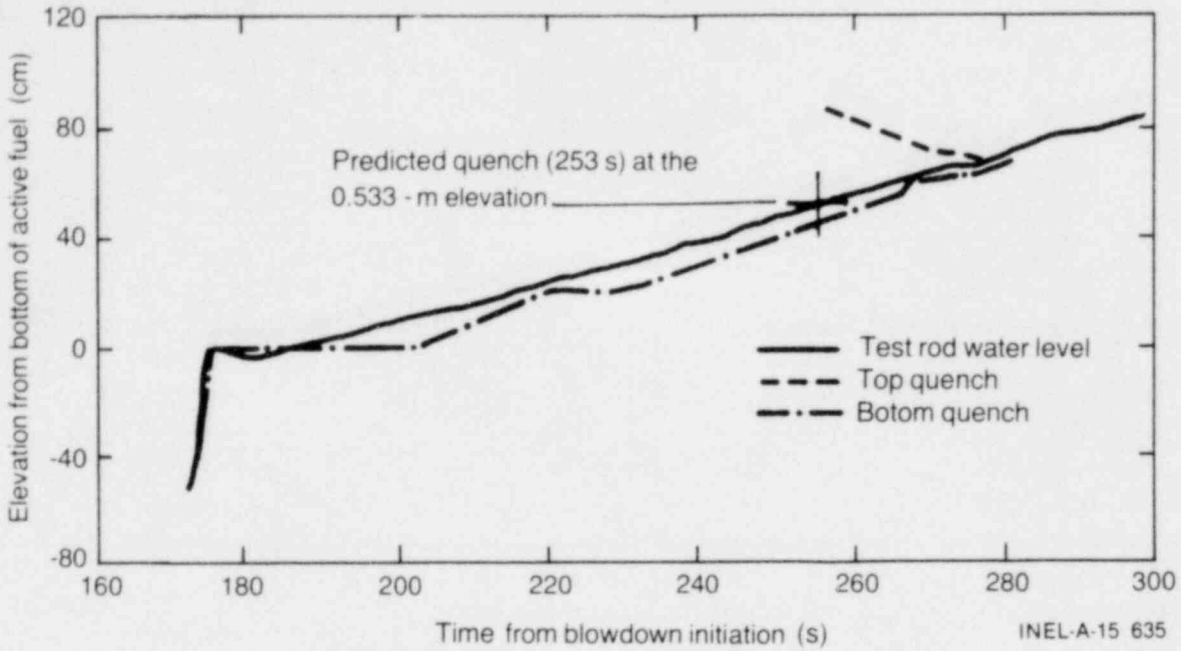

Figure 93. FLOOD4 water level prediction for Test LLR-5.

by transition boiling, nucleate boiling, and convective heat transfer to the liquid. The rods quenched from the top as well as from the bottom due to liquid entrainment. FLOOD4 predicts that at about the same time that quenching at the thermocouple location occurs, a quench front will also start moving down the rod from the top and that the two quench fronts will meet at about 280 s at the 70-cm elevation.

The reflood portion of Tests LLR-4 and -4A were invalidated by valve sequencing anomalies. From initiation of blowdown until approximately 15 s into the transient, the system thermal-hydraulic behavior for Test LLR-4 was essentially the same as for Tests LLR-3 and -5. At approximately 15 s, the primary coolant system isolation valves and the blowdown valves malfunctioned and began to flutter open and shut, permitting primary coolant to enter the in-pile tube and blowdown system. The unintentional valve sequencing resulted in premature quenching of the fuel rods at 15.5 s and again at 18.2 s, with subsequent increases and decreases in cladding temperature during the first 35 s of the transient. Beyond 35 s the rods remained in film boiling at relatively low temperatures. As shown in Table 10, the cladding thermocouples responded in unison with the elongation sensors. The conclusion reached is that for the thermal-hydraulic conditions that existed during the rapid rod quenching during Test LLR-4, no significant thermocouple perturbation effects occurred.

Figure 94 illustrates the long-term cladding temperature and elongation responses of Rod 399-2 during Test LLR-4A. The elongation response indicates that the rod responded to the initiation of reflood at 120 s, but reflood dynamics similar to those evidenced in Test LLR-5 were not witnessed after 125 s. This anomaly was attributed to the failure of the low flow reflood valve to open, thus invalidating the reflood. Quench was indicated by the elongation sensor at 245 s into the transient. The cladding temperatures decreased approximately 250 and 200 K at the 0-degree, 0.314-m and 180-degree, 0.457-m locations, respectively, for the first 120 s due to radiation heat losses. Beyond this time, the temperatures stabilized until quench occurred at 244.5 and 246.2 s at the 0.314- and 0.457-m locations, respectively. As shown in Table 10, the cladding temperatures responded in unison with the elongation sensors for the other rods of this test. Consequenty, the conclusion reached is that significant thermocouple perturbation effects did not occur in the rod rewet portion of Test LLR-4A.

The externally mounted cladding thermocouples of the LLR Test Series may have influenced the fuel rod thermal response during reflood, with the effect apparently being dependent on the reflood rate. At the low flooding rate of a few centimeters per second experienced during Test LLR-5, a comparison of the fuel centerline

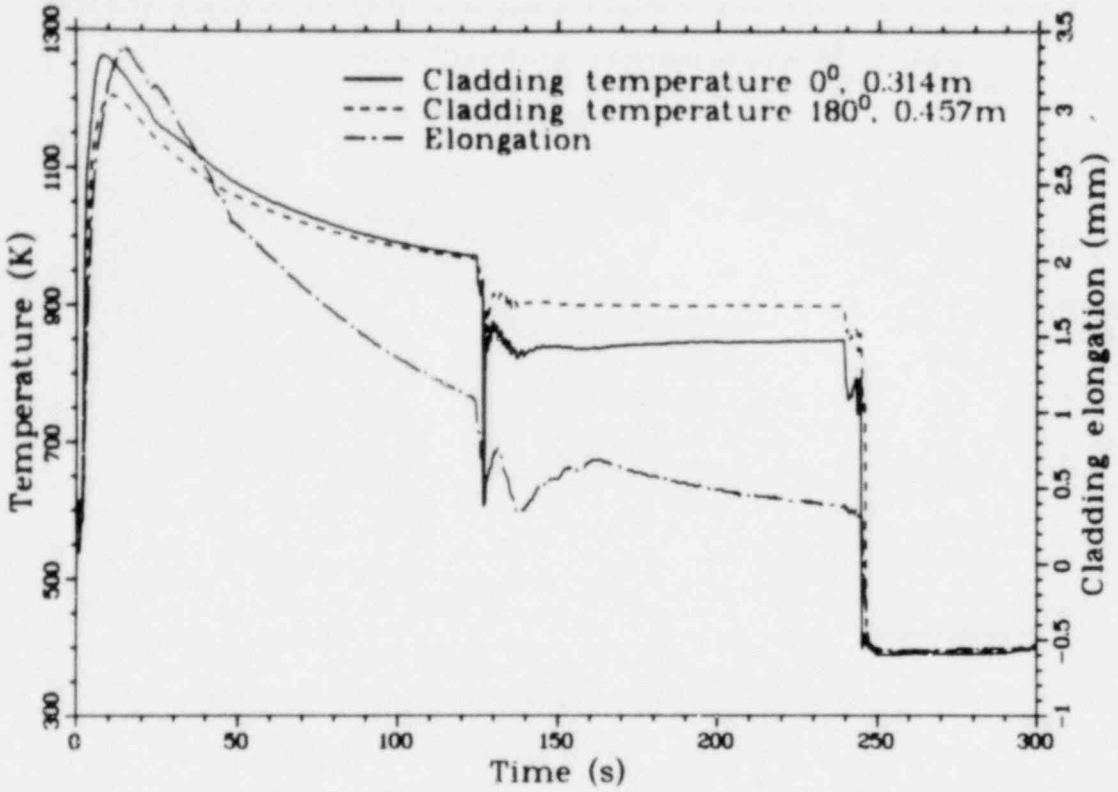

Figure 94. Long-term thermal and mechanical behavior of Rod 399-2 during Test LLR-4A.

temperatures of two rods, one with and one without externally mounted cladding thermocouples, demonstrates no apparent effects in fuel rod response due to the cladding thermocouples. At the higher flooding rates of from 10 to 50 cm/s experienced during Test LLR-3, a comparison is made of the cladding quench rate, as determined by cladding thermocouples and an integrated axial length measurement. The external cladding thermocouples during Test LLR-3 were prematurely quenched before the reflood quench front approached the thermocouple location. Finally, at extremely rapid flooding rates greater than 50 cm/s for Tests LLR-4 and -4A, the effects of externally mounted cladding thermocouples is speculated to again be small, since the reflood water front quickly quenched the cladding. The externally mounted cladding thermocouples may have resulted in a local quench at the thermocouple tips or a major quench of the upper section of the fuel rod in the region of cladding thermocouple leads during the LLR tests.

6. CONCLUSIONS

The PBF/LLR Test Program consisted of four sequential LOCA experiments during which the performance of seven, unpressurized, PWR-type fuel rods were evaluated. Measured cladding temperatures ranged from 880 to 1260 K when the rods were exposed to blowdown conditions similar to those expected in a PWR during an hypothesized double-ended cold leg break. The PBF/LLR fuel rods experienced the maximum mechanical deformation that would be expected to occur to the unpressurized LOFT fuel rods during the LOFT L2 Power Ascension Tests. The program demonstrated that previously deformed, low pressure, light water reactor design fuel rods, and, specifically, LOFT design fuel rods, are able to withstand successive preconditioning cycles and LOCA tests without failure.

Relative to the LLR tests themselves, several conclusions can be drawn. These include:

1. The mechanical deformation of the fuel rods that was observed during the postirradiation examination was consistent with Olsen's temperature-pressure criteria for fuel rod deformation.

2. The temperature and cladding elongation sensors indicated DNB was first observed at an elevation other than at the thermocouples, and probably on the lower portion of the rods during the high power Tests LLR-5, -4, and -4A.

3. On the basis of microstructure temperature estimates, the fuel rods achieved higher cladding temperatures at lower elevations on the rods than at the thermocouple elevations (except during Test LLR-3).

4. The delay in CHF and lower cladding temperatures at the peak power elevation during the high power tests could be attributed to thermocouple fin effects.

5. Measured cladding surface temperatures were in good agreement with the microstructural temperature estimates.

6. The RELAP4 code predicted the system thermal-hydraulic behavior, but underpredicted times to CHF, and predicted higher cladding temperatures than were measured at the thermocouple locations; however, on the basis of temperatures determined from postirradiation microstructure examination, the RELAP4 cladding temperature predictions may be close to the actual temperatures at locations without thermocouple attachments.

7. The FRAP-T5 code overcalculated the steady state centerline temperature for noncollapsed cladding, and undercalculated the centerline temperature for fuel rods with collapsed cladding. FRAP calculated more cladding collapse than measured for all the transients at all thermocoupl locations.

8. Significant thermal-hydraulic and fuel rod thermal and mechanical response data that can be used for evaluating and modifying the FRAP computer code for LOFT core requalification were obtained from the LLR Test Series.

6.1 System Coolant Response

Section 3 presented comparisons of the experimental data obtained at the measurement spool pieces, the fuel rod shrouds, and the IPT with RELAP4 calculations. The IPT coolant pressure, temperature, and mass flow rate data obtained from the LLR tests compared favorably with the calculations by RELAP4, which constituted the LOFT stipulated test conditions for the LLR Test Series. Minor differences existed in the magnitude of the fuel rod shroud volumetric flow and shroud coolant temperatures as measured and calculated. These differences resulted from various factors. The pressure differential between the upper and lower plenums was overcalculated for the first 4 s of the transients, which could have caused the error in the calculation of the lower shroud volumetric flow from 1.5 to 4 s. The presence of leakage flow paths in the flow shrouds during the transients could also have resulted in the discrepancy in fuel rod shroud volumetric flow. Finally, since the

code assumes homogeneous flow with thermodynamic equilibrium, the phase slip and separation that occurred in the flow shrouds could not be correctly computed.

Evaluation of the coolant conditions in the flow shrouds led to an evaluation of the flow patterns present in the flow shrouds. A flow map indicated an annular flow regime was probably maintained for the first 6.5 s of the transient when superheated conditions were attained.

On the basis of the preceding evaluation of the coolant conditions and the RELAP4 calculations, fuel rod surface heat transfer during the transient was deduced. The fuel rod surface experienced nucleate boiling during the first 1.6 to 2.8 s of the LLR transients. After CHF, film boiling was established and cladding temperatures maximized. The coolant quality approached unity at 6.5 s, and surface heat transfer changed to a combination of forced convection to steam and radiation to the flow shroud for the remainder of the transient.

Critical heat flux occurred on the fuel rods from 1.8 to 2.6 s during the low power (41 and 46 kW/m) Tests LLR-3 and -5, whereas the CHF time during the high power (57 and 56 kW/m) Tests LLR-4 and -4A ranged from 1.6 to 2.0 s.

6.2 Fuel Rod Response

Section 4 described the results of the investigation of the steady state and transient response of the fuel rods used for the LLR tests.

The measured cladding peak temperatures during the LLR tests ranged from 880 to 1260 K. At the elevated temperatures, the unpressurized fuel rods experienced cladding collapse and waisting. The measured cladding temperatures during Test LLR-3 ranged from 880 to 990 K. On the basis of these temperatures and Olsen's deformation criteria, no mechanical deformation is expected to have occurred to the rods during this test. Test LLR-5 achieved cladding temperatures in the range of 985 to 1015 K. On the basis of these temperatures, buckling would have been expected to occur at the thermocouple locations. However, since cladding temperatures are estimated to have been higher at lower elevations of the fuel rods due to possible thermocouple fin effects, buckling and incipient collapse probably occurred at locations lower than the thermocouples. The measured cladding temperatures during Test LLR-4 ranged from 1060 to 1165 K, which resulted in collapse and waisting of the fuel rods. This deformation was confirmed in the visual postirradiation examination for Rod 312-1 after Test LLR-4. Finally, Test LLR-4A achieved cladding temperatures in the range of 1075 to 1260 K, which resulted in waisting, as confirmed in the postirradiation examination, of the four rods of this test.

The posttest visual examination showed the seven LLR fuel rods to be uniformly covered with a dark-grey-to-black layer of zirconium dioxide. Except for Rod 312-3 (which was waterlogged and failed during Test LLR-3), none of the rods exhibited any visually discernible deformation (bowing or loss of diameter). However, cladding collapse occurred on all the rods, excluding Rod 312-3, resulting in permanent strains of approximately 0.5%. The deformation data obtained from the tests agreed well with Olsen's out-of-pile criteria.

The posttest analysis of the cladding microstructure was consistent with measured cladding peak temperatures during the high power Tests LLR-4 and -4A. Cladding temperatures, as estimated from microstructures, ranged nominally from 1050 to 1150 K at the 0.533-m thermocouple location, from 1150 to 1200 K at the 0.457-m location, and from 1200 to 1270 K at the 0.314-m location.

General conclusions from the postirradiation examination are:

1. No apparent circumferential or longitudinal temperature gradients occurred around most of the thermocouples.

2. The temperatures based on microstructure estimates were higher for the lower portion of the rods (from 25 to 40 cm), which could be indicative of a thermocouple fin effect on the upper half of the rods.

3. The fuel rod without thermocouples (Rod 345-2) reached slightly higher cladding temperatures, from microstructural temperature estimates and oxidation layer calculations, and experienced more mechanical deformation than companion Rod 345-1, suggesting a possible

thermocouple effect. This specific examination is detailed in Reference 5.

4. Evidence of fuel-cladding chemical reaction was found in most of the rods at random orientations.

5. The fuel-cladding gap opened in almost all cases. Almost no fuel was attached to the cladding after the tests.

6. The measured cladding surface temperatures are in reasonable agreement with the temperatures estimated from the cladding microstructures.

7. RELAP4 calculations at lower elevations (25 to 40 cm) on the fuel rods were in reasonable agreement with cladding microstructure estimates.

7. REFERENCES

1. D. L. Reeder, *LOFT System and Test Description*, NUREG/CR-0247, TREE-1208, July 1978.

2. K. R. Katsma et al., *RELAP4/MOD5 — A Computer Program for Transient Thermal-Hydraulic Analysis of Nuclear Reactors and Related Systems*, ANCR-NUREG-1335, September 1976.

3. L. J. Siefken et al., *FRAP-T5 — A Computer Code for the Transient Analysis of Oxide Fuel Rods*, NUREG/CR-0840, TREE-1281, June 1979.

4. R. J. Buckland and D. H. Schwieder, *Experiment Data Report for PBF/LOFT Lead Rod Test Series (Tests LLR-S0, -3, -4, -4A, -5)*, NUREG/CR-0927, TREE-1272, October 1979.

5. S. Shiozawa and D. E. Owen, *An Evaluation of LWR Fuel Rod Behavior during the PBF/LLR Tests* (to be published).

6. E. M. Feldman and D. J. Olson, *Semiscale Mod-1 Program and System Description for the Blowdown and Heat Transfer Tests (Test Series 2)*, ANCR-1230, August 1975.

7. J. R. Larson, *PBF-LOCA Test Series, Test LOC-11 Test Results Report*, NUREG/CR-0618, TREE-1329, April 1979.

8. G. E. Alves, "Co-Current Liquid-Gas Flow in a Pipeline Contractor," *Chemical Processing Engineering, 50*, 9, September 1954, pp 449-456.

9. J. G. Collier, *Convective Boiling and Condensation*, London: McGraw-Hill, 1972.

10. O. Baker, "Design of Pipelines for Simultaneous Flow of Oil and Gas," *Oil and Gas Journal*, July 26, 1954.

11. G. F. Hewitt, and D. N. Roberts, *Studies of Two-Phase Flow Patterns by Simultaneous X-ray and Flash Photography*, AERE-M 2159, 1969.

12. C. S. Olsen, *Zircaloy Cladding Collapse Under Off-Normal Temperature and Pressure Conditions*, TREE-NUREG-1239, April 1978.

13. R. J. Pryor et al., *TRAC-P1A, An Advanced Best-Estimate Computer Program for PWR LOCA Analysis*, NUREG/CR-0665, LA-7777-MS, May 1979.

14. L. S. Tong, *Boiling Crisis and Critical Heat Flux*. AEC Critical Review Series, August 1972.

15. R. W. Shumway, *Core Reflood Dynamics Code-FLOOD4*, EGG-SEMI-5055, October 1979.